UCLouvain

École polytechnique de Louvain

3D interconnected NiSn nanowire networks for Li-ion battery electrodes

Author: **Shana MASSAR**
Supervisors: **Luc PIRAUX, Alexandru VLAD**
Readers: **Jean-François GOHY, Pascal VAN VELTHEM**
Academic year 2018–2019
Master [120] in Chemical and Materials Engineering

Acknowledgements

This master thesis was a long process which would not have been possible without the help of many people I would like to thank here.

First of all, I would like to thank my supervisors, Professor Luc Piraux and Professor Alexandru Vlad for the opportunity they offered me to work on this project. They guided me in the right direction whenever I was confronted with a problem, they helped me with their experience to make the right decisions during the whole project.

My warm thanks are also addressed to Professor Jean-François Gohy who accepted to be the reader of my master thesis.

Then, I sincerely thank the entire laboratory team, for their warm welcome and their availability to help me with different tasks. A special thanks to Mrs Delphine Magnin for the SEM training.

I would like to express my deep gratitude to Mr Pascal Van Velthem and to Mr Joel Omale for having answered my numerous questions, for their laboratory training and for all their encouragements. And my warmest thanks to Mr Pascal Van Velthem for reviewing my drafts multiple times and who accepted to be one of the readers of my thesis.

Last but not least, I thank sincerely my master's colleagues Nicolas Marchal and Lancelot de Halleux that made this an unforgettable experience, Mr Luc Reginster for our fruitful discussions, and my family for their constant support through my whole master.

Abstract

The growing demand for electrical energy storage systems caused by the energy transition and the increase of portable electronic devices puts pressure on the creation of new batteries with higher performances, longer life-time and smaller size and weight.
In this context, Li-ion batteries currently appear as one of the best solutions. Indeed, thanks to the small Li ions shuttled between the electrodes of the battery, Li-ion battery can achieve high specific capacity along with long life-time. Li-ion batteries are commonly used for electric vehicles and portable electronics.
In parallel to the development of batteries composition, work on the architecture can also be performed to improve the battery characteristics.
Nanoscale 3D architectures are currently being developed in state-of-the-art batteries.
The main goal of this master thesis focuses on the combination of a new 3D nanostructure with a promising alloy composition for anodes in Li-ion batteries.
The developed anode is made of NiSn alloy (Ni_3Sn_4) in a shape of 3D interconnected nanowires having different diameters (230, 105 and 40nm). They are compared with 2D, i.e. films, structures and with pure Sn samples to highlight first the contribution of the 3D scale to the performances and secondly the advantage of alloyed materials (NiSn) compared to pure active material (Sn).
The samples are grown thanks to cathodic electrodeposition techniques in track-etched polycarbonate templates on copper (Cu) substrates. The electrodepostion results are characterized thanks to scanning electron microscopy and energy dispersive x-rays spectroscopy. The anodes are then assembled in a "half-cell" with Li as counter electrode and are cycled galvanostatically.

The surface morphology, the composition and the dimensions of the grown samples are analyzed with consideration to the parameters applied.
The resulting curves of the battery cycling tests are examined and linked with the intrinsic behaviours of lithiation and delithiation upon charge and discharge but also with side mechanisms as amorphization or SEI formation.
The intermediate-diameter size of nanowires (105nm-diameter) achieved the best results at low potential limitation (1V-0.01V) with a specific capacity of 1000 $\mu A/cm^2$ and a life cycle of 55 cycles compared to 325 $\mu A/cm^2$ and 35 cycles for 40nm-diameter nanowires, 750 $\mu A/cm^2$ during 45 cycles for 230nm-diameters nanowires and against 650 $\mu A/cm^2$ during 22 cycles for NiSn film.
Pure Sn samples achieved higher values of specific capacity for films (1600 $\mu A/cm^2$) at the expense of the life cycle of 10 cycles only. However, the deposition of Sn nanowires faced some issues and the resulting sample performances are very low and probably not representative of the real performances.
The low capacity and life cycle values achieved in this study are probably due to mass loss and lack of adhesion between the deposited anode and substrate, which seem to jeopardize the samples quality. It is therefore very important to work first on this problematic to be able to analyze more accurately the developed anode performances.

Contents

List of Figures

List of acronyms

C rate	Discharge current calculated in function of the capacity (see section 1.2.5)
DEC	Diethyl carbonate
DMC	Dimethyl carbonate
EC	Ethylene carbonate
EDX	Energy Dispersive X-ray spectroscopy
HOMO	Highest Occupied Molecular Orbital
LIB	Lithium-Ion Battery
LUMO	Lowest Occupied Molecular Orbital
NW	Nanowire
OCV	Open Circuit Voltage
PC	Polycarbonate
Redox	Oxydo-reduction reaction
SEI	Solid Electrolyte Interphase
SEM	Scanning Electron Microscopy
SHE	Standard Hydrogen Electrode
XRD	X-Ray Diffraction

Introduction

The energy demand is nowadays becoming a growing concern due to an exponential growth of world population combined with the huge and fast development of energy-consuming technologies. Our life style is becoming more and more dependant on the energy supplies.

At the same time, the negative impact on the environment and biosphere of the main energy source, fossil fuels, becomes unsustainable for our current lifestyle. A quick and efficient change of energy sources is becoming essential for the preservation of our environment.[1]
In this context, alternative, renewable and environmentally responsible energy sources are developed on a global basis.
Nuclear power plants are still an option for electricity production while avoiding any emission of carbon dioxide to limit the damage on the ecosystem but the problem of nuclear waste storage is still unsolved.
Belgium has fixed an objective of 13% of renewable energy in the total consumption for 2020. The proportion of renewable energy was of 9.1% in 2017.
The production of renewable electricity is mainly based on biomass by incineration, wind energy (on and offshore) and photovoltaic.[2]
At a larger scale, renewable energy starts to be implemented all around the world. But their inconstant output, due to their uneven distribution and the unpredictability of nature is still an issue for their applications. Developing efficient, sustainable and cost-effective energy storage systems is one of the big challenges of the energy transition.[1]

In the same context of limiting our emissions, one big desired development is about reducing the CO_2 emissions due to transport which represents around 25% of the total emissions.[3] A strong attention is paid to cars which represent around 75% of the CO_2 emissions related to transport.[4] Electrical or hybrid vehicle fleet is emerging but to allow a deeper and faster penetration of electrically driven vehicles, lightweight, long-life and more efficient batteries are needed.

In parallel with this energy transition, the development of miniaturized devices consuming more and more energy continues to grow with a performances duplication each 18 months according to the Moore's law.[5]
The development of long-life and highly efficient batteries along with a reduction of weight and size remains a key objective for research.
Battery technologies have been largely investigated and improved during the last years through electrochemical systems and new battery chemistries. The list of unexplored possible materials for active components of batteries becomes depleted.

The Li-ion batteries have proven efficiency and high performance and are becoming a must in the portable electronics field and in the sector of electric cars. Originally commercialized by Sony, Li-ions batteries are now in many electric devices and Tesla integrated some Li-ion batteries in its cars.[6] However the extraction of lithium has a non-negligible cost on the environment

through lands damages, the high consumption of water and the use of toxic products. Moreover the distribution of the lithium resources is largely unbalanced across the world, with around 60% of the resources in South-America. No cost-effective recyclable processes exist nowadays. But lithium, owing to its remarkable intrinsic properties, has become unavoidable in the battery development.
Indeed, the Li ion has the smallest reduction potential while being small and light. It allows to deliver high capacities in small and light batteries. In Li-ions batteries (LIB), Li ions act as charge carriers shuttled from the cathode to the anode and reacting with the electrodes by intercalation, alloying or conversion reactions. Research is still carried out to identify the most suitable electrodes for LIBs. A strong attention was paid on the anode material which was used to be graphite even if it did not achieve high specific capacity values.
Graphite uses the intercalation technique to react with Li ions which were inserted in between the layers of graphite.

Interest is now carried in lithium alloying materials anode. One issue with this anode type is the huge volume expansion caused by the alloying with Li ions. Some strategies were developed to buffer the volume expansion. One of them is to use an inactive metal as matrix to buffer the volume variation. Some combinations of nickel and tin were developed where tin (Sn) is the active material reacting with four atoms of lithium while nickel (Ni) is present as inactive matrix.

Research has now interest in working on the structure along with the composition of batteries. Great improvements could be achieved by changing the structure of our usual batteries without changing much their composition.
Different strategies were performed at the complete battery scale such as interdigited electrodes, continuous electrodes, sponge geometries, etc.
But a work on the electrode geometry can also be done.
Nanowire patterns present many advantages such as an easy access for the electrolyte ions to the active material of the electrodes thanks to a large surface area combined with free volume allowing to also buffer the volume variations of the electrodes. Transport properties (ions diffusion and electronic transport inside the solid electrodes) are also improved by the nanowires geometry and nanoscale.
Straight nanowires, core-shell structures, interconnected nanowires and many other possibilities exist.

This report studies one specific configuration for anode material composed of a NiSn alloy for Li-ion batteries: the 3D interconnected nanowires.
Different diameters nanowires were grown and cycled to analyze the effect of the diameter on the batteries performances. Simple 2D films were also grown to be compared with the 3D architecture results.
In addition to the geometry study, samples of pure tin were also grown to verify the necessity of an inactive matrix of nickel inside the samples.
The main objective of this study is to highlight the performances of 3D interconnected NiSn nanowire electrodes having different diameters compared to 2D structures or pure Sn samples.

This manuscript is divided in three chapters. The first one is dedicated to the theoretical aspect of the work with a context of power sources, some reminders about battery principles and characteristics. More specifications about Li-ion battery are then given followed by a discussion on 3D architectures.
The second chapter presents all the experimental techniques and conditions used to grow, assemble and test the samples. A description of the characterization techniques and the physics

principles behind them is also given. Some of the applied parameters are discussed to give perspectives to achieve higher quality samples.
In the last, but not least, chapter, all the results derived in the context of this work are presented, interpreted and discussed. Some conclusions and perspectives are finally drawn.
The appendix contains some information or results which were not interpretable but which still could be of interest for the reader.

Chapter 1

Theoretical background

Thanks to the context described in the introduction, it is now possible to understand why the development of batteries is so important today. This section aims to explain all the relevant features important to understand fully the science and parameters behind the battery design. First, a quick overview on other electrons producing power sources is given to illustrate the context in which batteries are developed.
Then a deep investigation on the batteries working principle, components and parameters is led.
After that, more details are given about Li-ion battery, which is the batteries type of interest: working principle, interphase formation, but also a study of the lithium resources and sustainability was performed.
After that, the study is developed around the choice of the anode's material.
Some justifications about the interest to work with Sn are given followed by the development of solutions leading to the NiSn alloy choice.
Finally, the interest for 3D batteries architectures, and more precisely for 3D interconnected nanowire networks, is described and the different parameters and the advantages of such structures are explained.

1.1 Electrons producing power sources

In a context of growing energy demand, different strategies were imagined with one purpose: the increase of the energy production efficiency. The Carnot-cycles limitations encouraged the researchers to look on other power sources than thermal machines. Electricity has attracted lots of attention.

Two main fields are related to electrons producing power sources. The first one, the one of interest in this study, is the electrochemical source of electrons.
The second one is linked to thermal/nuclear/mechanical-to-electricity fields. Common examples are thermoelectric, pyroelectric and nuclear sources.[7]
The main interesting features of electrochemical electrons producing power sources are:

- Capacitors
- Batteries
- Fuel cells
- Photovoltaic

Fuel cells Fuel cells work with the same electrochemical principle as batteries, by converting chemical energy into electricity. The main difference is the nature of the active material in the cell. In batteries the active materials are present as components of the cell while in fuel cells, the active materials are fed into the cell from external sources when power is needed.[5] The fuel cell can work continuously as long as the reactants are supplied and the reaction products are removed. This implies to used liquid or gaseous reactants and products.[8]
One of the most known system is hydrogen and air (O_2) with water generation (see figure 1.1). In the fuel cell, the reactants are not in direct contact but separated by a ionically conducting medium, otherwise, a thermal generation will lower the electrical generation.

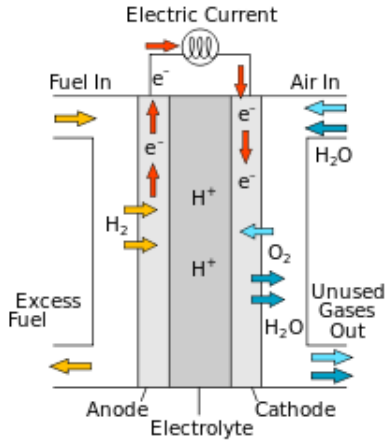

Figure 1.1: Schematic representation of a fuel cell (from [9])

Capacitors Capacitors are composed of two conducting parts separated by a non-conducting medium.
Capacitors can store and deliver charges in an electrical circuit as a battery. The charges of opposite signs are accumulated on each conducting side of the capacitor while charging, increasing the potential drop between the electrodes.
Supercapacitors use the Helmholtz double layer principle in liquid electrolyte to achieve higher performances.[10][8]

Photovoltaic Electrochemical solar cells use sun light to produce electricity thanks to electrons generating electrochemical reactions. A good example of this particular technology is the dye-sensitized solar cells.

Batteries The batteries are one very promising technology to store electricity. The chemical principles and parameters of batteries are discussed in this chapter.

1.2 Batteries

The battery is a device which uses oxydo-reduction reactions to convert chemical energy into electrical energy.
Batteries have a lower specific energy than common fuels but as the conversion is due to electrochemical reactions, batteries are not subject to the Carnot cycle's limitations at the opposite of heat or combustion engines. They are therefore capable of high energy conversion. [5][11]

To understand fully the working principle and the different outputs of a battery, an overlook on the principle of oxydo-reduction reactions is essential. This section explains the working principle of batteries before describing its components, parameters and performances.

1.2.1 Electrochemical oxydo-reduction reactions

An oxydo-reduction (as well known as redox reaction) is a reaction which implies a transfer of electrons from one reactant to another and, therefore, a change in the oxidation state of the reactants.
Spontaneous redox reactions transform reactants in more stable components.
Some of commonly known phenomena are due to redox reactions as the corrosion of metals or the combustion.
The oxidation occurs when a species loses electrons while the reduction occurs when the other species gains electrons.
These two reactions are complementary and are called "half-reactions".

Oxidation reaction:

$$\mathrm{X} \rightleftharpoons \mathrm{X^+} + 1\,\mathrm{e^-} \tag{1.1}$$

where the reducer X gets oxidized.
Reduction reaction:

$$\mathrm{Y^+} + 1\,\mathrm{e^-} \rightleftharpoons \mathrm{Y} \tag{1.2}$$

where the oxidant Y^+ gets reduced.
The global redox equation is therefore:

$$\mathrm{Y^+} + \mathrm{X} \rightleftharpoons \mathrm{Y} + \mathrm{X^+} \tag{1.3}$$

The redox couples are the two different oxidation states of one reactant. X^+/X and Y^+/Y.
These redox couples are classified thanks to standard reduction potential E° which corresponds to the cell potential at equilibrium under standard conditions where the cathode is the element of the couple and the anode is the oxidation of hydrogen chosen as reference (SHE, Standard Hydrogen Electrode):

$$\frac{1}{2}\mathrm{H_2} \rightleftharpoons \mathrm{H^+} + 1\,\mathrm{e^-} \tag{1.4}$$

A positive E° represents therefore an oxidizing agent for hydrogen while a negative E° represents a reducing agent for hydrogen.

In a classical redox reaction involving two different species, it is possible to determine which one will act as oxidizing agent and as reducing agent by comparing E°. The highest standard potential will do the reduction and the lowest, the oxidation. [12]
The standard potential depends on the nature of the components.

1.2.2 Battery components

A battery (or more precisely, a cell, which is the repeated unit of a complete battery) is composed of three main elements.

The electrodes

The cathode and the anode (the electrodes of the battery) are the active materials which are doing the redox reactions.
The anode and cathode materials will determine the working voltage and the performances of the battery.
In a cell, both oxidation and reduction reactions occur at a specific location.
At the anode the oxidation occurs while the reduction occurs at the cathode.
When the spontaneous reaction of discharge occurs, the anode generates electrons and cations due to the oxidation process. The anode is connected to a current collector and to the external circuit, allowing the electrons to flow from the anode to the external load. This electrical current flows in the external circuit to the current collector of the cathode and, finally, to the cathode, where the electrons recombine with cations though the reduction reaction.
To allow such a reaction, an ionic transfer is needed between both electrodes.

The electrolyte

The anode and the cathode must be separated to avoid internal short-circuits which would consume the electrical current, but they also need to be connected by a ionically conducting medium, the electrolyte. A flux of ions crosses the electrolyte to balance the electrons movements and to respect the charge neutrality of the device.
The electrolyte is therefore a good ionic conductor to allow a fast process while being an electronically insulator to avoid any electrical loss. It can be liquid or solid.

Another critical parameter to take into account is the reactivity of the electrolyte with the electrodes. Most electrolytes are aqueous with some important exceptions as for lithium-ion batteries since the working voltage of lithium batteries is higher than the decomposition voltage of water.
A scheme of a classical battery is depicted on figure 1.2. In practice an electrolyte-permeable separator is placed between the electrodes to avoid short-circuits while allowing ionic diffusion.
In discharge mode, the anode is the negative electrode and the cathode is the positive electrode. This is inverted upon charge as it can be seen on figure 1.2 and figure 1.3.

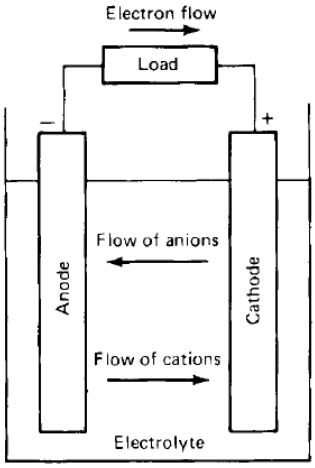

Figure 1.2: Electrochemical discharge of a cell (from [5])

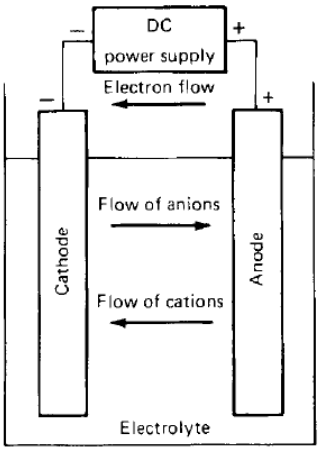

Figure 1.3: Electrochemical charge of a cell (from [5])

1.2.3 Types of battery

Batteries may be classified in many different ways as by applications, functional characteristics, chemistry or physical state. One fundamental distinction is the rechargeability of batteries. [13] Primary batteries are defined as non-rechargeable batteries. They usually present a good shelf-life (conservation time) , high energy density at low discharge rate and practical advantages as no maintenance needed or ease of use. One well-known common example is the alkaline zinc/manganese dioxide flashlight battery.

Secondary batteries can be recharged multiple times by passing an electrical current in the opposite direction of the discharging current. Some familiar examples are the lead-acid batteries used in automobiles and Li-ion batteries used in portable electronics. [13]

1.2.4 Battery potential

The potential of the cell is defined as:

$$E^{\circ}{}_{cell} = E^{\circ}{}_{cathode} - E^{\circ}{}_{anode} \tag{1.5}$$

This potential is also known as the electromotive force. It is the origin of the electrochemical reactions occurring in the cell and delivering the generated electricity. The standard potential $E^{\circ}{}_{cell}$ sign will determine whether the system is in charge or discharge. Indeed, the $E^{\circ}{}_{cell}$ is linked to the Gibbs free energy of the components formation during the electrochemical reaction by:

$$\Delta G^{\circ} = -nFE^{\circ}{}_{cell} \tag{1.6}$$

Where F is the Faraday constant and n is the number of exchanged electrons.
In other conditions than standard conditions, the Nernst equation can be derived:

$$\Delta G = \Delta G^{\circ} + RTlnQ \tag{1.7}$$

by substitution it becomes:

$$-nFE_{cell} = -nFE^{\circ}{}_{cell} + RTlnQ \tag{1.8}$$

and finally, it can be wrote as:

$$E = E^{\circ} - \frac{RT}{nF} ln(Q) \tag{1.9}$$

where R=8.314, T is the temperature and Q the reaction quotient of the electrochemical reaction.

The reaction is spontaneous (discharge) if the Gibbs free energy is reduced, therefore, if the E_{cell} is positive.[5]

1.2.5 Battery performances and parameters

After the description of the working principle, some knowledge about the internal characteristics of batteries and the influence of the chosen parameters is important to understand better the results achieved by the batteries.

Theoretical voltage

The open-circuit voltage (OCV) is the highest difference of potential which could be generated by the battery. It can be calculated from the reduction potential of the electrodes or thanks to the Gibbs free energy of the system as explained in the previous section. In practice the real potential delivered by the system is lower due to different non-ideal characteristics but also because the battery does not get discharged completely.

Non-ideal characteristics

1. Self-discharge One first reason of non-ideal battery performances is the self-discharge which occurs due to internal chemical reactions without delivering any energy to the external circuit. One possible mechanism of this process is if the anode and cathode directly react together (if one element is slightly soluble in the electrolyte for example). Other mechanisms, usually called *parasitic* reactions, are possible as reactions between the electrodes and other substances, the electrolyte for example. These reactions are most of the time very slow and become important only in the case of long storage times. [13]

2. Polarization and internal impedance Polarization effects are all effects which induce a loss of voltage during discharge.[5]

- Active polarization which drives the reaction to occur at the electrodes surface due to the kinetic of electrons transfer at the electrode/electrolyte interface.
- Concentration polarization which comes from mass transfer leading to a difference of concentrations of reactants and products at the surface and in the bulk of the electrodes
- Ohmic polarization (internal impedance) is due to the ionic resistance of the electrolyte, the electronic resistance of active materials and current collectors, the contact resistances between electrodes and current collectors,... Please note that the term *Ohmic polarization* is commonly used even if the impedance of a complex device such as a battery is not only composed of a real resistance term and should be measured in alternative current (AC) in place of a constant current (DC).

At the same time, the presence of impurities at the electrodes and the ionic conductivity of the electrolyte imply also to use a higher voltage than OCV during the recharge of the battery.[14] All these effects lead to a real voltage output E:

$$E = E^{\circ} - (\eta_{act} + \eta_c)_{anode} - (\eta_{act} + \eta_c)_{cathode} - R_i I \tag{1.10}$$

With E°, the open-circuit voltage of the cell,
η_{act} the activation polarization, η_c the concentration polarization,
R_i the internal resistance, I the current. As it can be seen on the figure 1.4

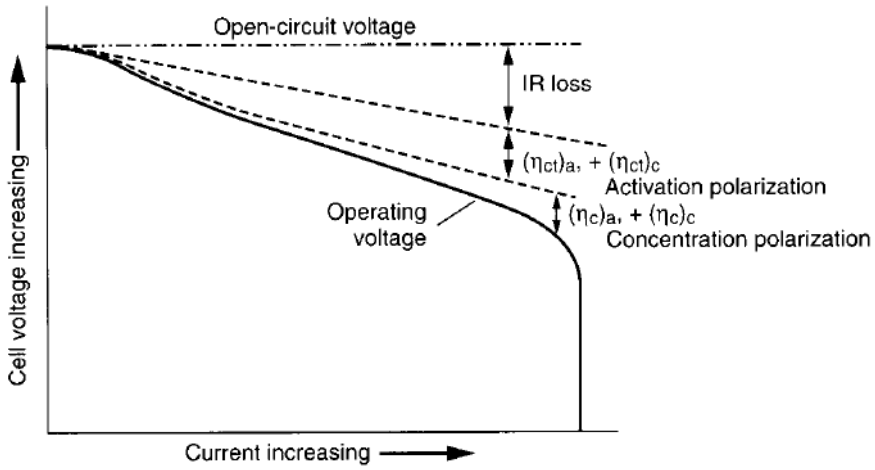

Figure 1.4: Cell polarization in function of operating current (from [5])

Energy

The unit of measure is the Joule (J) but in the case of batteries, the energy is usually expressed as Watt-hour (Wh): the power delivered by the cell over a certain time, 1Wh= 3600J. The energy density is the energy by unit of mass or volume, depending on the application.
The energy proportion effectively delivered by a real battery under optimal conditions is approximately 25 to 35% of the theoretical energy which can be delivered by the given amount of active materials.[5]

Capacity

The capacity is defined as the current delivered by the battery times the duration of delivering, it is usually expressed as Ampere-hour (Ah).
The capacity depends on the quantity of accessible active material in the cell and the delivered capacity upon discharge depends on the discharge rate: higher is the discharge rate, lower will be the capacity.[11] Due to this effect, it is important to normalize the current of discharge.

Current

One discharge rate widely used is the "C" rate. This discharge current is define as a fraction (M) of the rated capacity given for a time n.

$$I_{discharge} = M * C_n \tag{1.11}$$

To have the right units, the C_n, is commonly divided by 1h in literature. [5]

The battery performances are influenced by the operating temperature. Performances are better at higher temperature due to an increasing internal resistance and a reduction of chemical activities while the temperature is decreasing.
The components nature is chosen to achieve the highest capacity and voltage as possible while keeping it possible to produce in a safe, sustainable and efficient way. The nature of the components will be discussed in more details later.

1.3 Li-ion batteries

The high increase of miniaturized circuits and devices provokes a growing demand for micro-batteries of larger capacities and faster charging rates. At the same time more powerful and efficient batteries are required for the new set of electrical applications which are currently developed to replace combustion engines such as for electrical vehicles.
The use of small ions as charge carriers into the batteries allows a high ionic conductivity while providing a faster diffusion within the electrodes considering that solid state diffusion is the rate-limiting step of the batteries electrochemical reactions.
Furthermore small and light ions allow a higher energy and power density (gravimetric or volumetric).
The interest goes mainly on 2 possibilities:

- Li-ion batteries which provide great battery performances because Li is the smallest usable ion with a low atomic number and the lowest reduction potential.
- Na-ion batteries since sodium is cheaper and more abundant than lithium. Na-ions are close to Li-ions even if they have lower electrochemical properties (such as a larger radius and a higher reduction potential). Morever the mass of Na is higher than Li which has to be taken into account for mobile applications where the mass is an important parameter.[1]

Li-ion batteries provide a high working voltage and a high energy density, specific capacity but also a long service life (see en figure 1.5 and 1.6).
This section aims to focus on the Li-ion battery, by giving information on its working principle, characteristics, advantages and drawbacks before going more into details on the Li-ion batteries anodes which are the main topic of this study.

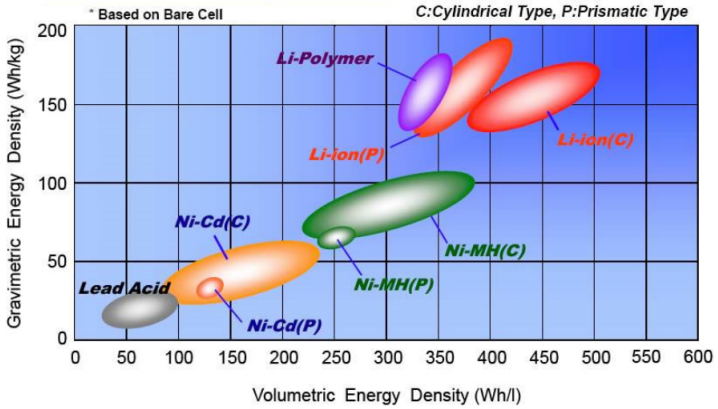

Figure 1.5: Comparison of Energy Density in Battery Cells (from NASA [15])

Battery chemistry	Type	Voltage/V	Theoretical specific energy/W h kg^{-1}	Practical specific energy/W h kg^{-1}	Practical energy density/W h dm^{-3}
Zn/MnO_2 (alkaline)	Primary	1.5	358	145	400
Li/I_2	Primary	2.8	560	245	900
Pb/acid	Secondary	2.1	252	35	70
Ni/Cd	Secondary	1.3	244	35	100
Ni/MH	Secondary	1.3	240	75	240
Na/S	Secondary	2.1	792	170	345
$Na/NiCl_2$ (ZEBRA)	Secondary	2.6	787	115	190
lithium–ion	Secondary	4.1	410	150	400

Figure 1.6: The voltage, theoretical specific energy values (considering only the mass of the active materials in the electrodes), values achieved in practice and energy densities for the major battery systems (there is a large range of values for lithium–ion batteries owing to the great variety of available electrode materials, both for the positive and negative electrodes) (from [16])

1.3.1 Working principle

In Li-ion batteries, Li-ions diffuse in the electrode via intercalation, alloying or conversion reactions (see on figure 1.7), crossing the electrolyte upon charges and discharges. [17]

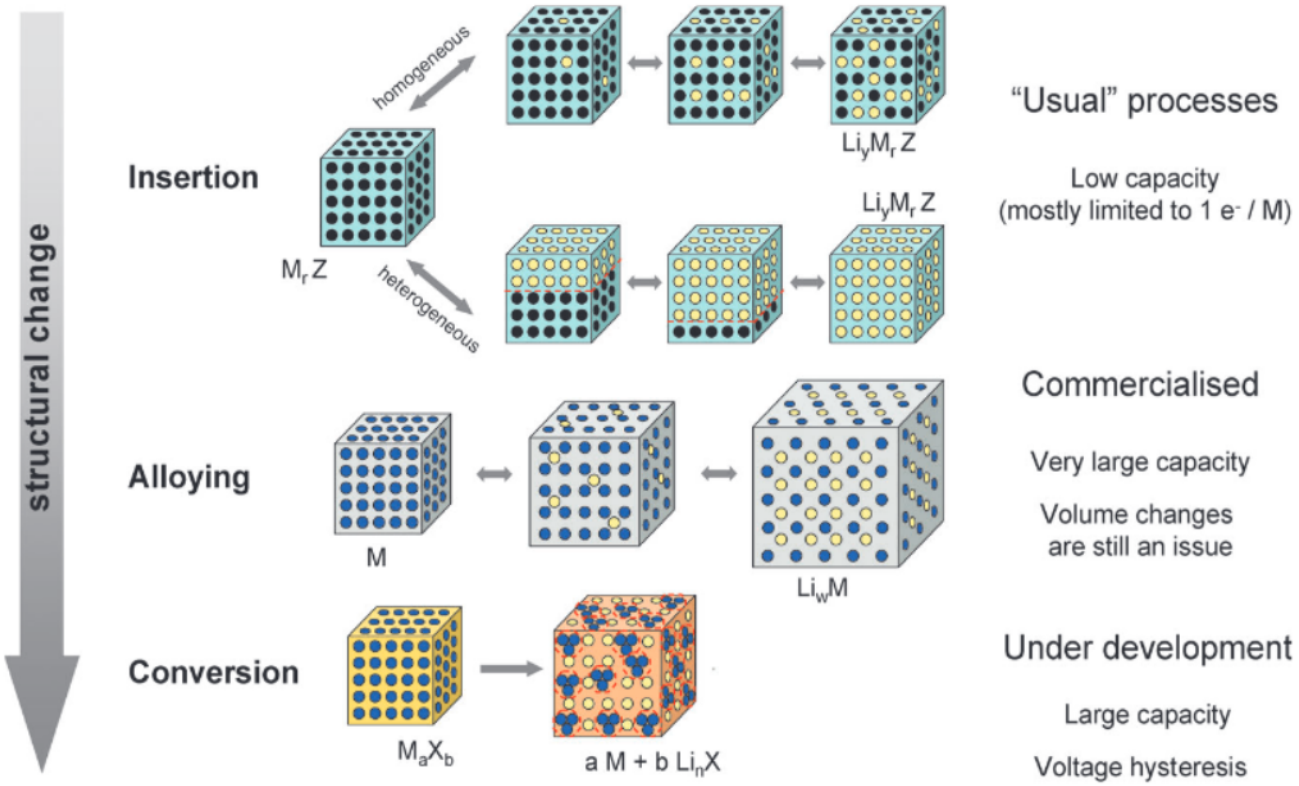

Figure 1.7: A schematic representation of the different reactions mechanisms observed in electrode materials for lithium batteries. Black circles: voids in the crystal structure, blue circles: metal, yellow circles: lithium. (from [16])

Intercalation The Li ions are intercalated in between the layers of the electrode material such as graphite.

Alloying The Li-ions react with the active material of the electrode to form alloys. This process is investigated in this study with Sn as active material alloying with Li.

Conversion reaction This term is used to describe the reaction between the Li ions and a binary transition metal compound M_aX_b, M being the transition metal while X= O,S,N,P,F,... to produce metallic nanoparticles surrounded by a Li_yX matrix. [16]

During the discharge, the anode releases Li ions and electrons. The electrons flow from the anode to the cathode trough the external circuit, allowing to provide electricity to the external load. At the same time, the Li ions (Li^+) generated travel through the ionically conductive electrolyte to the cathode and recombine with the electrons as it can be seen on figure 1.8 (note that the current direction is defined as the opposite direction of electrons flow). The overall reaction rate depends greatly on the ions movements through the electrolyte/electrode interface.

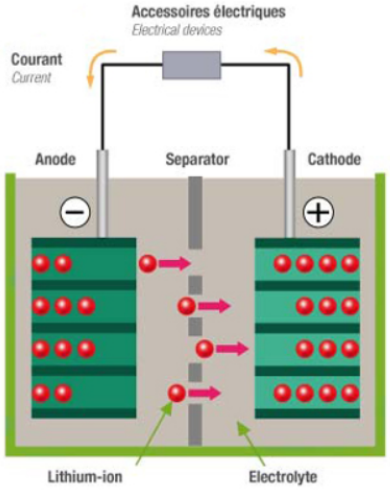

Figure 1.8: Li-ions battery (from [18])

The electrolyte is chosen in function of the working voltage which should be within the window of the electrolyte (between the HOMO and LUMO energy levels) to allow a long shelf and cycle life as it can be seen on figure 1.9. The Li^+ ionic conductivity of the electrolyte has also to be taken into account.[19]
Conventional electrolytes of Li-ions batteries are composed of $LiPF_6$ dissolved in organic solvents. These solutions are highly ionically conductive ($> 10^{-3}S/cm$) and are compatible with the voltage application window. The basis of the mixture is carbonate solvents which are aprotic, polar and having a high dielectric constant. This allows a high concentration of dissolved lithium salts.[16]

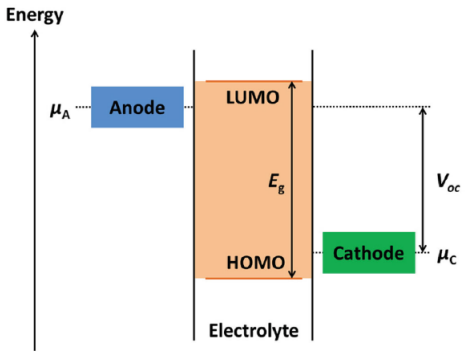

Figure 1.9: Relative energy diagram of electrode potentials and the electrolyte energy gap in rechargeable ion batteries (from [1])

1.3.2 SEI

Solid electrolyte interphase (SEI) layer is generated by decomposition of the electrolyte at the electrode surface. This layer plays a critical role by being permeable to Li-ions and preventing electrons transfer reactions between electrode and electrolyte.
Indeed, if the Li-ions can not cross correctly the SEI layer, the impedance of the cell increases while if the electrons transfer is not blocked, the SEI continues to grow, consuming more electrolyte and Li-ions. This would lead to a decrease of the capacity delivered. The stability and performance of the SEI film are important parameters to control in order to achieve long-life and efficient batteries. [20]
The SEI characteristics such as morphology, impedance, porosity and composition depend on the conditions of formation. Indeed, the voltage of formation, the organic or inorganic composition influence greatly the SEI characteristics. Here below, on figure 1.10, are suggested some possible reactions which can occur between lithium and $LiPF_6$ organic solvents electrolyte.

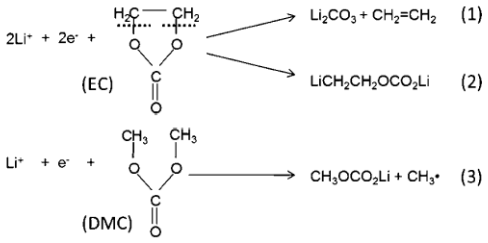

$$Li^+ + e^- + \text{Trace } H_2O \rightarrow LiOH + {}^1/_2\, H_2 \quad (4)$$

$$LiOH + e^- + Li^+ \rightarrow Li_2O + {}^1/_2\, H_2 \quad (5)$$

$$LiPF_6 \leftrightarrow LiF + PF_5 \xrightarrow{Li^+ + e^-} LiF + Li_xPF_y \quad (6)$$

Figure 1.10: Possible reactions of electrolyte decomposition (from [20])

In the case of intercalation electrodes such as graphite, it also prevents other solvent molecules from co-intercalating with Li-ions within the layers, leading to exfoliation and disintegration of the graphite electrode.

1.3.3 Advantages and Drawbacks

Li-ion batteries have open new possibilities in term of batteries weight, size, storage performance, life, capacity,... They also need few maintenance thanks to the absence of *memory effects*.

But these Li-ion batteries are also more expensive to produce than lead batteries and, moreover, less robust. One still controverted question is about the resources of lithium metal. The situation is briefly described below. [21]

Each year around 43000 tons of lithium are produced mainly for batteries applications (46% dedicated for batteries applications, as seen on figure 1.11) and the demand is expected to grow up to 50 000 tons in 2025. [22][23]

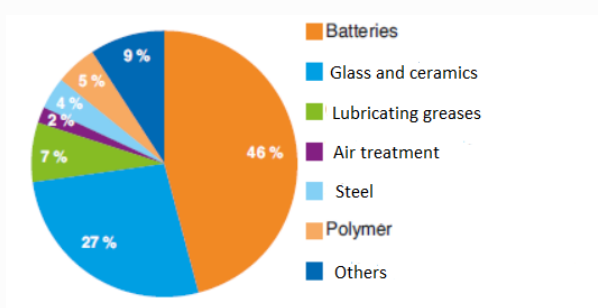

Figure 1.11: Sector using lithium (modified from USGS 2018 [24])

Lithium resources are geographically constrained (see figure 1.12) and were suspected to be too limited to meet the global demand for energy storage systems in the context of the rising amount of portable electronic devices. The discovery of new resources has allowed to be more confident in the abundance of lithium according to recent reports.
It is estimated that around 60% of the lithium resources are located in South-America ("Lithium triangle" figure 1.13, figure 1.14) which is producing more than the half of the world production (55% in 2017). South-America resources are exploited from brine while the rest of the lithium resources in the world is mainly under mineral deposits form. Lithium costs more when produced from mineral deposits than from brine.[23]

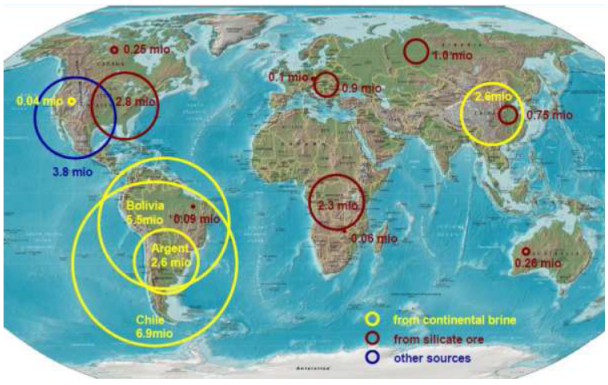

Figure 1.12: Global Lithium resources (from [25])

Figure 1.13: "Lithium triangle" (from [26])

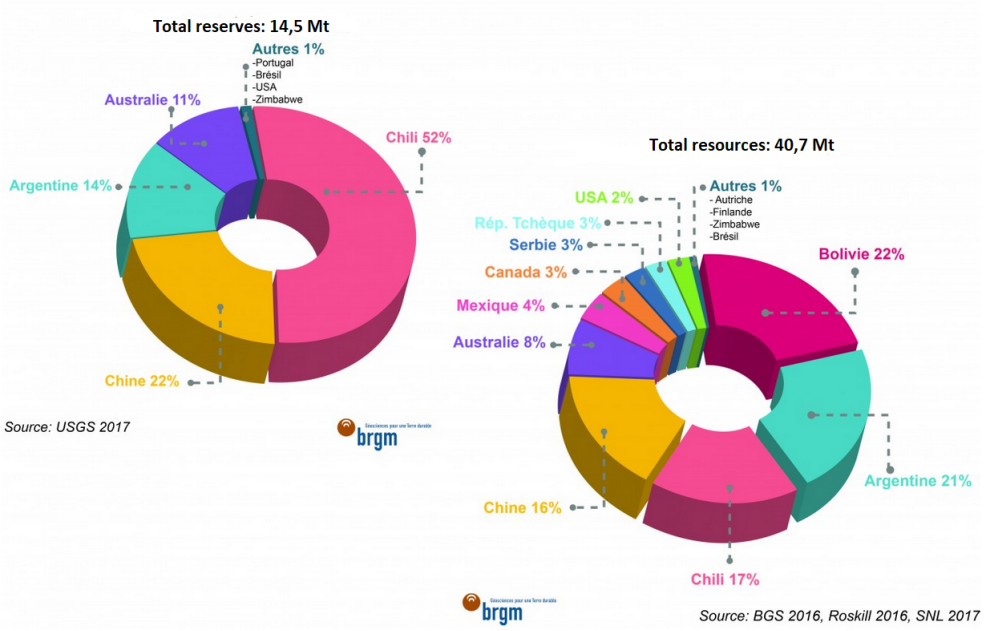

Figure 1.14: Resources and reserves distribution of lithium in 2016-2017 (modified from [23])

The lack of a more even distribution across the world could lead to some geopolitical complex situations. As seen on figure 1.14, Europe is not well represented in the distribution even if some potential projects could emerge.
From a more environmental point of view, the extraction of lithium uses lots of water in arid regions mainly in South-America (figure 1.16): 500 gallons of water are needed for 1 ton of lithium [27], toxic leaks are also a risk, the lands are damaged by the extraction and no efficient and cost-effective recycling process is available for now.

Figure 1.15: Lithium mines in Chile (from [18])

Figure 1.16: Lithium exploitation Chile (from Mathieu Colin/Hemis)

1.3.4 NiSn anode for Li-ions battery

After the description of the batteries and more precisely, the Li-ion batteries, this chapter focuses on the anodes material of Li-ion batteries. The ideas behind the NiSn alloy studied in this report are developed step by step in this section.
The anode material of Li-ion batteries stores and releases Li-ions during charge and discharge respectively.
The choice of the anode material will greatly influence the reaction process and the performances of the batteries.
Moreover the electrolyte decomposes during the charge at the anode's surface. This decomposition causes the formation of a solid electrolyte interphase (SEI) and prevent electron transfer reactions between the anode and the electrolyte.
An anode has to fulfill some specifications to work correctly in a Li-ion battery:[14]

- The anode material should have a low potential (related to a standard potential) and the cathode/anode couple should provide a high cell potential.
- The structure should not vary upon reactions with Li-ions. Variations of structure cause strains and decrease the life cycle of batteries.
- Anode and Li-ions reactions should be highly reversible.
- Fast diffusion of Li-ions within the anode material is necessary to improve the performances.
- Anode electronic conductivity should be high to allow fast movements of the electrons to the external circuit during electrochemical reactions.
- Anode material should store as much charges as possible
- As a design factor, the anode active material should be as dense as possible to enhance battery energy.

At the beginning of the Li-ion batteries conception, pure lithium was used as anode because of its high specific capacity. But the formation of dendrites and its high reactivity with water makes it dangerous and complicated to manipulate.
Carbon materials such as graphite were investigated to replace lithium metal. Li-ions intercalate within the material without deforming it. This components lead to an high energy density and long life cycle batteries but a low volumetric capacity.
In order to increase the specific capacity of the anodes, noncarbon-based alloying materials such as Sn or Si were investigated. Indeed, while 6 atoms of carbon are needed to uptake 1 Li, Sn can accommodate approximately 4 Li-ions leading to a theoretical specific capacity of 994 mAh/g against only 372 mAh/g for graphite (see figure 1.17). [17]

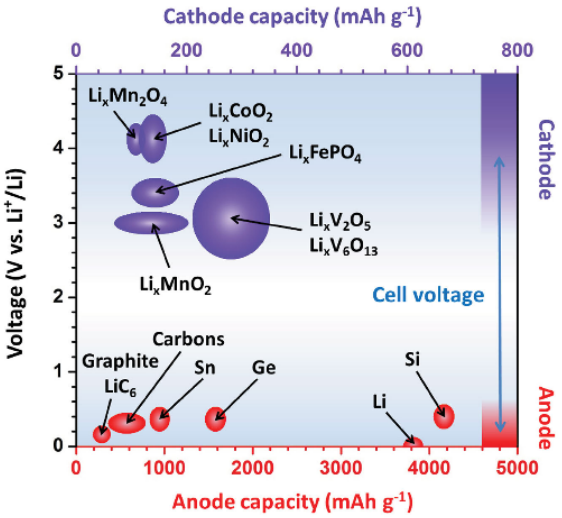

Figure 1.17: Diagram illustrating the capacities and electrochemical potentials of important cathode and anode materials with respect to Li metal and the cell voltage of LIBs (from [1])

Sn-based anode

On figure 1.18, some of the possible elements used as cathode or anode in Li-ion batteries are described in function of their availability and volumetric and gravimetric capacity. With the constant improvement of lightweight devices, higher energy densities are becoming nowadays more and more important. These parameters have to be taken into account during the material selection but other parameters such as the reduction potential will also play a role.
It can be seen that Ge and Ga are very interesting but far too expensive, P and Sb are toxic, Al suffers from fractures and Zn, Cd, Pb have low gravimetric capacity.[28]
From these values, Si and Sn are noticed to be interesting choices. Sn has in general lower properties than Si except for the electrical conductivity.

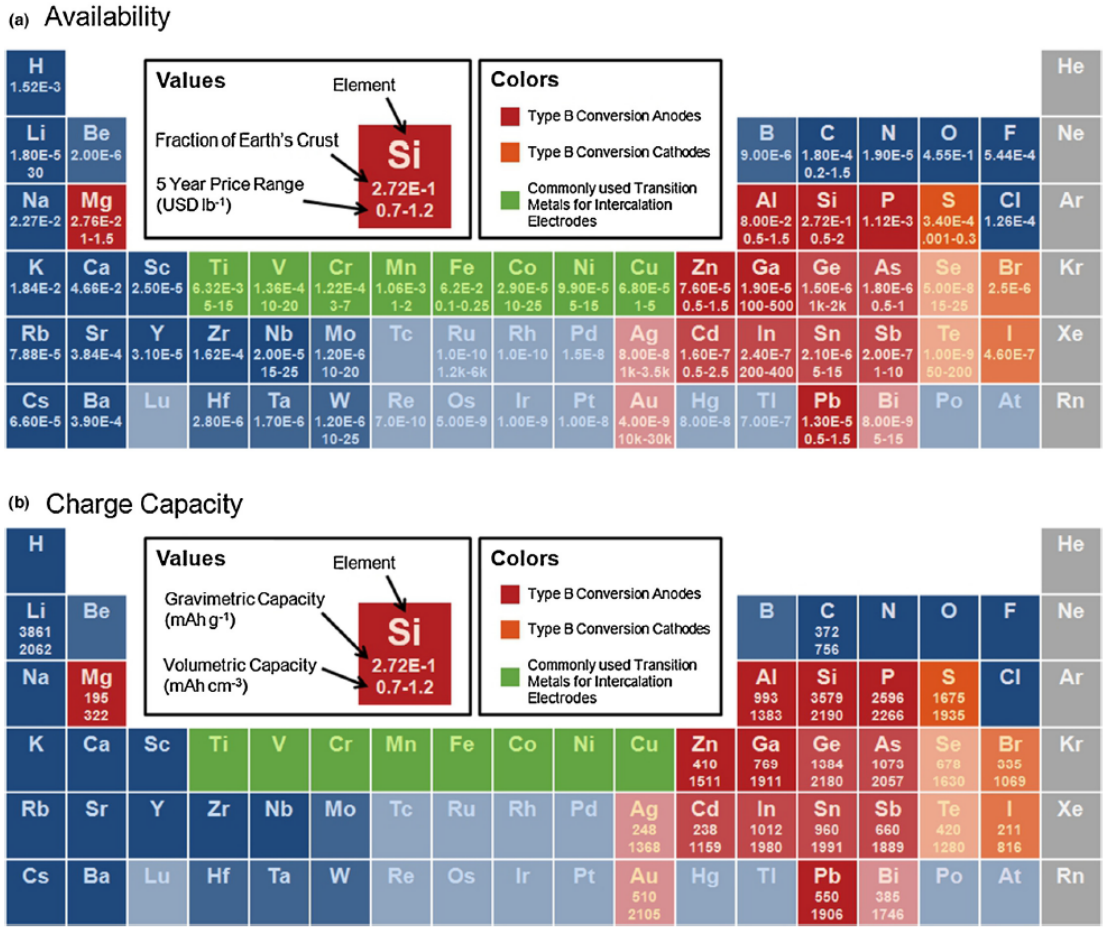

Figure 1.18: (a) Availability and (b) capacities of elements that may host Li as electrodes. Elements with abundance (as fraction of Earth's crust) below 10^{-5} are slightly faded, and elements below 10^{-7} are faded further. Prices are approximate 5-year ranges of metal prices (except Ge, which is a 3 year range), 80–100 mesh natural graphite for carbon, and the Vancouver/USGS prices for sulfur. Gravimetric and volumetric capacities are theoretical values calculated based on delithiated mass and lithiated volume (from [28])

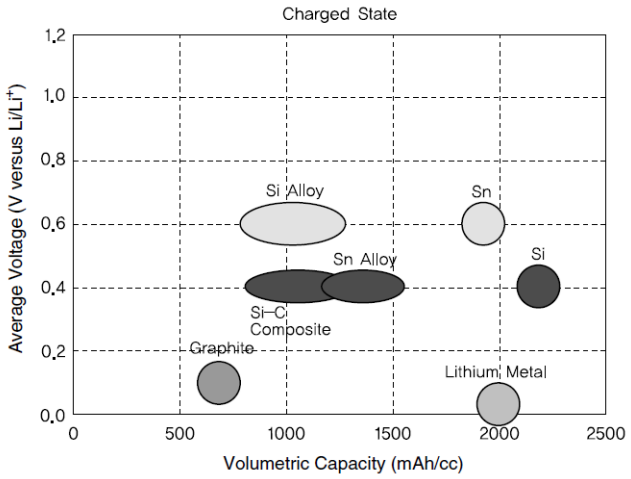

Figure 1.19: Voltage and capacity of metal elements that form alloys with lithium (from [14])

Lithium is able to alloy and dealloy (unlike the intercalation/deintercalation within graphene) with different metals as Sn and Si which makes it a favored material for rechargeable batteries.[29]

In the case of Sn, lithium can make different alloys such as Li_2Sn_5, $LiSn$, Li_5Sn_2, $Li_{13}Sn_5$, $Li_{22}Sn_5$. The various compositions and high amount of lithium in the alloys induces a high specific capacity.
The formation of alloys with lithium is accompanied by a decrease of voltage as it can be seen on figure 1.20 with a comparison between Sn and Si.

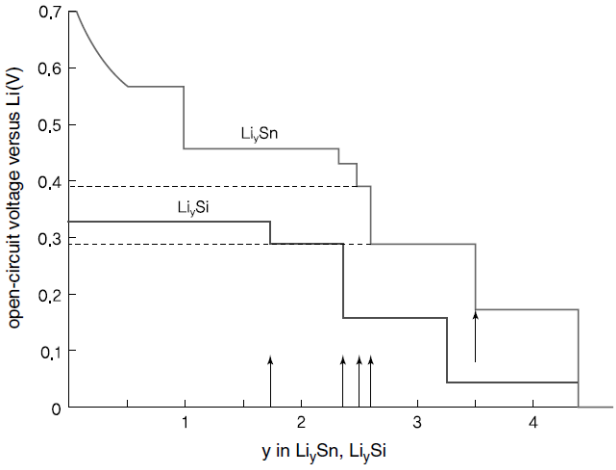

Figure 1.20: Change in potential of Sn–Li and Si–Li with varying lithium composition (from [30])

The integrity of the anode materials during alloying with lithium upon charge and discharge is one of the main challenges as an important volume variation can occur during the formation of the alloys, degrading the capacity very fast.[31] Indeed, the volume variation is due to a larger lattice constant, as the voids between metal atoms are filled with Li-ions during the formation of alloys as it can be seen for Si on figure 1.22. Since one Sn atom can react with up to 4.4 lithium ions, this expansion in volume may reach 400%.[14]

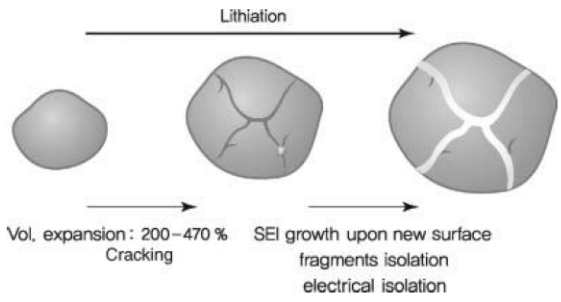

Figure 1.21: Schematic diagram of cracking during lithiation (from [14])

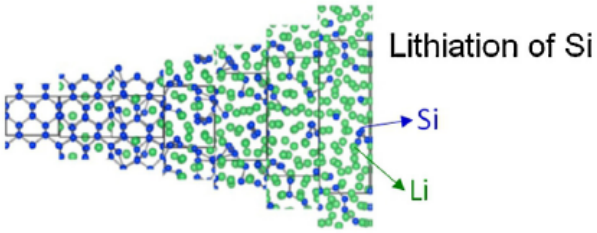

Figure 1.22: Volume expansion and deformation of Si upon lithiation (from [28])

The volume expansion as described on figure 1.21, creates first cracks in the material. This generates new surfaces in contact with the electrolyte and which can eventually creates new SEI (and therefore, consumes more active material and increases cell impedance, see figure 1.24). If the crack length increases some fragments of the active material can become isolated and no longer participate in the electrochemical reactions as described on figure 1.23, inducing a

huge loss of capacity.[14] At the same time, the volume expansion can produce a loss of contact between the active materials and the current collector which degrades drastically the cycling performances.[16] Volume expansion and contraction can also induce destruction of the sample or morphological changes, effect which is strongly pronounced on films and called *delamination* (see figure 1.25).

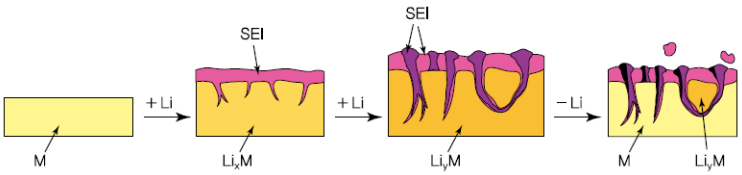

Figure 1.23: SEI formation in metal anode during volume expansion (from [14])

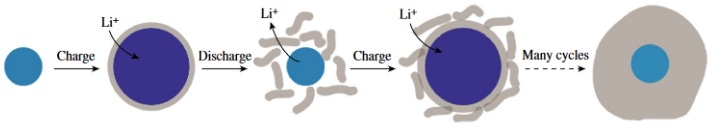

Figure 1.24: SEI formations around spherical particles (from [32])

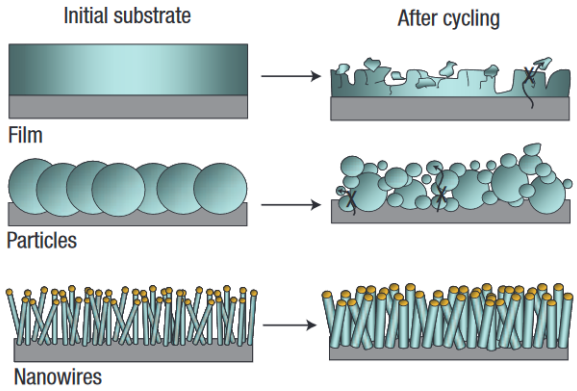

Figure 1.25: Morphological changes during cycling (from [33])

Modifications of the anode materials (structure and composition) to resist against this volume expansion/contraction were investigated.
The addition of an inactive material to the active material in the electrode has been proved to be efficient to buffer the volume variation (other techniques exist but will not be investigated in this study [14]).
The concept of volume variation buffered by the inactive material matrix where the active material is dispersed is illustrated on figures 1.26 and 1.27.

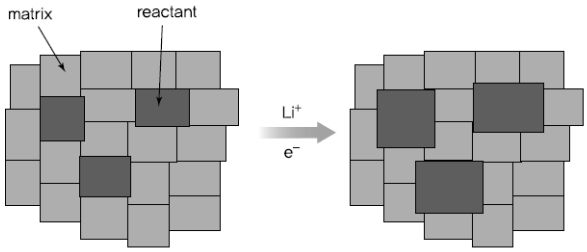

Figure 1.26: Volume expansion of the active material upon lithiation in a inactive matrix (from[14])

Inactive materials such as oxides are not used because oxygen reacts irreversibly with lithium and consumes a large amount of lithium leading to a high capacity loss. Inactive metals are preferred in this context, such as Ni, Fe, Mn, Co.

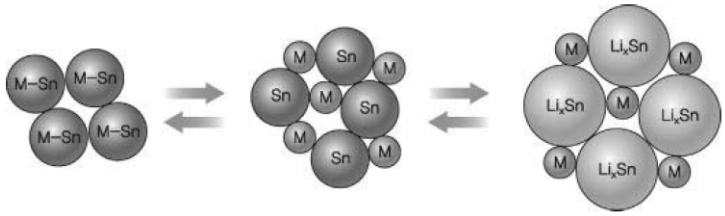

Figure 1.27: Reaction of Sn-M during lithiation (from[14])

The inactive metal has good electronic conductivity properties but hinders the ionic movements leading to a decrease of the rate capability characteristics.

Moreover, the structure of the anode was also investigated since it greatly influences the batteries performances.
In this context, composites, core-shell structures, faom, nanowires were developed.
The geometry of the anode will be investigated in details later.
The combination of Sn with Ni is investigated in this work to buffer this volume change by the presence of an inactive material (Ni).

NiSn anode

During the first irreversible cycle of Ni_3Sn_4 battery:

$$\mathrm{Ni_3Sn_4} + 17.6\,\mathrm{Li^+} + 17.6\mathrm{e^-} \longrightarrow 4\mathrm{Li_{4.4}Sn} + 3\,\mathrm{Ni} \tag{1.12}$$

The next cycles are reversible:[34]

$$\mathrm{Li_{4.4}Sn} \longrightarrow \mathrm{Sn} + 4.4\,\mathrm{Li^+} + 4.4\,\mathrm{e^-}(charge) \tag{1.13}$$

$$\mathrm{Sn} + 4.4\,\mathrm{Li^+} + 4.4\,\mathrm{e^-} \longrightarrow \mathrm{Li_{4.4}Sn}(discharge) \tag{1.14}$$

1.4 3D structures

To improve the batteries performances, it is interesting to not only work on the components but also on the architecture of the final device. Great differences of performance exist between batteries of same composition but of different configurations.
Some examples are given in this section. Then, the chosen pattern of 3D interconnected nanowires is described followed by the advantages of such a structure and the different parameters to be taken into account.

1.4.1 Architectures

This study focuses on the architecture of only one electrode, the anode. But to achieve interesting results, the whole battery design has to be thought.
The chosen pattern of the anode is an array of interconnected 3D nanowires in this case.
Before focusing on the chosen system, a quick look is taken on what could be made at the full battery scale.
Some 3D architectures existing for battery application are depicted on figure 1.28.

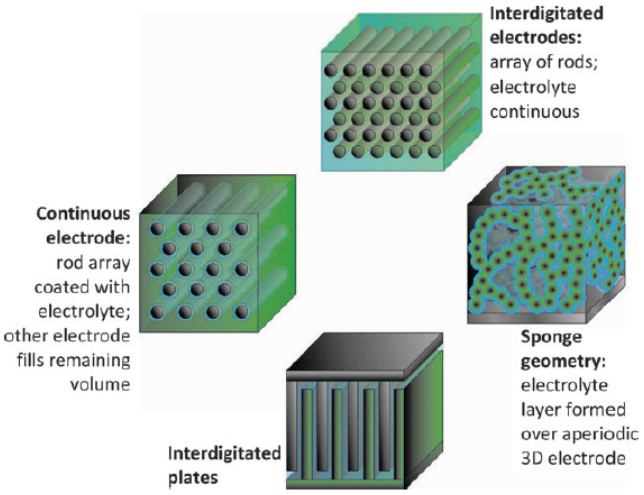

Figure 1.28: Three-dimensional designs for batteries (modified from [7])

One of the first design to come to mind for battery application is the interdigited electrodes. The anode and cathode are alternating arrays of rods. The interdigited structure allows a shorter ionic diffusion pathways resulting on a smaller ohmic polarization. A variation of alternating rods is to use plates. The current densities linked to this kind of structure are uniform due to the 1D nature of the transport between anode and cathode.
One can also imagine a structure in which the electrolyte is not the continuous phase: as it can be seen in the continuous electrode system on figure 1.28, the anode can be shaped into parallel rods coated with the electrolyte layer and surrounded by the continuous phase being the other active material (the cathode in this example).
The electrolyte layer can be of different thicknesses but has to be larger than 1 nm, in order to avoid electronic coupling of the electrodes by tunneling which could therefore act as shortcuts. Another parameter to take into account is the electrostatic contact of electrodes through overlapping of double layers. This phenomena is not fully understood for now but it influences very likely the ions transport.[7] The last idea illustrated is to use an aperiodic system where all the phases are continuous trough the "sponge" matrix. [7] All these examples show that there is only limit of imagination to new batteries designs.

However, this study focuses on the architecture of only one component: the anode. Therefore, the global battery design will be kept quite classical: two electrodes separated by a liquid electrolyte. The main purpose is to understand the improvements brought by the promising anode architecture of 3D interconnected nanowires even if the final purpose is to integrate it in the future in more advanced complete battery systems.

1.4.2 3D interconnected nanowires electrodes

The chosen pattern of the anode is an array of connected nanowires grown along 2 directions, creating a 3D interconnected structure as it can be seen on figure 1.29.

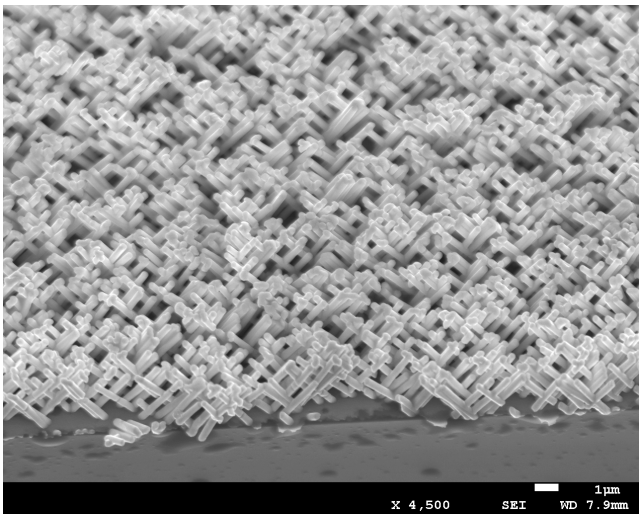

Figure 1.29: NiSn 230nm-diameter interconnected nanowires

1.4.3 Advantages of the 3D interconnected nanowires structure

In addition to have a very large surface area and a small diameter which generate a high interactive surface between electrodes active sites and Li-ions in the electrolyte (a much larger active surface than a simple 2D film electrodes), the 3D interconnected nanowires arrays allow an easy access for the electrolyte ions to all the active material, each nanowire can participate in the electrochemical reaction.
Indeed, in the case of films (2D) electrodes, when the active mass is increased, the biggest part of the active materials is far inside the electrode and large ionic diffusion within the solid electrode is needed to use all the active mass. At the opposite, in 3D nanowires structures, the electrolyte surrounds all the active materials and only small ionic diffusion is needed to have access to the active mass.
Moreover an efficient accommodation of volume variations of the electrode during the charge and discharge can take place thanks to the large free space between the different nanowires.[35]
The connections between the interconnected nanowires allow a better structural stability of the device and a continuous conductivity of the structure to the current collector even when some parts are not in direct contact with the current collector.
The nanowires have moreover the benefits of the nanoconfinement such as the shorter diffusion pathway inside the solid electrodes, rapid charge collection and a facile accomodation of mechanical constraints.[36][37]
The interconnected network directly grown on the current collector allows a direct flow of the generated electrons from the electrodes to the circuit through a directional pathway (see features on figure 1.30).[35]

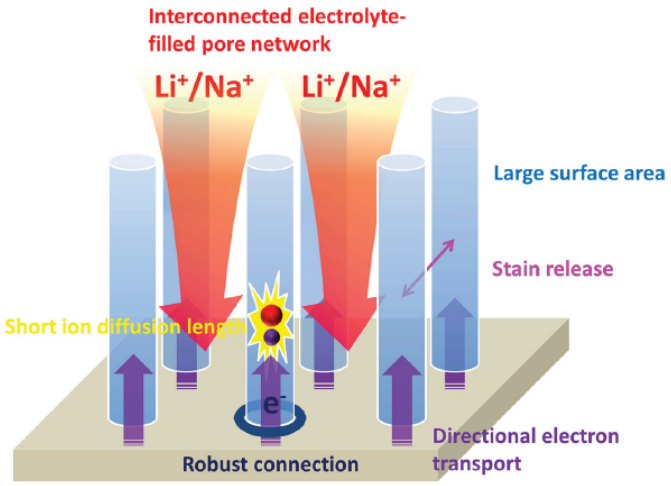

Figure 1.30: Schematic of straight nanowires illustrating their prominent features (from [1])

1.4.4 Parameters

This section present the influence of the height, the diameters and the composition of nanowires on the expected performances of batteries.

Height

The height and the geometry of the nanowires have to be carefully chosen.
Long nanowires tend to agglomerate. Agglomerations have dramatic effects on batteries efficiency. Indeed, agglomeration reduces the surface area of reaction, prevents Li-ions diffusion and increases stresses in the array.[35]
Moreover straight nanowires performances are proved to be very sensitive to the nanowires length which comes along with the agglomeration risk. Life cycle and gravimetric capacity are drastically reduced when the length of straight nanowires increases. To avoid this reduction of performance, others geometric patterns were investigated. 3D-patterns (straight nanowires with nanoconnections, as it can be seen on 1.31 and 1.32) were proved to be much more efficient. Indeed, the spacing between nanowires is conserved and allows a constant Li-ions diffusion for different nanowires lengths. The electrochemical performance of such geometry is length-independent while the cycle life is prolonged due to a reduction of stress at the roots of the nanowires.[35] The interconnected nanowires can have the same advantages.
As example, the gravimetric capacity of both geometries are shown for different nanowires lengths on figures 1.33 and 1.34.

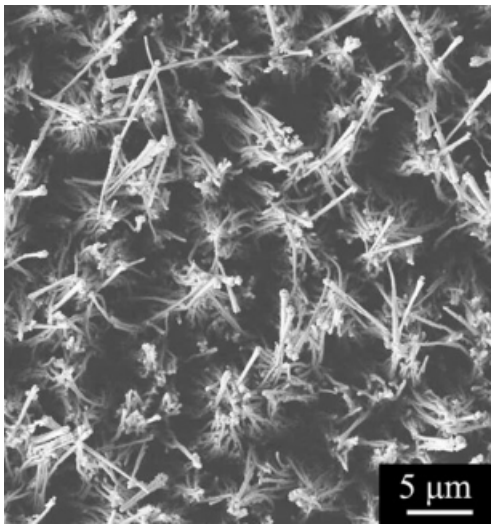

Figure 1.31: 20μm straight nanowires, top view (from [35])

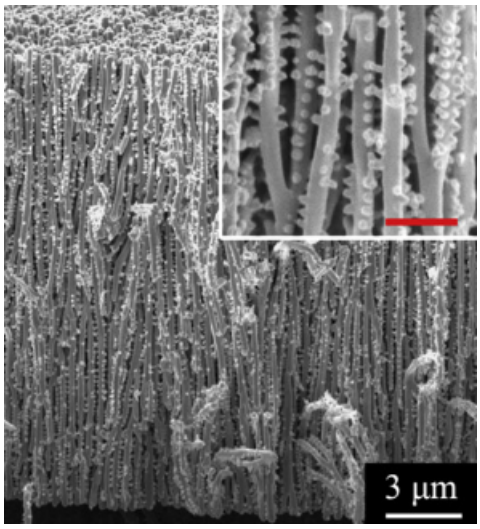

Figure 1.32: 20μm 3D nanowires, side view (from [35])

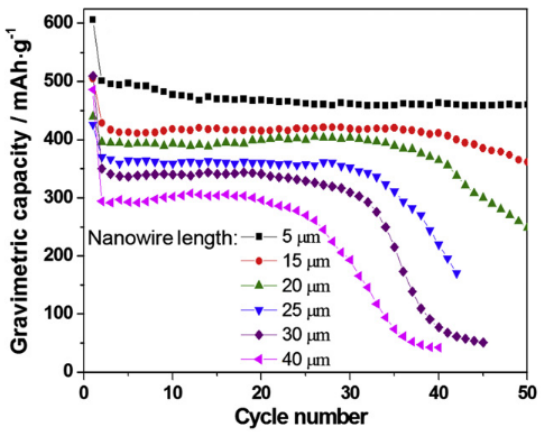

Figure 1.33: Gravimetric capacity of straight nanowires (from [35])

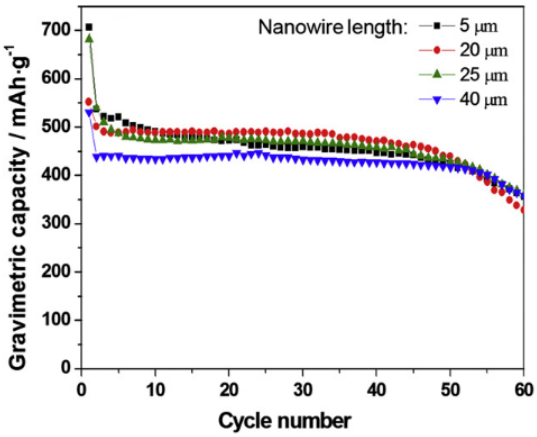

Figure 1.34: Gravimetric capacity of 3D nanowires (from [35])

Diameters

The diameter of the nanowires influences directly the generated structure. Smaller diameters generate larger surface areas but smaller free volumes between the nanowires and a more fragile sample is expected while larger diameters generate stronger and more stable nanowires arrays with larger free volumes between nanowires but smaller surface areas.
This study analyzes the influence of the diameter on the battery performances.

Composition

The NiSn alloy has a high capacity and is considered as easy to create. The combination of Sn with Ni can reduce the volume expansion/contraction upon cycling which makes it more resistant to mechanical disintegration.[34] Ni_3Sn_4 is one of the promising identified composition for battery applications.[38] A proportion of 62% Sn has been proved to be necessary to achieve the formation of Ni_3Sn_4. At lower concentration of Sn, lithium can not alloy with Sn while at higher concentration of Sn, it is segregated during the cycling and the capacity is therefore reduced. [31]

1.4.5 Fabrication of 3D structures

The fabrication methods of 3D battery structures depend on many parameters such as the nature of the architecture, the geometry and the scale.

Devices can be built naturally on a substrate, or with the use of templates as well as by etching techniques as illustrated for nanowires growths on figure 1.35.

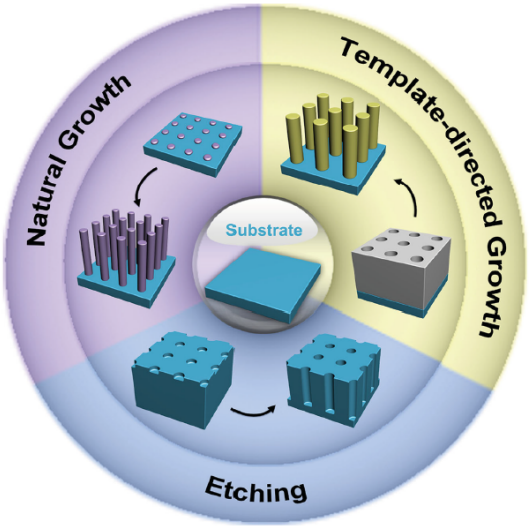

Figure 1.35: Schematic illustration of the fabrication of the nanowires electrodes.

Natural growth comprises vapor-phase growth, solution-phase growth, thermal oxidation,... while etching (dried or wet) can use physical or chemical reactions. Finally 3D growth can also be performed in templates.[1][7]
Another approach to form 3D structures is based on various folding strategies as for *origami*. [7]

In this work, the electrodeposition technique in template was chosen. More details about the deposition and nanowires growth are given in the Methods chapter 2.
Indeed, electrochemical deposition techniques are able to generate interesting architectures:

- The structure can be directly grown on the current collector
- The growth can be directly controlled by the deposition parameters as ions concentrations, current of deposition, temperature,...
- Alloying is easily performed by mixing salts ions
- Complex structures can be grown (core-shell)

[31]

Chapter 2

Experimental: materials and methods

This chapter details the fabrication and the characterization techniques chosen in this study in addition to the parameters which were used and the discussions about the decisions and the assumptions made.
First is described the fabrication by cathodic electrodeposition of the films and of the interconnected nanowires array in polycarbonate track-etched templates. The fabrication methods of the important parts of the setup are explained (polycarbonate template and pressing membrane) followed by the choice of the electrolytes and the whole setup. Then, a description of the cathodic electrodeposition process is added with a discussion on the chosen parameters (applied potential) and on the resulting samples (mass and dimensions calculation). Finally the characterization techniques used during this work are detailed (SEM,EDX).
A second part is dedicated to battery tests. The whole process of cells fabrication and the testing techniques are explained followed by the chosen parameters to achieve results of interest during the cycling tests.

2.1 Electrodeposition

Different techniques exist to make Ni-Sn alloy films or nanowires, electrodepostion is one of the most used because it allows to modulate easily the form and size of samples.[34]

2.1.1 Manufacture

The manufacture of the setup pieces is explained first, followed by the fabrication of the final product (the NiSn and Sn nanowires) through the setup, the components needed (electrolytes composition), the electrodeposition principle, the parameters and the post-deposition process.

Polycarbonate template fabrication

The polycarbonate (PC) template is fabricated by nuclear track-etched technology in which a polycarbonate film is bombarded by energetic heavy ions (Ar^{9+}, 5.5 Mev/amu) under vacuum (10^{-2} mbar) at room temperature in the Cyclotron Resource Center at Louvain-la-Neuve (Belgium) by the company *It4ip*.
The interconnected system is created by exposing the PC film two times at different angles (α of $+25°$ and $-25°$ with respect to the normal of the film) to the energetic heavy ions.[39]
The tracks of the heavy ions in the PC membrane are chemically etched by 0.5M NaOH aqueous solution at 70° C to form nanopores of desired diameters (40nm, 105nm and 230nm in this case). The volumetric porosity iss $\approx$ 23%. The process can be seen on figure 2.1. Layers of Cr and Cu of different thicknesses depending on the nanowires diameters (see table 2.1) are

then evaporated (with Plassys MP500S device) on one side to promote the adhesion with the substrate during electrodeposition.

Nanowires diameter	Cr layer	Cu layer
230nm	10nm	150nm
105nm	5nm	50nm
40nm	5nm	25nm

Table 2.1: Layers evaporated on PC template

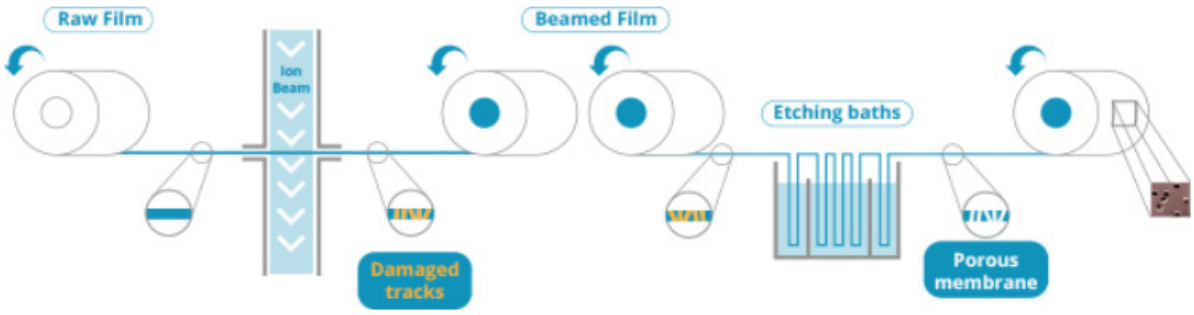

Figure 2.1: Track-etching technology process (from [40])

"Pressing" membranes

In the setup for electrodeposition of small-diameter nanowires, a microporous pressing membrane is used to improve the adhesion between the substrate and the nanowires by pressing homogeneously the PC template on the substrate. Alumina membranes were used to be employed but their fragility was a problem since a new membrane was often needed. To counter this problem, Si membranes from Smart Membranes with straight pores of $1\mu m$-diameter were used (see figure 2.2). However, some metallic depositions occurred during electrodeposition, clogging the pores. A coating of Al_2O_3 of 20nm was made by atomic layer deposition (150 layers) to insulate it. See section 3.1.5, for precision and images about the undesired metallic depositions.

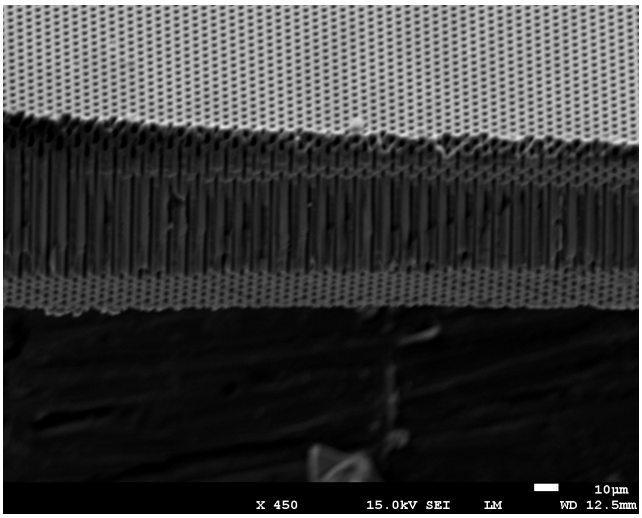

Figure 2.2: Broken edge of the coated Si membrane

Electrolytes

The electrolyte solutions used to depose NiSn come from recipes found in articles [41] and [38]. The electrolyte for Sn formation was the same without the Ni salts (see tables 2.2 and 2.3). The solution is stirred until complete dissolution of the salts.

Compound	Origin	Concentration (M)	Solution volume (L)	Mass (g)
$NiCl_2.6H_2O$	Aldrich Chemistry	0.075	0.5	8.9
$SnCl_2.2H_2O$	Sigma-Aldrich	0.175	0.5	19.7
$K_4P_2O_7$	Aldrich	0.5	0.5	82.6
Glycine (NH_2CH_2COOH)	Sigma Life Science	0.125	0.5	4.7
NH_4OH	Sigma-Aldrich	5mL/L		

Table 2.2: Electrolyte for NiSn deposition

Compound	Origin	Concentration (M)	Solution volume (L)	Mass (g)
$SnCl_2.2H_2O$	Sigma-Aldrich	0.175	0.5	19.7
$K_4P_2O_7$	Aldrich	0.5	0.5	82.6
Glycine (NH_2CH_2COOH)	Sigma Life Science	0.125	0.5	4.7
NH_4OH	Sigma-Aldrich	5mL/L		

Table 2.3: Electrolyte for Sn deposition

Electrodeposition setup

A thin strip of copper foil is cut and washed by different solvents. First, it is degreased in alcohol and in acetone, then in a H_2SO_4 bath (2.5M from TitriPUR) and washed with distilled water between each step. Then the copper foil is dried.

After that, the electrodeposition cell can be assembled. The Cu foil is first placed, then the polycarbonate template is placed for nanowires growth, for films growth, the polycarbonate template is removed.
The pressing membranes is then placed for small-diameter nanowires. A sequence of seal (circular rubber, 6mm of internal diameter, a surface of $0.283cm^2$ in contact with the electrolyte), Teflon piece, another larger seal (circular rubber) and finally, a large Teflon piece aiming to contain the electrolyte are placed one on the top of another (see figures 2.4, 2.5). The rubber seals and the polycarbonate template are cut with a punch.
Once the cell assembled and maintained by springs and bolts, the electrolyte is poured in the large Teflon piece. The film of copper act as the cathode electrode while a platinum piece is plunged in the electrolyte to act as the anode (see figure 2.3). A reference electrode (Ag/Ag^+ from Hamilton) is placed right above the sample, in the electrolyte.

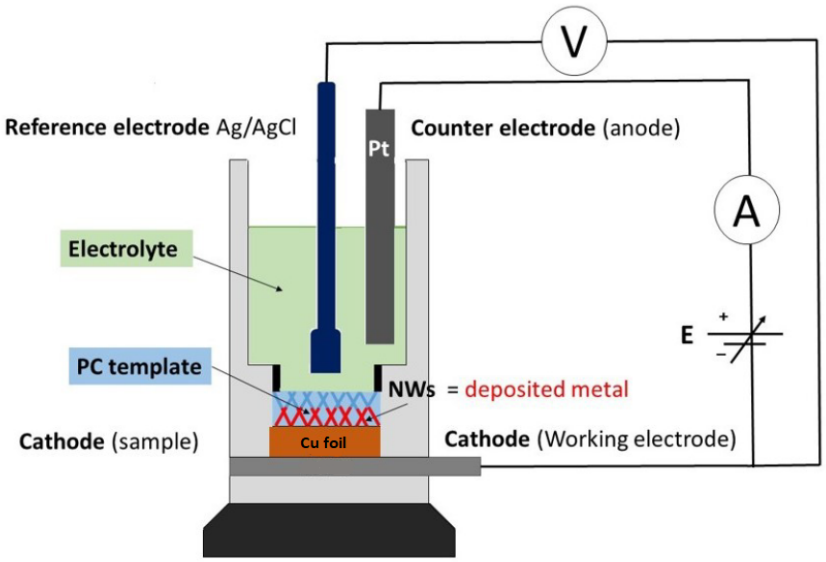

Figure 2.3: Schematic representation of the electrodeposition setup (from [42])

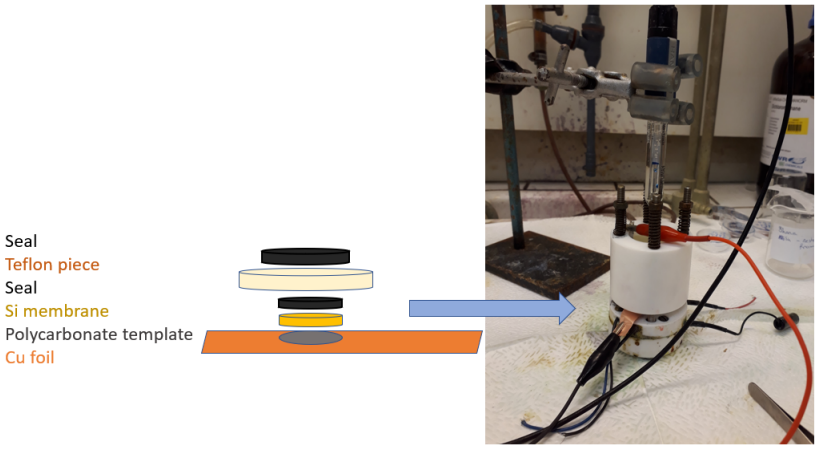

Figure 2.4: Electrodeposition setup

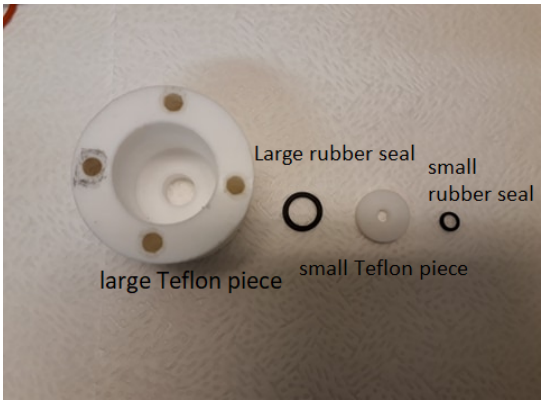

Figure 2.5: Rubber seals and Teflon pieces

Cathodic electrodeposition principle

The electrodeposition consists of depositing elements on an electrode thanks to electrochemical reactions. Three electrodes are necessary: the working electrode which is the electrode of interest where the cathodic electrodeposition occurs, the counter electrode which closes the electrical circuit and the reference electrode (Ag/Ag^+) which measures the potential applied.[43] The counter electrode nature is not important as long as it does not interfere with the reaction of interest.
The deposition reaction at the cathode is:

$$\mathrm{M^{Z+}} + \mathrm{Ze^-} \rightleftharpoons \mathrm{M} \tag{2.1}$$

While the equation at the anode is:

$$\mathrm{H_2O} \rightleftharpoons 2\,\mathrm{H^+} + \frac{1}{2}\mathrm{O_2} + 2\,\mathrm{e^-} \tag{2.2}$$

To grow the NiSn sample by electrodeposition, we impose a chosen potential and a desired charge. An overpotential is applied to achieve higher deposition rate. But the overpotential has to be not to high to avoid side reactions as hydrogen evolution. The deposited charge Q after a time t is calculated by integrating the deposition current over time.

$$Q = \int_0^t i dt \tag{2.3}$$

From the charge deposited, a theoretical calculation of the deposited mass/number of moles can be made thanks to Faraday's law:

$$Q = nFN \tag{2.4}$$

where n is the change of metal's charge, F is the Faraday constant and N the number of deposited moles which can be linked to the mass by being multiplied with the molar mass.
The electrodeposition was carried out with a Potentiostat/Galvanostat Model 263A from Princeton Applied Research.
Typical curves of electrodeposition currents with the 4 steps (nucleation, deposition, caps, overfilling) are compared with the currents measured during experimentation and conclusions about overfilling are drawn in the results part (section 3.1).

Electrodeposition parameters

Deposition of Sn Potentials between -1.02V to -1.2V were applied in the investigation for efficient conditions to depose Sn. No relation between the deposition and potential was found since the deposition seems to also depend on other parameters such as the ageing of the solution or its storage conditions, due to the low reproducibility of samples. The electrodeposition of Sn is discussed in more details in the Results chapter (see section 3.1). A cyclic voltammetry could be performed to identify an appropriate potential which gives a high enough depositing current.
The Pourbaix diagram can be used to identify the reasons to the difficulties met when depositing Sn (figure 2.6).

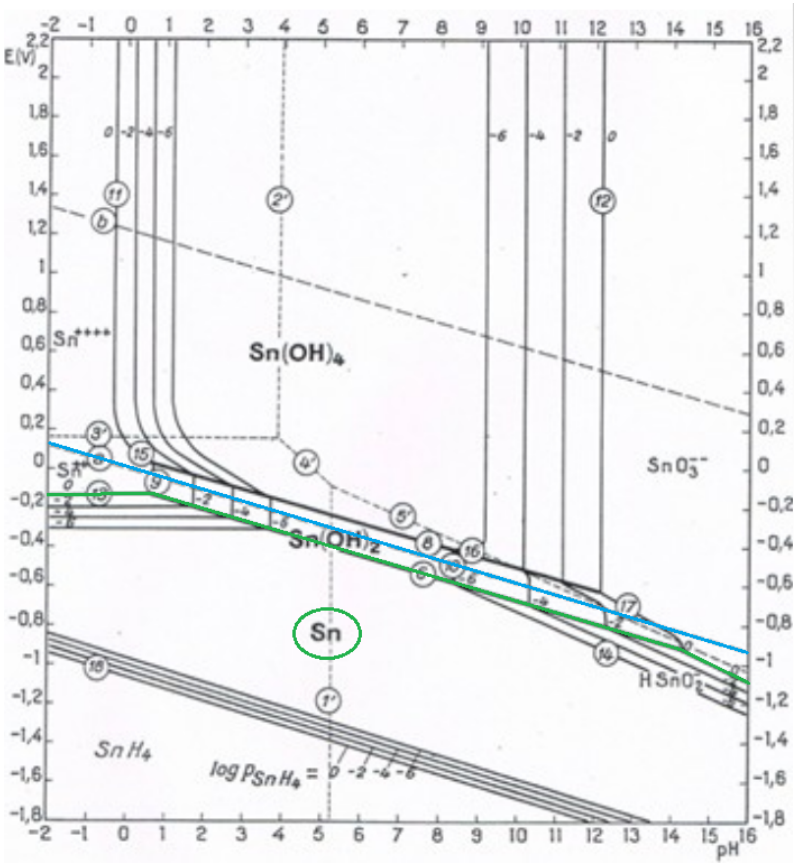

(a)

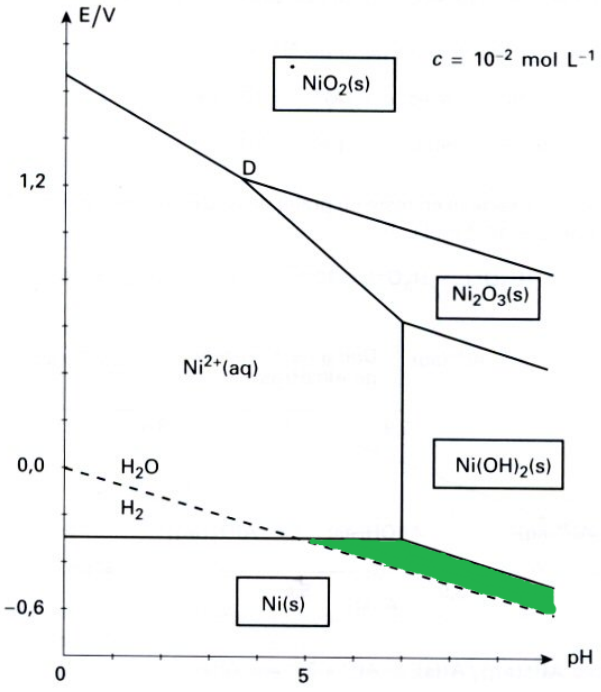

(b)

Figure 2.6: Pourbaix diagram of Sn-H2O and Ni-H2O systems at 25 °C (from (a)[44], (b)[45]). The potential given is related to SHE.

The pH of the Sn electrolyte is 9.3. It can be seen that the stability region of Sn (green line, for the concentration of the electrolyte used) is outside the stability region of the solvent, water (delimited by the blue line). It means that pure solid Sn is not stable in water and reactions between Sn and water could occur. Moreover, side reactions of water reduction are suspected to occur since the applied potential is outside the stability region of water (please, note that the Pourbaix diagram is given in function of SHE).[46]
However the kinetic of reactions is not shown on this diagram which is calculated based on the thermodynamic equilibriums. It is therefore complicated to know exactly which parameter is of most importance in practice.
A last parameter seems important to be noted: the Sn^{4+} region is not stable at high pH values, which could explain also the issues met during depositions and for Sn solutions conservation. Acidifying the solution could be tried to analyze the influence of the pH on the deposition. If the Pourbaix diagram of Ni is compared with the Sn system, it can be seen that a common stable region of Ni and H2O (the green region on figure 2.6) at higher pH than 7 is found which suggests stable deposited Ni in water. Moreover the stability region of Ni ions is larger which could lead to a much more stable solutions conservation.
This comparison has to be read with some distances since the samples used in this study are NiSn and not Ni and the systems are probably influenced by the other compounds present in the solution. But the idea is only to show the difference in stability between both systems which could help to find more suitable conditions in order to achieve a better quality Sn deposition.

The amount of deposited material can be theoretically calculated with the Faraday equation:

$$N(mol) = \frac{1C}{2 * 96485(C/mol)} = 5.18 * 10^{-6} mol \tag{2.5}$$

which gives:

$$m = 5.18 * 10^{-6}(mol) * 118.7(g/mol) = 6.15 * 10^{-4} g \tag{2.6}$$

The deposition efficiency is not 100% and an error is therefore expected.

Deposition of NiSn A potential of -1V is applied to depose NiSn in standard conditions (room temperature).
The calculation of the expected mass of alloys deposited is less straightforward than for pure elements.
First a constant is introduced for each material:

$$K = \frac{M}{F * Z} \tag{2.7}$$

where M is the molar mass of the element, F is the Faraday constant and Z, the charge change of the metal.
If K is calculated for Ni and Sn:

$$K_{Ni} = 3.04 * 10^{-4}(g/C); K_{Sn} = 6.15 * 10^{-4}(g/C) \tag{2.8}$$

The K value of the alloy can be calculated thanks to the weight fraction of each component:

$$\frac{1}{K_a} = \frac{\omega_{Ni}}{K_{Ni}} + \frac{\omega_{Sn}}{K_{Sn}} = \frac{0.22}{3.04 * 10^{-4}} + \frac{0.78}{6.15 * 10^{-4}} \tag{2.9}$$

$$K_a = 5.02 * 10^{-4}(g/C) \tag{2.10}$$

The weight fraction was calculated on the basis of a global composition of $Ni_{38}Sn_{62}$ as described in the literature.[38][47]
The mass of Sn (active material) is therefore

$$m_{Sn} = 0.78 * m_{NiSn} = 0.78 * K_a * 1C = 3.92 * 10^{-4}(g) \tag{2.11}$$

Knowing the mass deposited and the density of the alloy, the theoretical height of film deposited can be estimated.
The density of the alloy ρ_a is calculated first:

$$\rho_a = \frac{\rho_{Ni} * \rho_{Sn}}{\rho_{Ni} * \omega_{Sn} + \rho_{Sn} * \omega_{Ni}} = 6.23(g/cm^3) \tag{2.12}$$

Knowing that the sample has a diameter of 6mm, the surface of the sample is $0.283cm^2$. The height of deposited film is therefore of $2.84\mu m$

Post-deposition processes

After deposition of the desired charge, the electrodes are removed and the electrodeposition cell is disassembled. The deposited sample on the Cu foil is plunged in a bath of dichloromethane from VMR to dissolve the polycarbonate template (in case of nanowires growth). A first dissolution of 10 minutes is performed, followed by a second one of 5 minutes and a last one of 30 minutes to remove efficiently the residual template from in between the nanowires. Some residue can remain in the sample if the dissolution is not performed during enough time (see figure 3.41 in Appendix 3.3.2).
On figure 2.8, is illustrated the deposition procedure in PC template for the growth of nanowires arrays with a more detailed view on the electrodeposition within the pores of the PC membrane on figure 2.7.

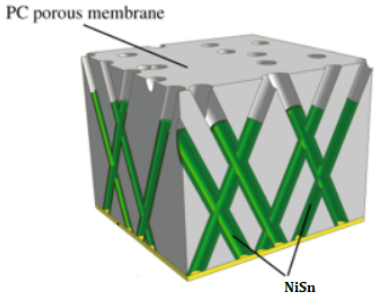

Figure 2.7: Manufacture of 3D interconnected nanowires from [48]

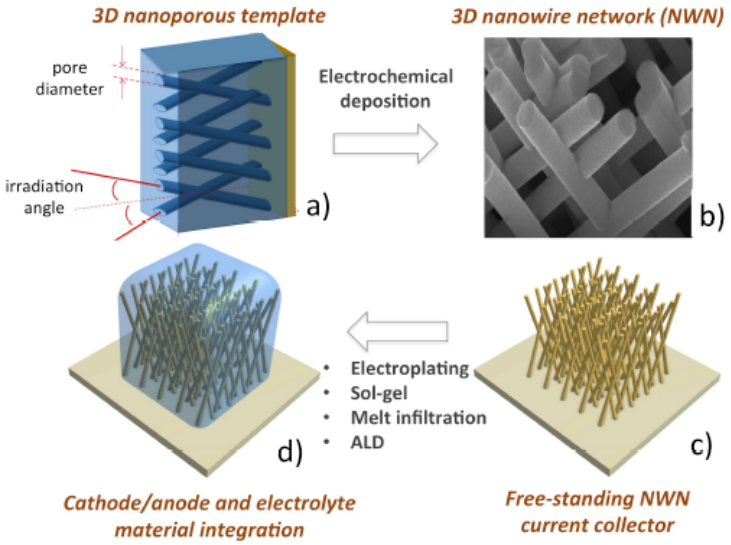

Figure 2.8: 3D track-etch polymer template prepared by the successive irradiation steps under various angles relative to the out-of-plane direction (a) SEM image of the 3D interconnected network of subsequently electrodeposited Ni nanowires (b) Illustration of the direct growth of free-standing NWN on a rigid substrate (c) and of an infiltrated 3D metal scaffold (d) (from [49])

2.1.2 Characterization

The characterization of many 3D architectures presents some challenges beyond those present for planar systems. Some of them are: [7]

- The dominant contribution of the surface resulting from a high surface-to-volume ratio
- The bulk of the architecture being sub-surface
- The disorder of the solid nanostructure
- The aperiodic pore structure of some systems
- The difficulty of characterising multi-components system
- The interparticle interactions

In this case of interconnected 3D nanowires, the electrodeposited structure is studied thanks to a Scanning Electron Microcope (SEM) and the composition is roughly measured thanks to an Energy-dispersive X-ray spectroscopy (EDX) measurement.
It could be interesting to perform other tests such as X-Ray Diffraction (XRD) to have a more precise idea of the predominant phase of the sample.

Scanning Electron Microscopy (SEM)

Scanning electron microscopy is an imaging technique which uses a beam of electrons to generate an image of the surface topology of conducting samples. For non-conductive sample a metallic coating is needed. Fortunately, in this study, the samples are all conducting.
The electron beam is thermionically emitted from a cathode filament in the electron gun. The electrons are accelerated in vacuum by 0.2 up to 40kV. The electrons beam is then condensed by lenses and orientated by a scanning coil.
When the electrons beam interact with the sample, secondary electrons, back-scattered electrons and characteristic X-rays are emitted from the sample to the detectors which analyze them to produce an image. The setup and the volume of interaction can be seen on figure 2.9. The interaction volume of the sample depends mainly on the beam energy and on the sample density. The low-energy secondary electrons give information about the surface topology while the high-energy back-scattered electrons emitted from deeper in the sample and X-rays inform about phase compositions. Indeed, as it can be seen on figure 2.10, the topology influences the number of secondary electrons emitted in a direction while the number of back-scattered electrons emitted depends on the nature of the sample.
The resolution is typically of 5nm.[50][51][52]
The SEM used during this work was JSM-7600F from JEOL, whose primary electron source is a Schottky Field Emission Gun (FEG), and has Semi-Inlens secondary electron detector and back-scattered electron detector.

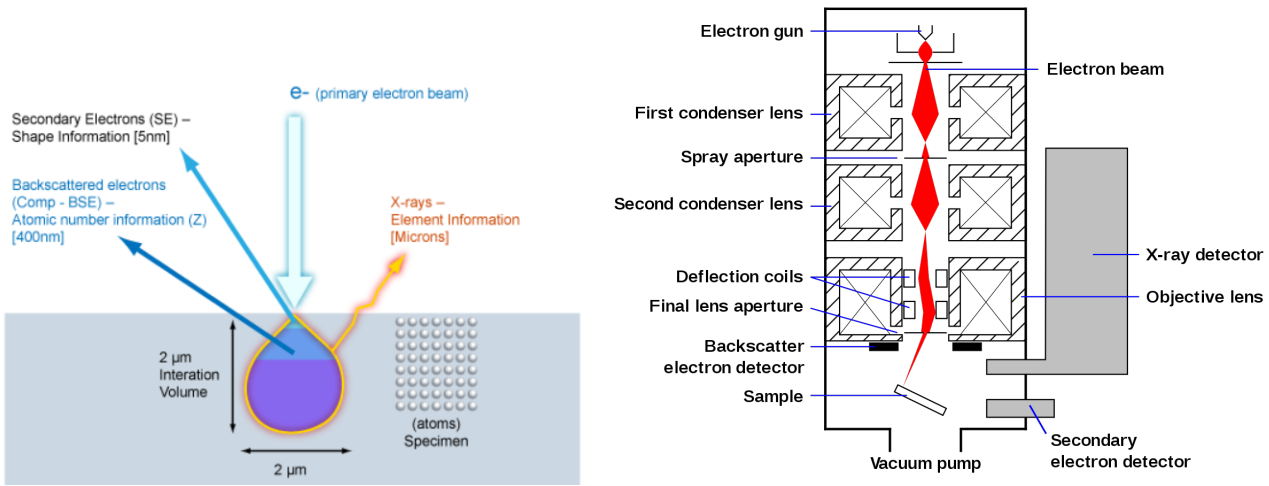

(a) (b)

Figure 2.9: (a) SEM interaction region with sample (from [53]), (b) SEM schematic setup (from [54])

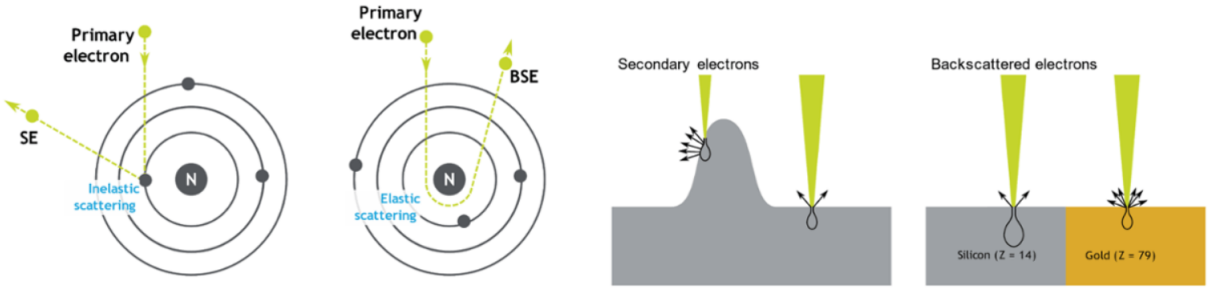

(a) (b)

Figure 2.10: (a) Physical meaning of secondary and back-scattered electrons, (b) Secondary electrons give information about topology while back-scattered give information about composition (from [55])

Energy-Dispersive X-ray spectroscopy (EDX)

As it can be seen on figure 2.9, the incident beam of primary electrons which hits the sample in a SEM can also induces X-rays generation. The Energy-Dispersive X-ray spectroscopy (EDX or EDS) takes place in the SEM device and analyzes the X-rays emission which gives information about the composition of the sample. Indeed, when a sample is hit by an electron beam, some electrons are rejected, creating holes the electronic inner shells of the elements. Some other outer electrons fill the holes. But the change of energy between the 2 electrons shells is compensated by an emission of characteristic X-rays associated with the elements nature.

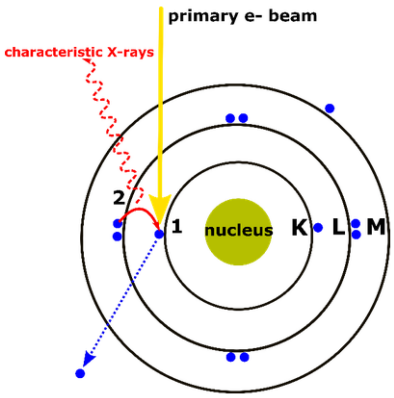

Figure 2.11: X-ray generation process: 1) The energy transferred to the atomic electron knocks it off leaving behind a hole, 2) Its position is filled by another electron from a higher energy shell and the characteristic X-ray is released (from [56])

2.2 Battery performances

To test the performances of the anode, the electrode is placed in the cell with lithium metal as reference. The electrodeposited electrode act therefore as cathode since its reduction potential is higher than pure lithium.
Even if, in practice, the NiSn electrode aims to be an anode and work with a different type of cathode. The potential results are therefore given with lithium as reference during the cycle tests performed. In this section, the sample assembly and preparation is first described, followed by test conditions and principles. And finally, the post-cycling characterization is detailed.

2.2.1 Batteries assembling

Sample preparation

The electrodeposited nanowires are first dried at 70°C under vacuum overnight in the furnace (Vacuum Drying Oven Heraeus Vacutherm). The Cu foil is then cut (maximum 1cm/1cm) to fit onto the battery cell. The samples are then put in the Argon filled glovebox from MBraun to ensure an inert environment.

Cell assembling

The cell is assembled in the gloveboxe in coin-cells of 20mm diameter (CR2032). The sample is placed on the positive can and impregnated with 4 drops of the electrolyte 1M LiPF6 in EC:DMC (from DodoChem). A 13-mm diameter Whatmann 1823-150 glass microfiber filters (separator) is placed above and impregnated with 8 drops of the electrolyte. Then, a Li piece is scraped to remove the protecting grease and Li is placed as counter electrode on the separator impregnated with electrolyte. Indeed, Li is very reactive and grease coatings are covering the metal to avoid any reactions. Finally, a stainless steel current collector and a spring are added before closing the cell with the negative can. The cell is pressed with a pressure of 500 psi to seal it. The assembly can be seen on figure 2.12.

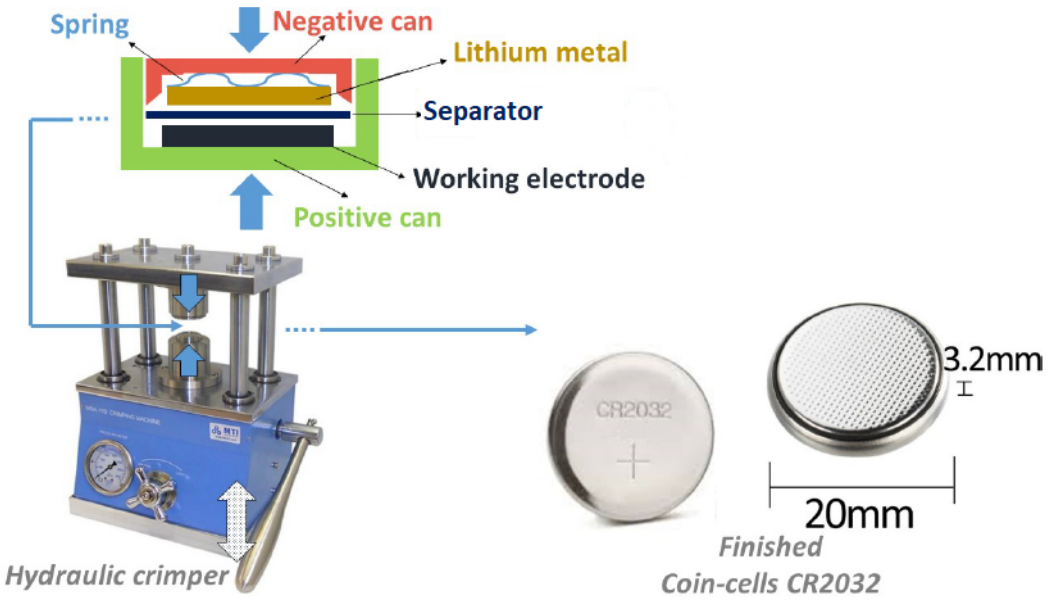

Figure 2.12: Half-cell assembly (modified from [57])

Cell verification

Once assembled, the OCV of the cell is measured thanks to a classical multimeter to verify that no short-circuit occurred during the assembly.

2.2.2 Cycling conditions and cycle test

The cycle test allows to simulate batteries under repeated charge and discharge cycles with at least one fixed parameter and given conditions. In this case of galvanostatic cycling with potential limitations, the current is imposed and the upper and lower limits of potential are fixed. Power and external resistance could also have been fixed. All the tests are performed in the same conditions to avoid influence from the temperature. The evolution of the capacity of the cell is recorded with the potential delivered as function of the cycle number. The values of interest in this experiment are the life cycle of these new batteries, the capacity delivered and the influence of the discharge rate.

The cells were cycled with galvanostatic cycling potential limitations from a varying (0.01, 0.1, 0.35V) lower potential value up to 1V at room temperature and with a cycling current of C/10 (see Theory section 1.2.5 for the definition of C rate) which is equal to $35.36\mu A$ for NiSn samples and to $45\mu A$ for pure Sn samples.
The C rate is calculated on the approximation of 4 electrons exchanged for each Sn atom which gives a theoretical specific capacity of 0.903 Ah/g with the estimated mass of the sample of $5.02 * 10^{-4} g$. The tests were performed with a Neware battery testing system model BTS4000 Series and BioLogic Science Instruments (BT-Lab software) which record the capacity of the cell at a given cycle number and potential.
For the different rating tests, the samples were cycled from 0.01V to 1V (see table 2.4 for the different rates used to cycle the samples).

Rates	C/20	C/10	C/5	C/3	1C	5C	10C	20C	50C	C/20
Number of cycles	10	10	10	10	10	10	10	10	10	10

Table 2.4: Rates and cycles number of the different rates test

2.2.3 Post-cycling process and characterization

Once cycled, the cell is disassembled thanks to the same hydraulic crimper as before. The electrodeposited sample is plunged in three successive DEC baths (from Aldrich Chemistry) for at least 3 hours each. The post-cycled samples were then analyzed thanks by SEM.

Chapter 3

Results & discussion

After that the main theories about batteries were explained in order to understand correctly the results and behaviours of the samples, and after that the parameters applied were described and discussed, the main results of this study are now given in the following chapter.
First, the grown samples are illustrated thanks to SEM images and EDX measurements, then are given the measured performances of galvanostatic cycling of the batteries with some potential-capacity and specific capacity-cycle profiles. The coulombic efficiency of selected samples is also measured. And, finally, some SEM images of cycled samples are described.
All these results are discussed and strategies to improve them are suggested through the chapter.

3.1 Electrodepositions

The electrodeposition is the first step of the anode production. High quality grown samples with defined characteristics are essential to achieve high battery performances. Films and interconnected nanowires of NiSn and Sn were created thanks to cathodic electrodeposition. In this section, the deposited samples are observed and analyzed, first the NiSn films and nanowires followed by an analysis of the membranes used to maintain the structure which were actually interacting with the deposition process, and finally the Sn films and nanowires. To conclude this section, some ideas are given to improve the adhesion between the substrate and the sample which is still one of the main issues faced.

3.1.1 NiSn films

Beside the growth and the characterization of nanowires, a first test was performed on films to have an idea about the deposition process, the thickness to expect and the chemical composition. The first samples which were characterized are films of NiSn deposited on Cu foil. A study of their morphology and thickness was made for different charges: 0.5C (figure 3.1), 1C (figure 3.2), 2.5C (figure 3.3).

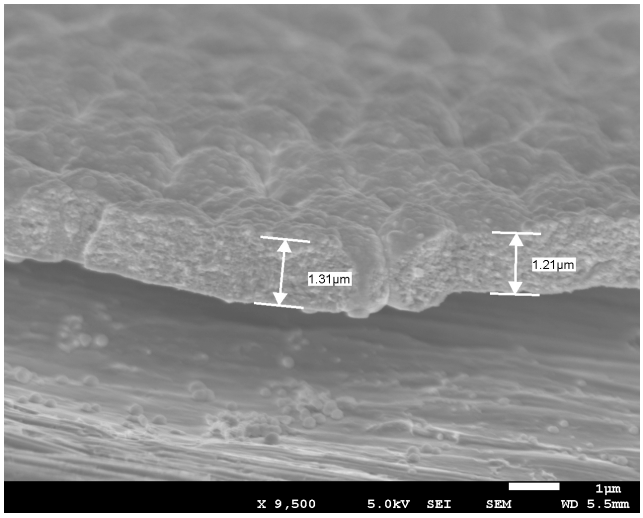

(a) Side view (x9500)

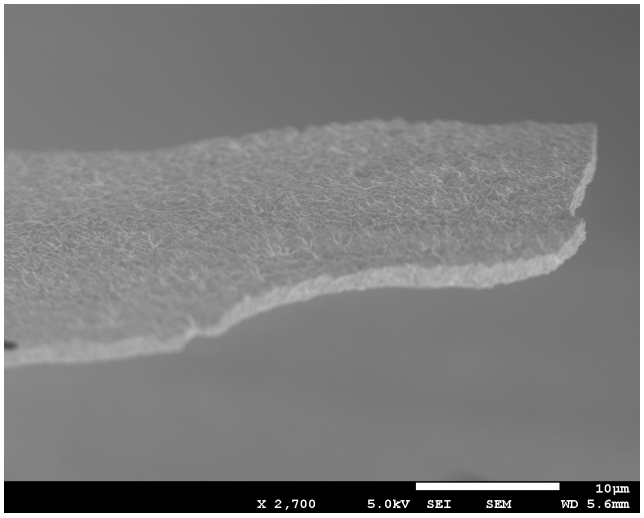

(b) Tilted view (x2700)

Figure 3.1: NiSn film of 0.5C deposited on Cu foil (a) NiSn film on Cu foil, (b) NiSn film

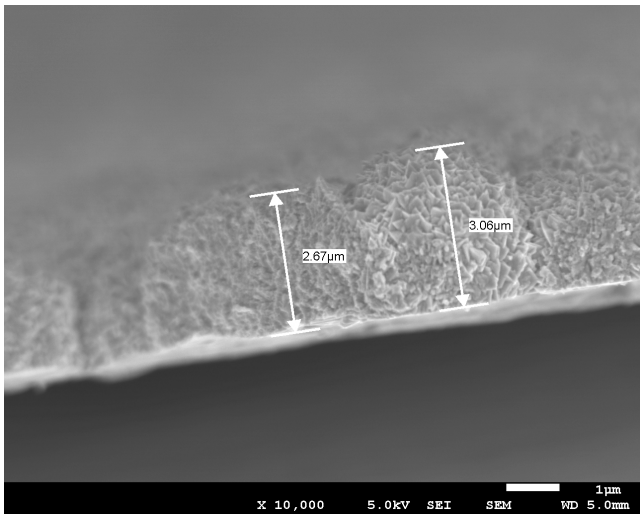

(a) Side view (x10000)

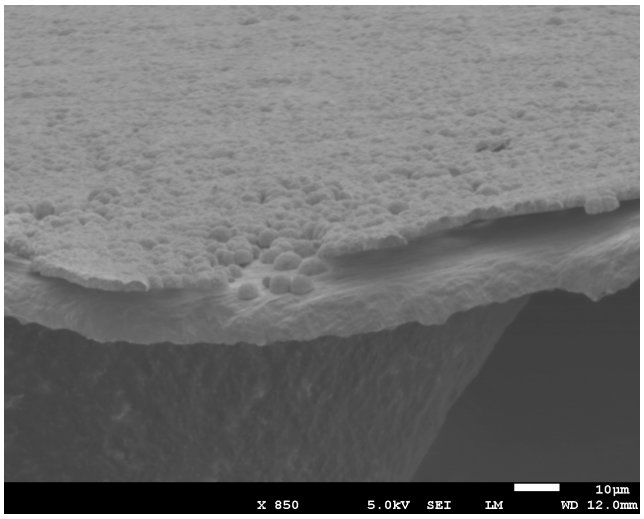

(b) Tilted view (x850)

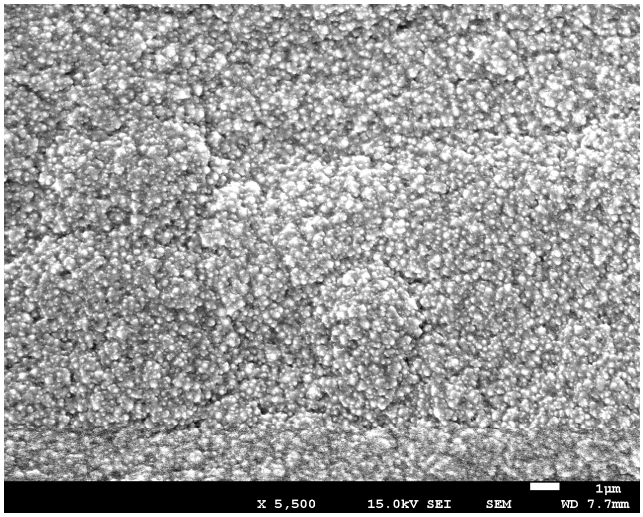

(c) Top view (x5500)

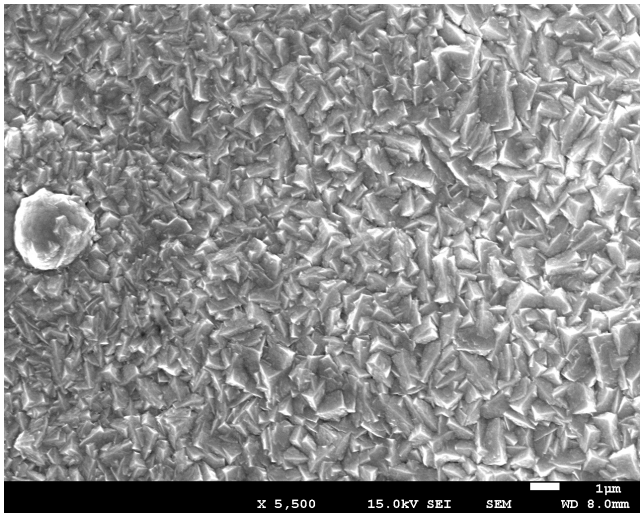

(d) Top view (x5500)

Figure 3.2: NiSn film of 1C (a),(b) NiSn film on Cu foil, (c),(d) top view of NiSn film

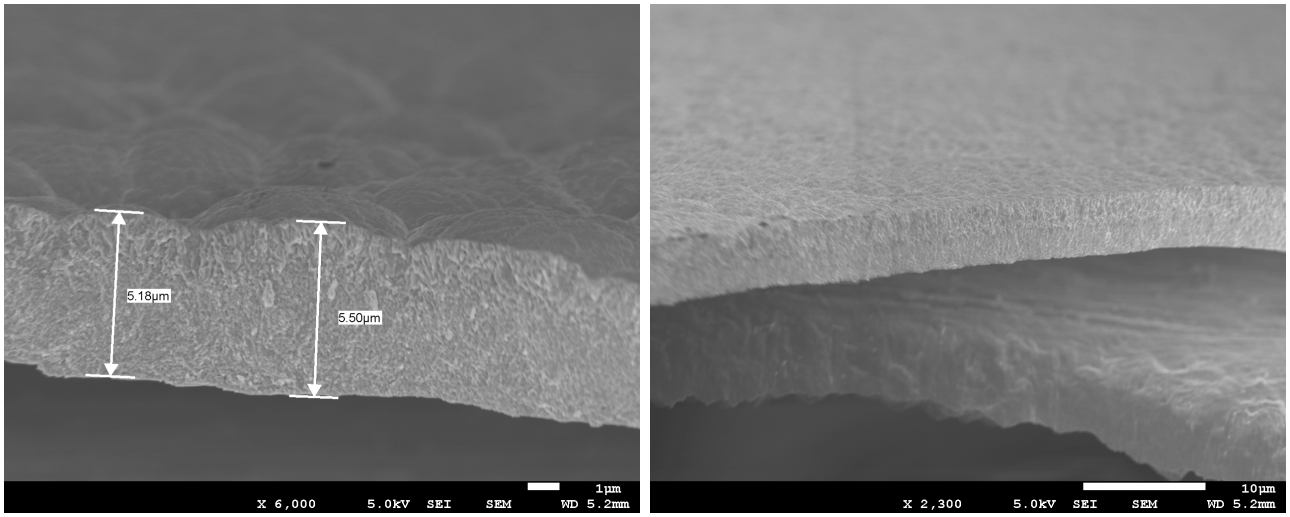

(a) Side view (x6000) (b) Tilted view (x2300)

Figure 3.3: NiSn film of 2.5C deposited on Cu foil (a) NiSn film, (b) NiSn film on Cu foil

The surface morphology of the films seems to change with the charge, while the thickness looks proportional to the imposed charge (an approximation of the relation is showed on figure 3.4). The thickness corresponding to 1C is consistent with the thickness theoretically calculated with the Faraday's law ($2.84\mu m$) in the Experimental section 2. Please note that the thickness values are not accurate due to the non constant view angle on the cross-section. The values measured are consistent with the literature. [58]
Film deposition do not face many challenges. The deposition duration is directly linked to the concentration of the electrolyte and the imposed charge.
The electrodeposition conditions (temperature, pulsed or constant current,...) have a great influence on the morphology (grain size, compactness,...) which, in turn, influences the electrochemical properties of the electrodes as it is explained in more details in the following section.

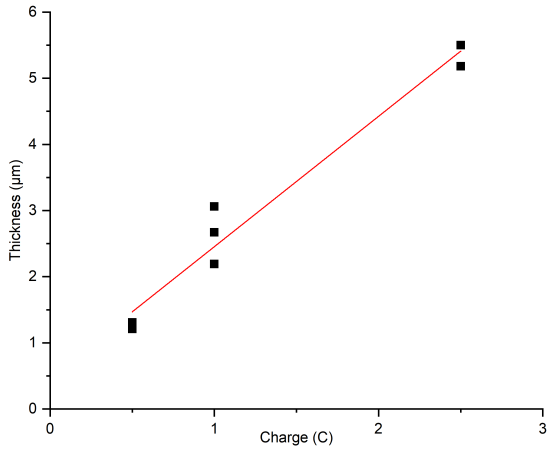

Figure 3.4: Evolution of NiSn film thickness as function of the applied charge

A study of the chemical composition as function of the charge was performed on films (figures 3.5, 3.6) thanks to an EDX study:

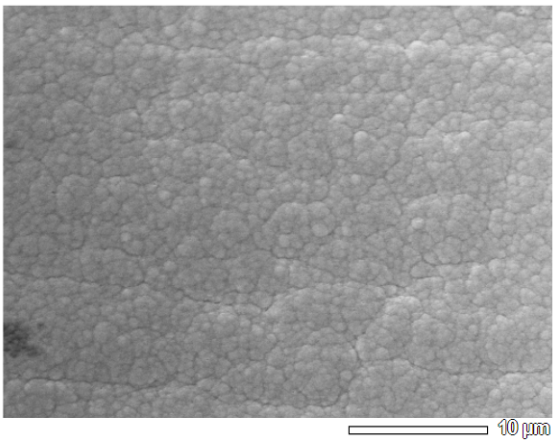

(a) Top view-2C

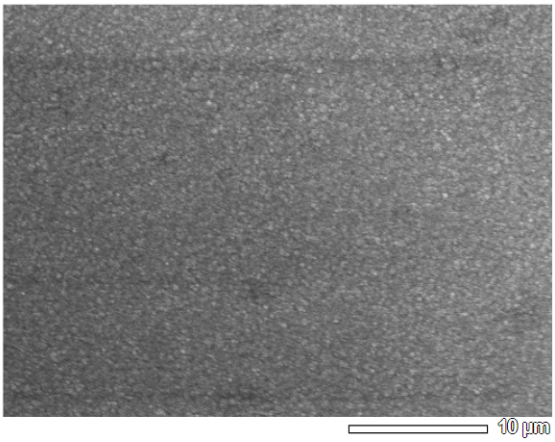

(b) Top view-5C

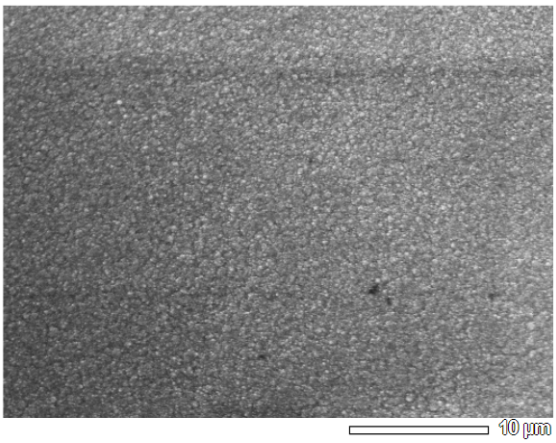

(c) Top view-10C

Figure 3.5: Top view of NiSn film analyzed by SEM-EDX

The atomic ratio of Sn/Ni measured:

- 5.67 for 2C
- 3.3 for 5C
- 2.85 for 10C

The desired ratio is 1.33 for Ni_3Sn_4 (see Theory section 1.4.4). These results are not completely representative of the sample nature since the accuracy of the EDX device is not perfect (an error of 5%-10% is suspected). Different NiSn phases can coexist in the structure and their proportions are influenced by the electrodeposition parameters.
For this study, a constant charge of 1C was imposed to keep constant conditions.

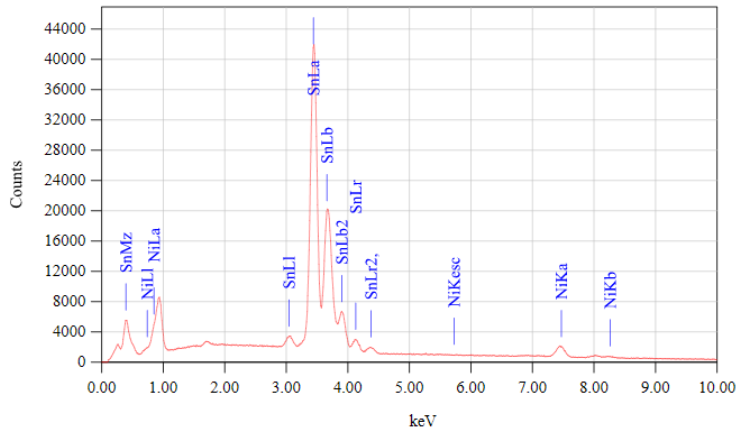

ZAF Method Standardless Quantitative Analysis
Fitting Coefficient : 0.2520

Element	(keV)	Mass%	Sigma	Atom%	Compound	Mass%	Cation	K
Ni K	7.471	8.04	0.94	15.03				9.5447
Sn L	3.442	91.96	0.34	84.97				90.4553
Total		100.00		100.00				

(a) 2C

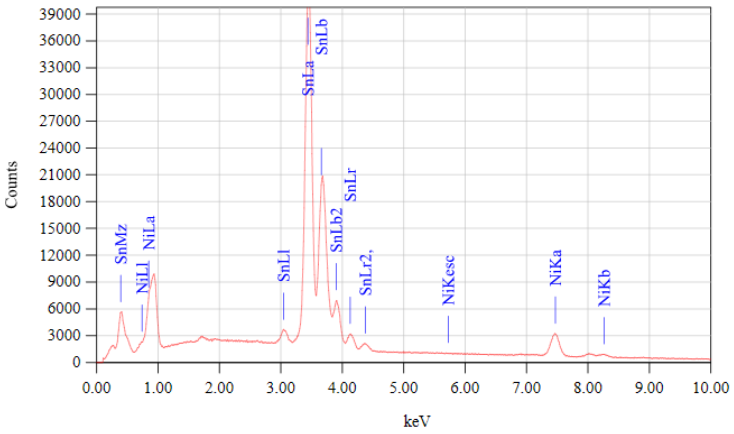

ZAF Method Standardless Quantitative Analysis
Fitting Coefficient : 0.2967

Element	(keV)	Mass%	Sigma	Atom%	Compound	Mass%	Cation	K
Ni K	7.471	13.41	1.10	23.84				15.7803
Sn L	3.442	86.59	0.40	76.16				84.2197
Total		100.00		100.00				

(b) 5C

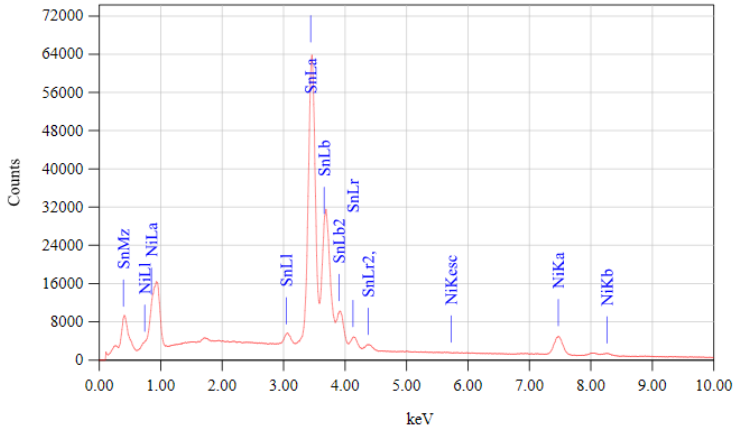

ZAF Method Standardless Quantitative Analysis
Fitting Coefficient : 0.4441

Element	(keV)	Mass%	Sigma	Atom%	Compound	Mass%	Cation	K
Ni K	7.471	14.76	2.03	25.93				17.3427
Sn L	3.442	85.24	0.74	74.07				82.6573
Total		100.00		100.00				

(c) 10C

Figure 3.6: EDX analysis of NiSn films 2C-5C-10C

3.1.2 NiSn nanowires (230nm)

The largest-diameter (230nm) nanowires were grown with the same conditions as for films. The nanowires were first grown through polycarbonate template on Si substrate and then on Cu foils with an alumina membrane or with a Si membrane or without any membrane (see chapter on Methods,section 2, for more information). The membrane was added to improve the contact between the substrate and the polycarbonate template, to allow a better adhesion between the nanowires and the substrate. Since the membrane did not perform perfectly its task (by preventing a good and homogeneous contact between the electrolyte and the substrate, see section 3.1.5: Membranes) and being not essential for the adhesion of 230nm-diameter nanowires on flat enough substrates, they were finally grown without any membrane. Images of the nanowires array can be obtained by SEM analysis (see figure 3.7). The resulting samples show a regular array of well-defined interconnected nanowires with a homogeneous height of approximately $9\mu m$ for 1C applied.

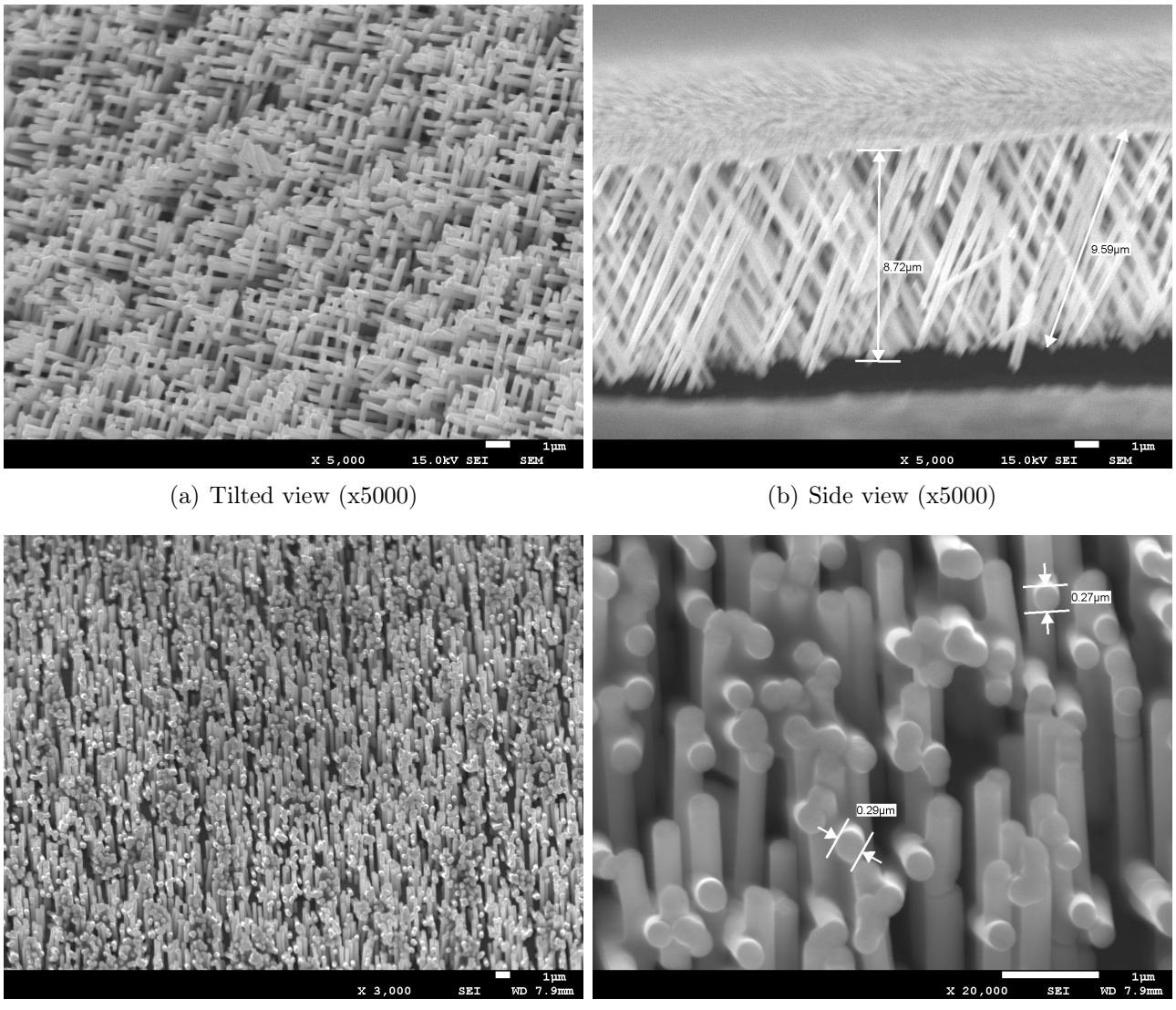

(a) Tilted view (x5000)

(b) Side view (x5000)

(c) Tilted view (x3000)

(d) Tilted view (x20000)

Figure 3.7: NiSn 230nm-diameter nanowires deposited on Cu foil (a),(c),(d) nanowires array, (b) cross-section view: Cu foil on the top, nanowires below

An EDX experiment was performed on one sample to learn more about the atomic ratio of Ni and Sn (figure 3.8). A ratio of 1:1 was found.

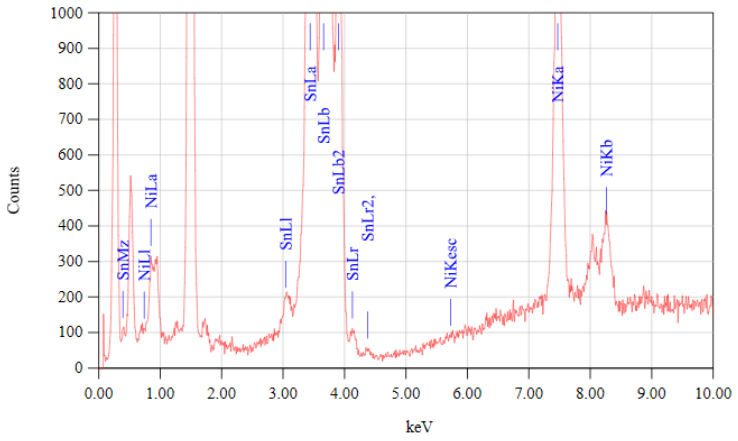

ZAF Method Standardless Quantitative Analysis
Fitting Coefficient : 0.5487

Element	(keV)	Mass%	Sigma	Atom%	Compound	Mass%	Cation	K
Ni K	7.471	34.09	2.40	51.12				38.8093
Sn L	3.442	65.91	0.88	48.88				61.1907
Total		100.00		100.00				

Figure 3.8: EDX analysis of NiSn 230nm-diameter nanowires

A classical deposition current for nanowires devices is depicted on figure 3.9. The peak at the beginning is due to the first germination on the substrate, then the growth in the nanotubes of the template stabilizes the deposition current. The average current measured is about 1.2mA, which is of the same order of magnitude as for films.

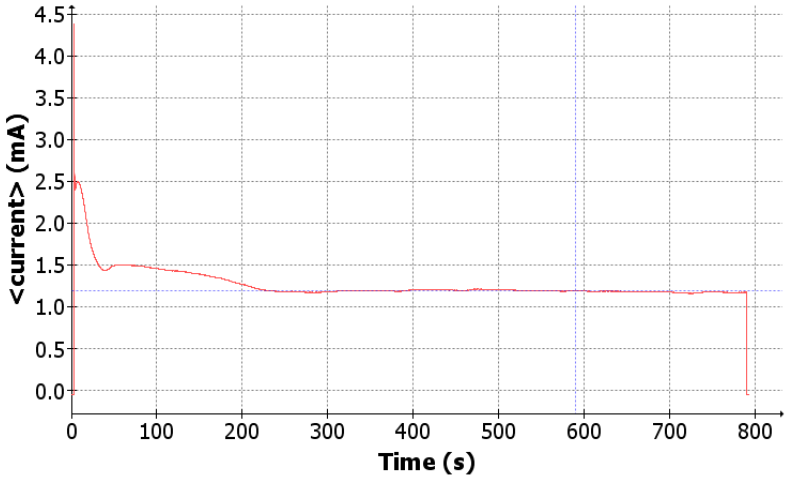

Figure 3.9: Deposition current for NiSn 230nm-diameter nanowires

3.1.3 NiSn nanowires (105nm)

NiSn nanowires with smaller diameter (105nm) and same packing factor were then grown to analyze the change of interstitial volume and the increase of interface area in battery applications (see figure 3.10).
The 105nm-diameter nanowires were first grown with the help of the Si membrane but it appears to be more interesting for achieving homogeneous samples to work without any membrane even if the adhesion is less favoured in such conditions. Indeed, with the "pressing" membrane, the deposition current was very low and the resulting sample seems to be non-homogeneous.
105nm is a diameter large enough to have a sufficient adhesion without "pressing" membranes. The network is well-defined and regular.

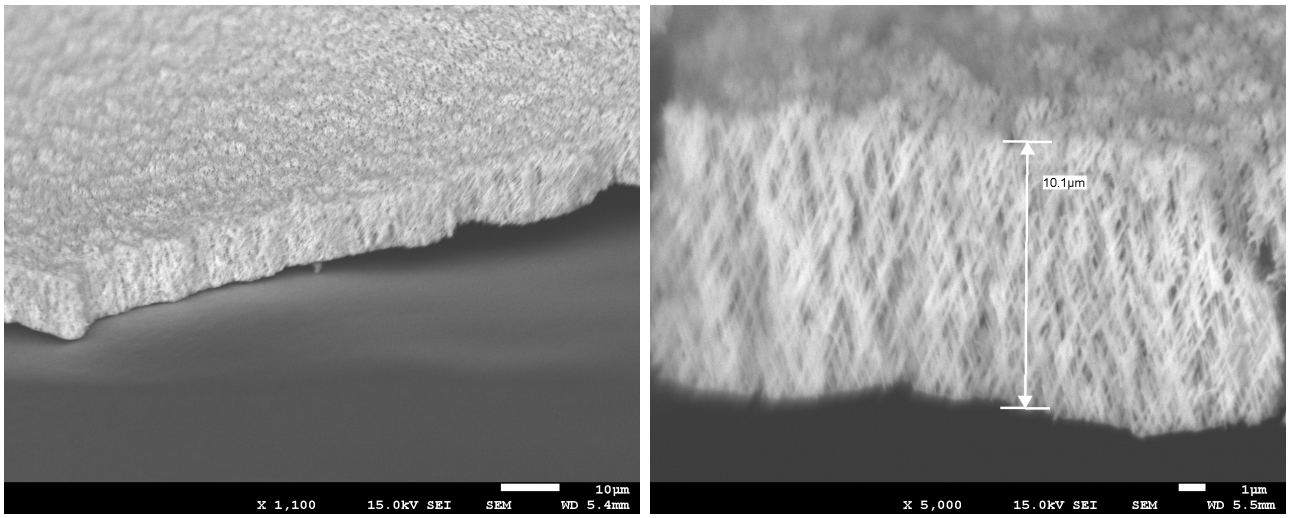

(a) Tilted view (x1100) (b) Side view (x5000)

Figure 3.10: NiSn 105nm-diameter nanowires

3.1.4 NiSn nanowires (40nm)

For a device with small contact area with the substrate, the silicon "pressing" membrane is essential to achieve the minimum adhesion required to grow the object.
The 40nm-diameter nanowire array presents a less regular structure with some nanowire ends packing at the surface (figure 3.11).

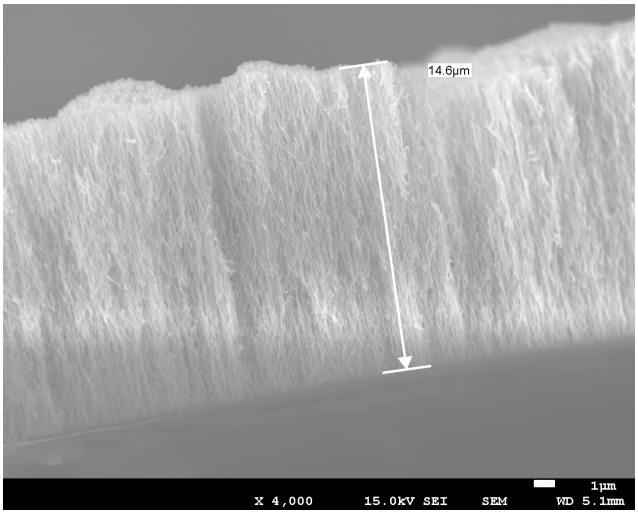

(a) Side view (x4000)

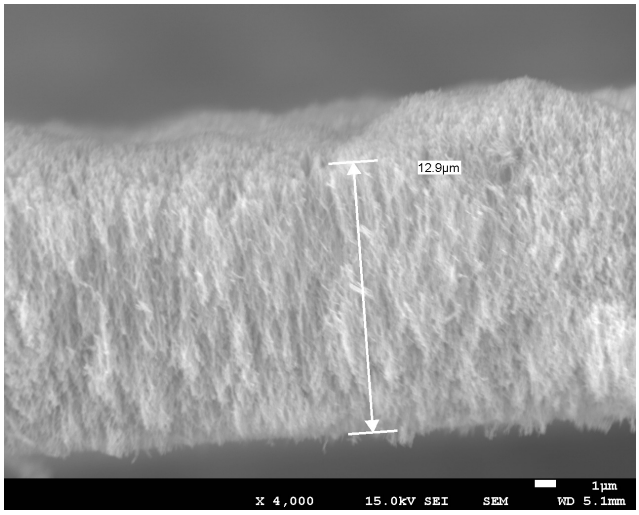

(b) Side view (x4000)

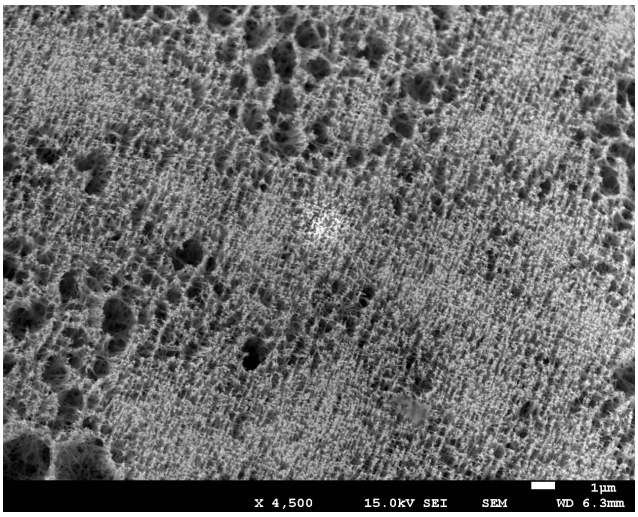

(c) Top view (x4500)

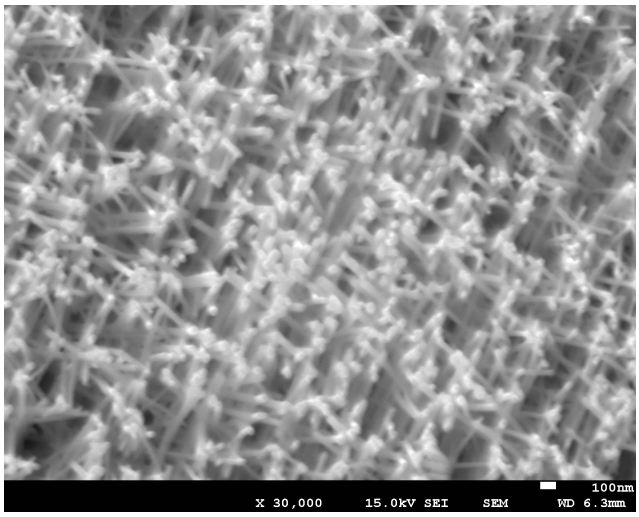

(d) Top view (x30000)

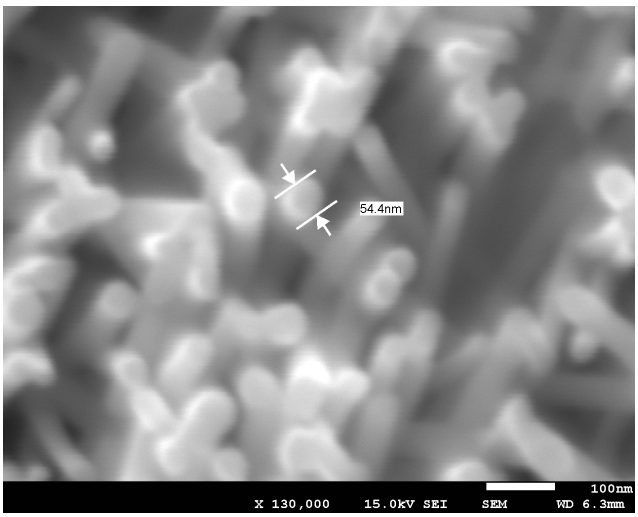

(e) Tilted view (x130000)

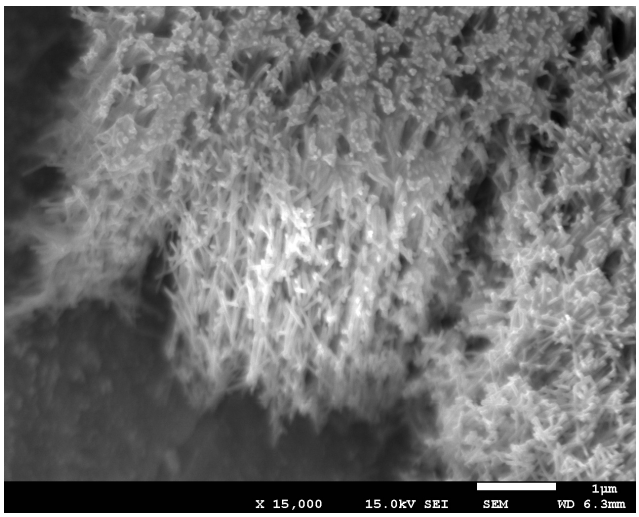

(f) Tilted view (x15000)

Figure 3.11: NiSn 40nm-diameter nanowires

3.1.5 Membranes

In the setup for the electrodeposition process, a microporous membrane can be added to press homogeneously the polycarbonate template on the substrate. This is done to achieve a better adhesion between the growing nanowires and the substrate. This membrane is not indispensable for large diameter nanowires where the adhesion surface is large enough to maintain the nanowires array on the substrate but is necessary for smaller-diameter nanowires.
First, alumina membranes were used but the fragility of such devices makes them not very efficient since the membrane has to be renewed for each setup.
Then a silicon microporous membrane was used, but the possible conductivity of the device allows deposition of the ions in pores and on the surface of the membrane, preventing a homogeneous and efficient growth of nanowires (figure 3.12). More information about the membranes nature is given in "Materials" section 2.
A coating of Al_2O_3 was made on this membrane, but the different manipulations of the object may have damaged the coating and the deposition occurs one more time on the microporous membrane as illustrated in figure 3.13.
The efficiency of a supporting microporous membrane has been proven by increasing highly the adhesion between small diameter nanowires and the substrate. But research have still to be made to improve the coating resistance to scratches and to find more suitable membranes allowing a higher deposition current and homogeneous deposition.

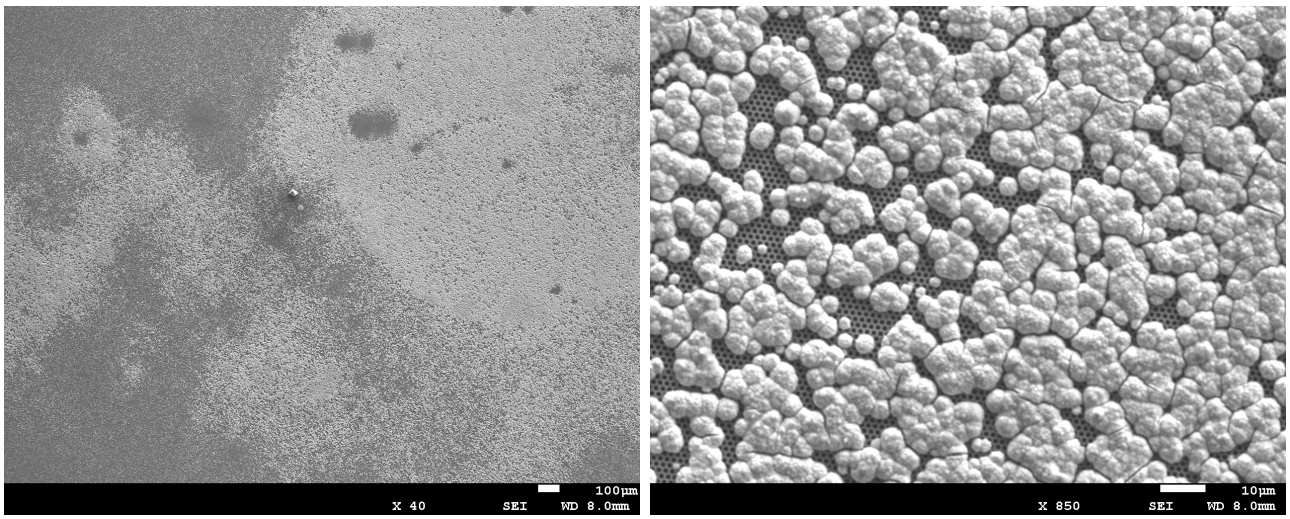

(a) Top view (x40) (b) Top view (x850)

Figure 3.12: Silicon microporous pressing membrane after electrodeposition, top view. The light zone is the metallic depositions while the darker zone is the original membrane

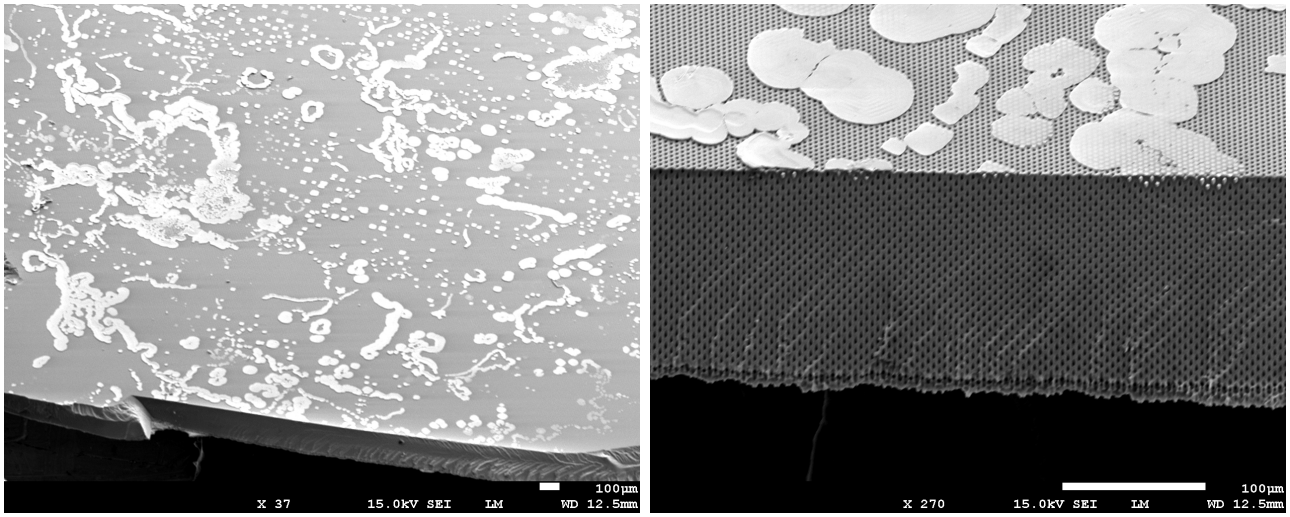

(a) Top view (x37)

(b) Tilted view on the edge (x270)

Figure 3.13: Coated silicon microporous pressing membrane with metallic depositions

3.1.6 Tin

The deposition of pure Sn did not give as constant and reproducible results as for NiSn. Two main figures were seen for Sn deposition of 230nm-diameter nanowires:

- "Nanowires planes" such as corals as it can be seen on figure 3.14
- Short nanowires and crystals as on figure 3.15
- An intermediate state with preferential growing spots without crystal formation, figure 3.16

The growth of pure Sn nanowires seems to be strongly limited, forming a carpet of small Sn nanowires of 1-2μm high. Some sites seem to be of preferential growth, allowing a located growth leading to both structures we observed: along some preferential lines, a planar structure looking as corals was grown while on some preferential spots, high nanowires (reaching the surface of the polycarbonate template) are topped with crystals which are formed on the upper surface of the template.
The adhesion does not seem to be a problem in this case since the substrate is completely covered with small nanowires. The homogeneous growth, at the opposite, is the key issue. To confirm this aspect, some NiSn nanorods were grown on the substrate, followed by pure Sn deposition. The issue of preferential growth stays present and no improvement was noticed.

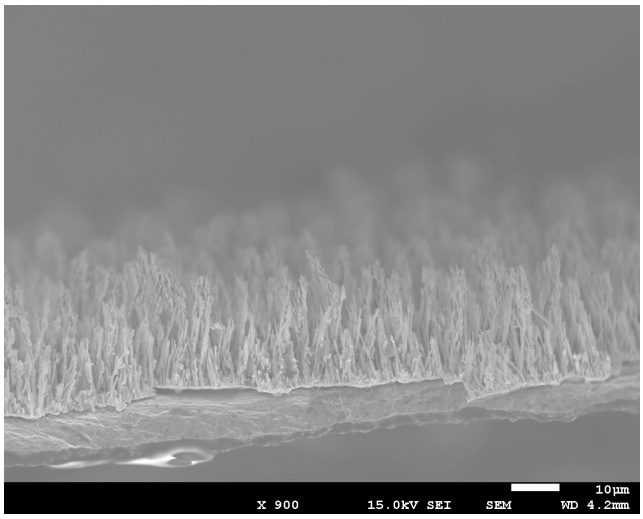

(a) Side view (x900)

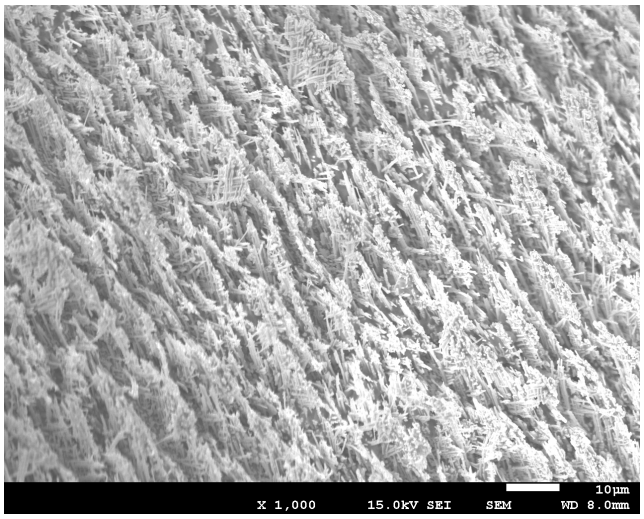

(b) Top view (x1000)

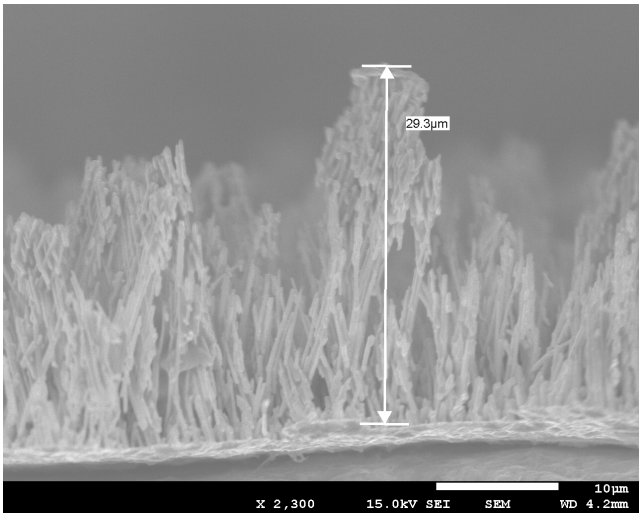

(c) Side view (x2300)

Figure 3.14: Sn nanowires 230nm diameter in "planes" configuration deposited on Cu foil

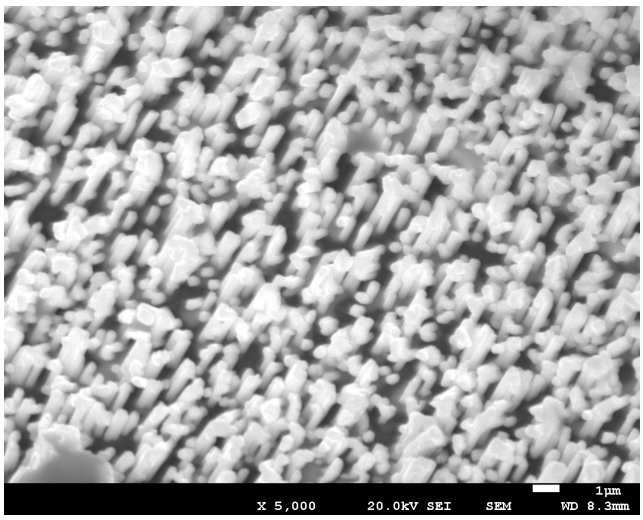

(a) Tilted view (x5000)

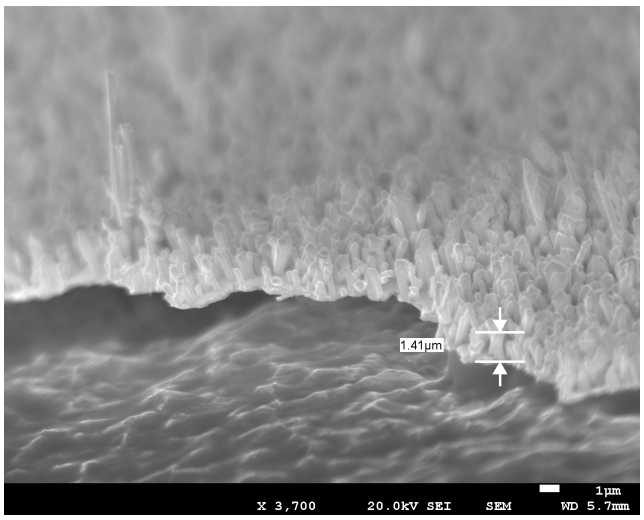

(b) Tilted view (x3700)

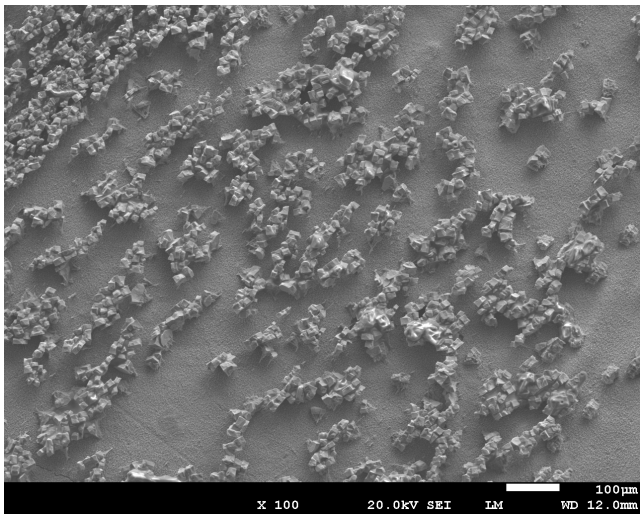

(c) Top view (x100)

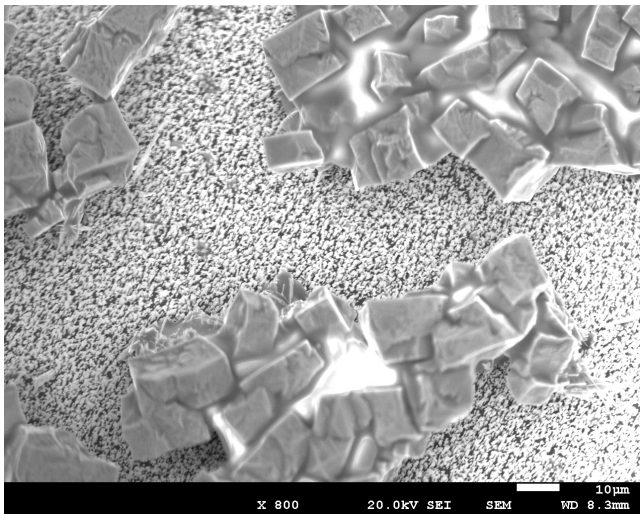

(d) Top view (x800)

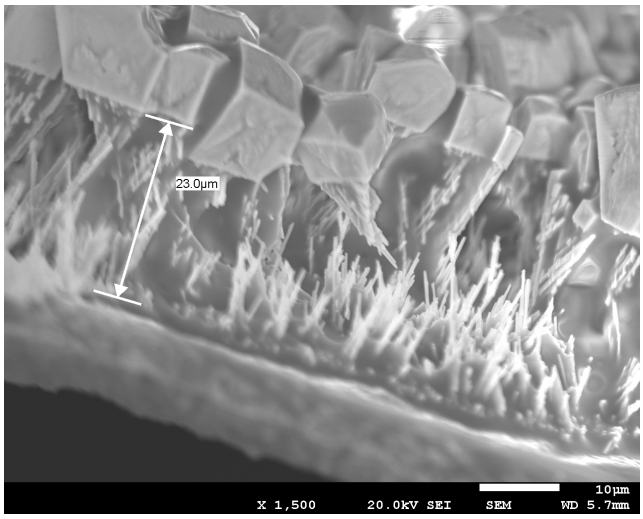

(e) Side view (x1100)

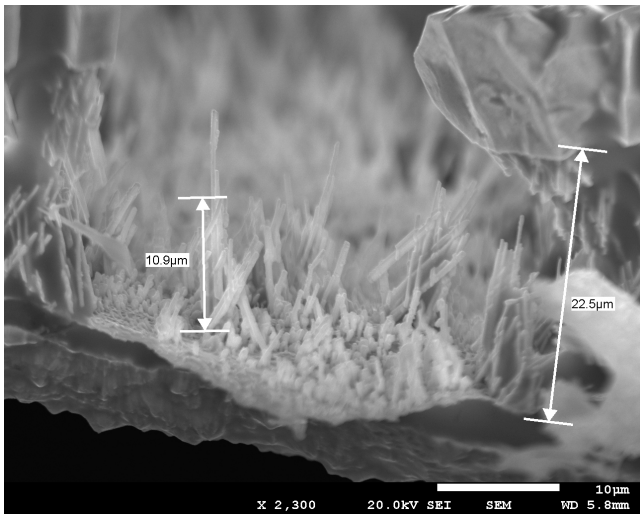

(f) Side view (x2300)

Figure 3.15: Sn nanowires 230nm diameter deposited on Cu foil with overflowing and crystals formation (a),(b) homogeneous "carpet" of small nanowires, (c),(d),(e),(f) crystals formed on the top of the nanowires array

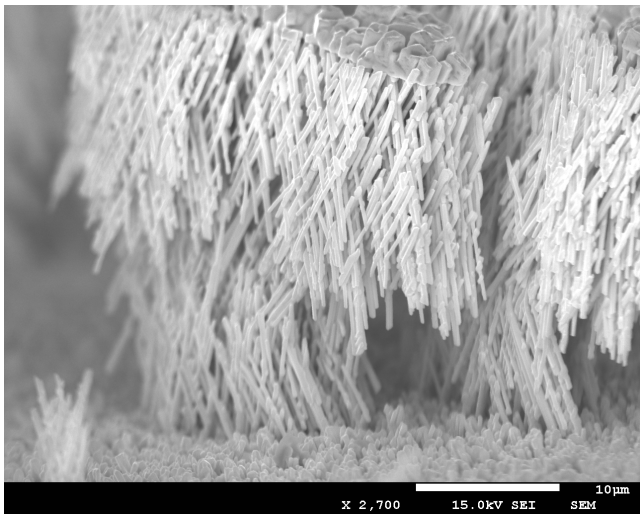

(a) Side view (x2700)

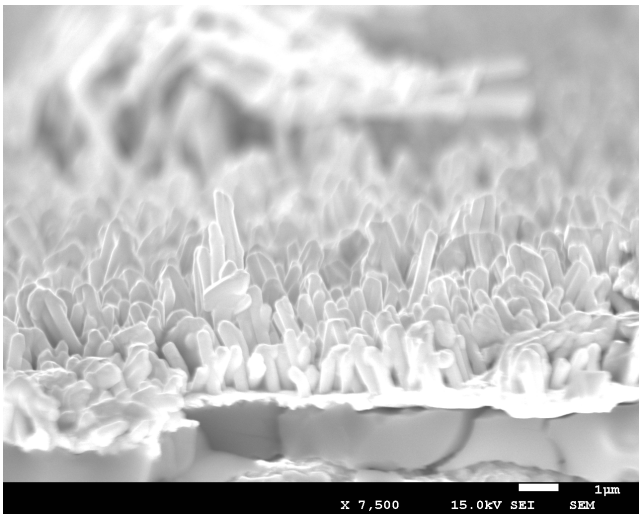

(b) Side view (x7500)

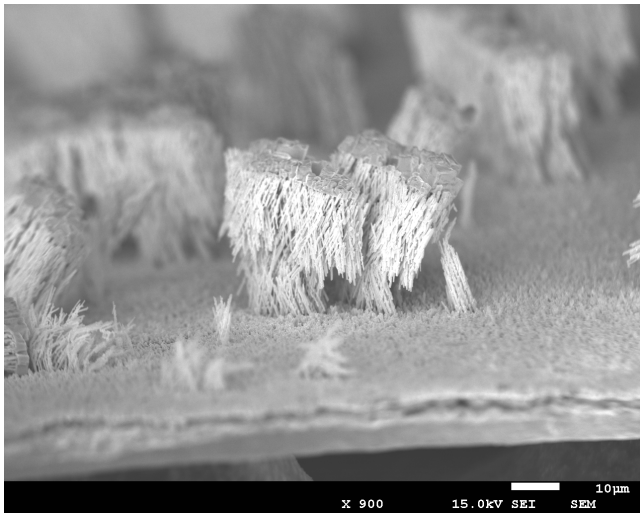

(c) Tilted view (x900)

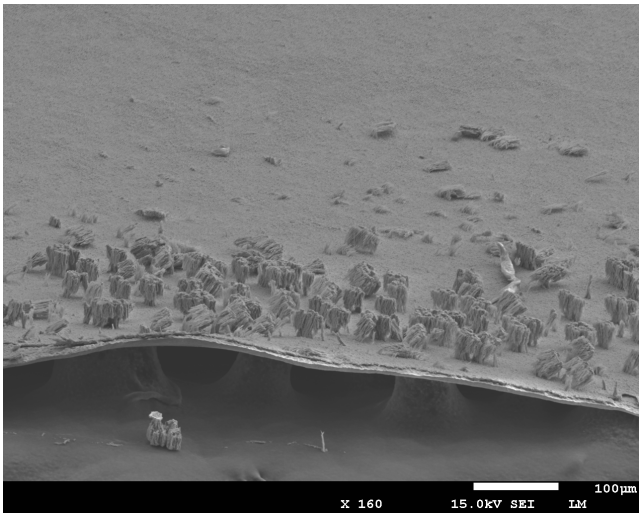

(d) Tilted view (x160)

Figure 3.16: Sn 230nm-diameter nanowires deposited on Cu foil with preferential growing sites. (a),(c) preferential growing sites, (b) small nanowires background,(d) global view of the sample (Pascal Van Velthem images)

The identification of the parameters influencing the structure is complex.
Indeed, for a constant potential applied in the electrodeposition process, the growth speed (deposition current) can strongly vary from one sample to another, leading to the formation of multiple configurations.
Moreover, the solution seems to be sensitive to time or storage conditions (as light) and that could be one of the reasons of so different results.

A typical shape of deposition current is depicted on figure 3.17. The increasing step is a sign of overflowing when deposition occurs above the template.

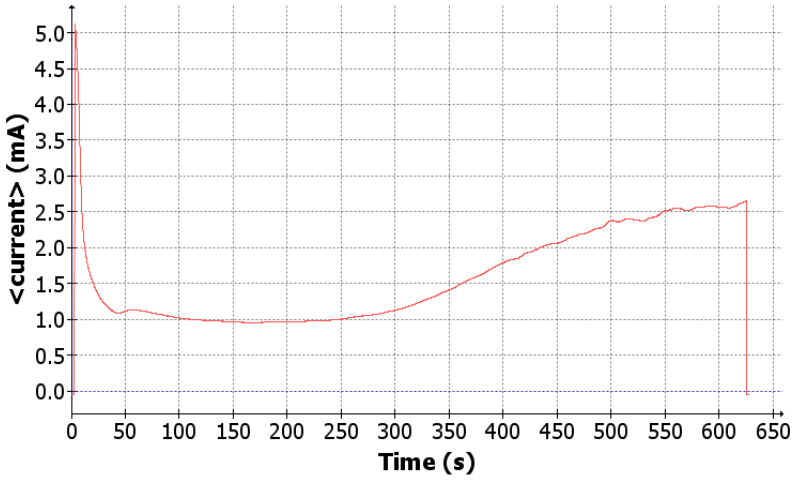

(a)

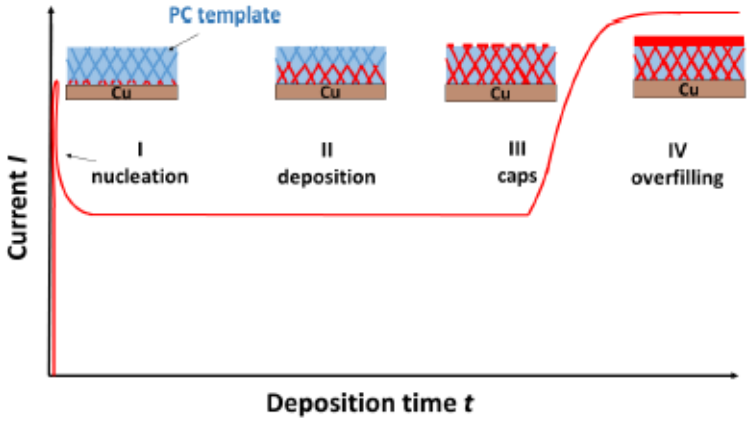

(b)

Figure 3.17: (a) Deposition current of Sn 230nm-diameter nanowires with overflow, (b) example of overflowing deposition current (from [57] and [59])

A deeper study of the right electrodeposition conditions (focused on the applied potential) is discussed in the experimental conditions chapter (see section 2.1.1). Moreover some changes in the electrolyte solvents, pH or composition could improve greatly the deposition, as discussed in the experimental chapter section 2. Indeed, the stability regions of the species of interest do not seem compatible with the characteristics of the current electrolyte.

3.1.7 Possible improvements

The results of the electrodeposition have a direct influence on the batteries performances. Indeed, the morphology, the predominant phase, the shape (the surface area, the height, the mechanical stability,...) change the performances of the battery. All these parameters are influenced by electrodeposition conditions such as temperature, current (pulsed or constant, high or low), time, setup used (pressing membranes),...
Moreover, a lack of adhesion can limit strongly the life cycle of batteries as well as being responsible for active mass losses.

The lack of adhesion between the nanowires array and the Cu substrate is one usual issue which occurs during electrodeposition and which leads to a loss of electrical contact between the active material and the current collector. The lack of adhesion is due to a large strain mismatch between the active/inactive materials interface (Cu foil and NiSn film deposited at the roots of the nanowires, see figure 3.42 in Appendix 3.3.2). Different ideas were investigated through research to find efficient improvements.
One solution which could be investigated is the growth of short Cu nanorods on the Cu substrate in the polycarbonate template (see figure 3.18). They act as "screws" and bind the template to the substrate as done in articles. [35][60] This could improve the structural stability and therefore the battery performances.

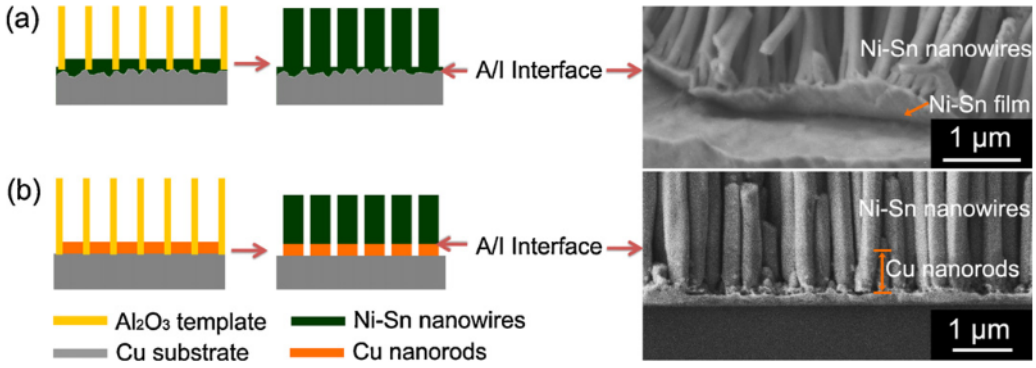

Figure 3.18: Schematics and SEM images of NiSn straight nanowire arrays with (a) NiSn bonding (b) Cu bonding to Cu foil (from [60])

Other techniques were used in literature to improve the performances by improving the adhesion. For example, working with pulsed electrodeposition allows a finer structure and surface morphology with a better adhesion.[61] But pulsed deposition is more complicated in the case of alloys deposition. Using conductive glue between the created anode and the current collector can also allow a stronger adhesion.
Annealing and alteration of the current collector interfaces could also be an interesting solution.[60] Moreover, heat treatments of the sample can generate alloying of the film deposited with the substrate, reinforcing the adhesion strength.[62]

Different ideas are described in the following performance results.
From another point of view, a deeper study of the influence of the "pressing" membranes on the deposition kinetics could also be performed.

3.2 Battery performances

The battery performances were tested by cycling them galvanostatically from 1V to a varying lower limit of potential. The life cycle and the value of specific discharge capacity were compared for different configurations (3D interconnected nanowires or 2D films) of NiSn electrode with pure Sn electrode.

The discharge is linked to the lithiation process which is the main process of interest and this is the reason why this study focuses on discharge capacity.
Two types of results are given for each sample:

- Potential-capacity curves
- Capacity-cycle curves

A short description of the general conclusions which can be drawn from both graphs and trends is given. More specific results and comparisons for each sample follow, with first a comparison between the different diameters of NiSn nanowires and NiSn films, followed by a comparison between the NiSn and Sn systems.
Finally, some coulombic efficiency curves are shown and analyzed.

3.2.1 Potential-Capacity curves: a general description

The charge and discharge curves allow to examine the battery performances. Charge/Discharge curves give in general the difference in capacity and potential for the electrodes from the half cells according to lithium as reference. High values in potential give a better output while high values in capacity give an improved operating time.
During the discharge of a cell, multiple measurement configurations are possible.

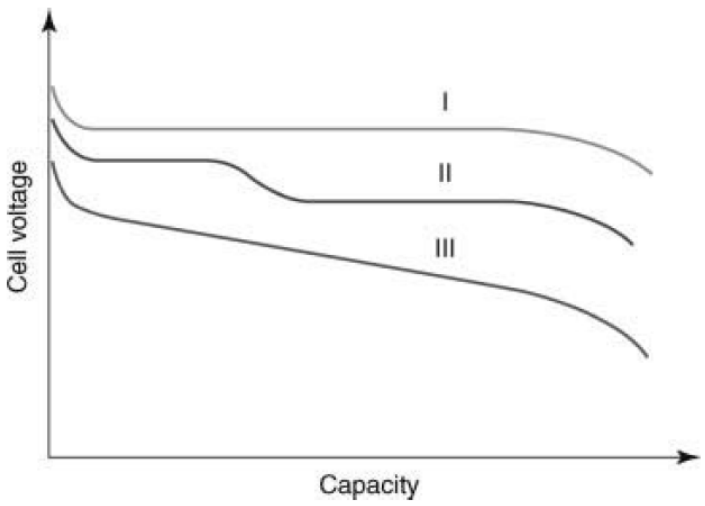

Figure 3.19: Discharge curves (from [14])

In figure 3.19, the potential of the curve I is hardly influenced by the reactions of the battery. In the case of the curve II, the presence of the step implies a change in the reaction mechanism. In curve III, the reactants, products and internal resistance change during the whole process. [14]

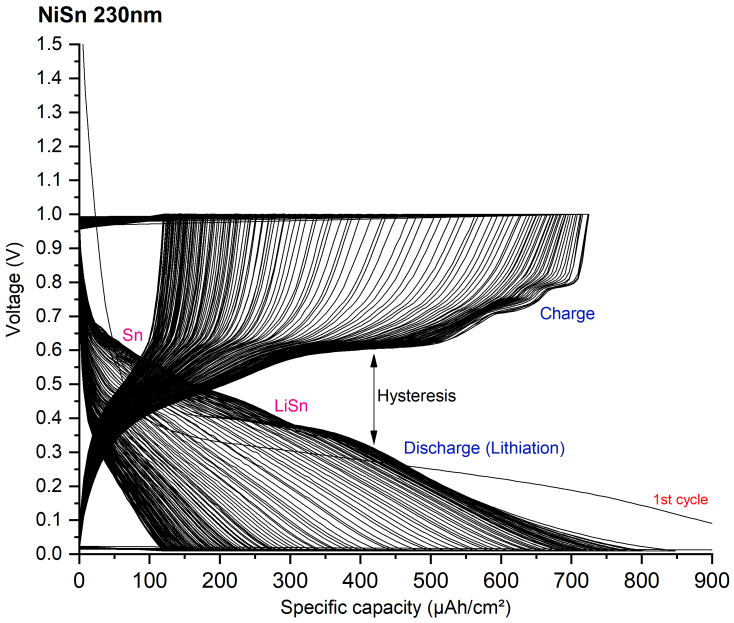

Figure 3.20: NiSn 230nm-diameter nanowires: Ecell-Capacity curves

Typical potential-capacity curves are shown on figures 3.21 and 3.20 for the case of NiSn nanowires of 230nm-diameter.
We can see that the curves are a mix of state II and III of figure 3.19. The sample is, therefore, presenting an evolution in the reaction mechanism and a change in the products and internal resistance during the process.
The colors in the diagram represent the evolution of the curve depending on the cycle number. This evolution follows a logical path since at first cycles, the capacity stays high under charge and discharges while after some cycles, the capacity decreases strongly and the curves move to the left.

The higher part of the graph represents the charge of the cell which is associated with the delithiation process of our sample, Li ions leaving the cathode.
The lower part is associated with the discharge of the cell, the alloying process between the lithium and the Sn of the cathode. Since Sn is the only active material within the sample (nickel does not react with lithium), the graphs of NiSn samples and pure Sn samples present the same trends.

The different steps of the discharge curve are associated with phase transformations occurring in the Sn-Li crystal due to the increasing content of Li ions in the structure (figure 3.20). The first step is the crystal structure of Sn changing in LiSn structure according to figure 1.20. The potential values differ because on figure 1.20 the equilibrium potential is given while in these measurements, the discharge current is not infinitely slow and therefore not at the equilibrium. One can see that if the phase transformations are well defined for first cycles, at higher cycle numbers, the charge and discharge processes look more as constant linear slope. This gives information about a change of behaviour at low and high cycles number along with a less important lithiation process. A possible transformation of crystalline Sn to an amorphous phase is suggested in the following articles thanks to observations and similar behaviours of silicon. [63] [64].

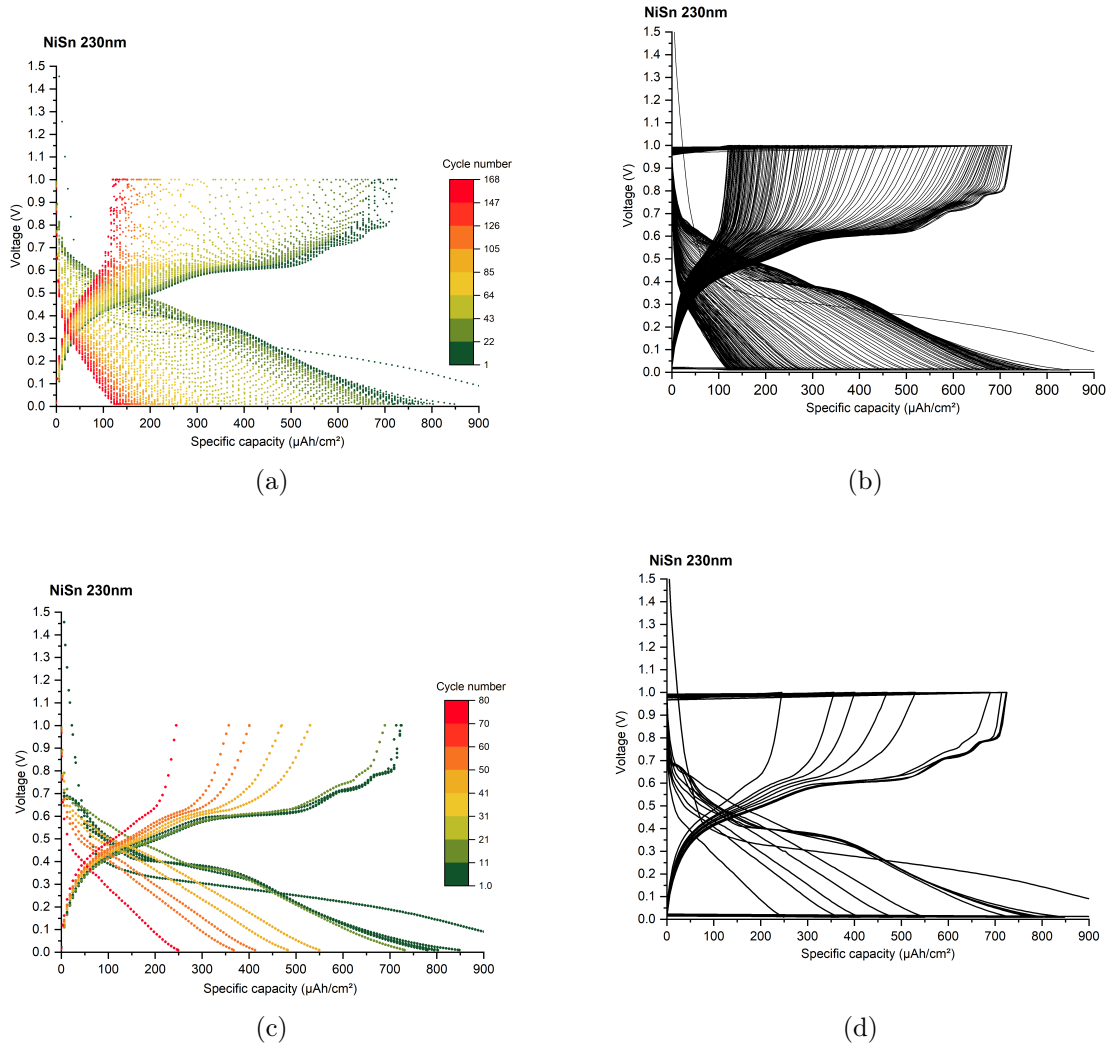

Figure 3.21: NiSn 230nm diameter nanowires: Ecell-Capacity curves. (a),(b) all cycles, (c),(d) few selected cycles

The first discharge curve has a particular shape differing from the other discharges curves. This is caused by some imperfections of the material as oxidation (SnO reacting in place of Sn) and a high irreversible capacity before SEI formation.
Another parameter we can observe on these diagrams is the hysteresis between the charge and discharge curves.
The potential value related to the formation of Li_ySn phases is linked to the Gibbs free energy of the structures formation. The addition of ions inside the structure induces strain and stress and modify the link between the Gibbs free energy and the equilibrium potential.

$$\Delta G = \Delta G_r - eE - \Omega\sigma_m \tag{3.1}$$

Where ΔG_r is the Gibbs free energy linked to the lithiation reaction, E is the potential, $\Omega\sigma_m$ are the volume change due to the addition of one Li atom and the mean stress in the core.[65]

3.2.2 Capacity-cycle curves: a general description

The capacity-cycle curves give general information about the battery performances. The maximum specific capacity achieved by the cell and the life cycle of the cell are detailed.

3.2.3 Specific results and comparison: NiSn

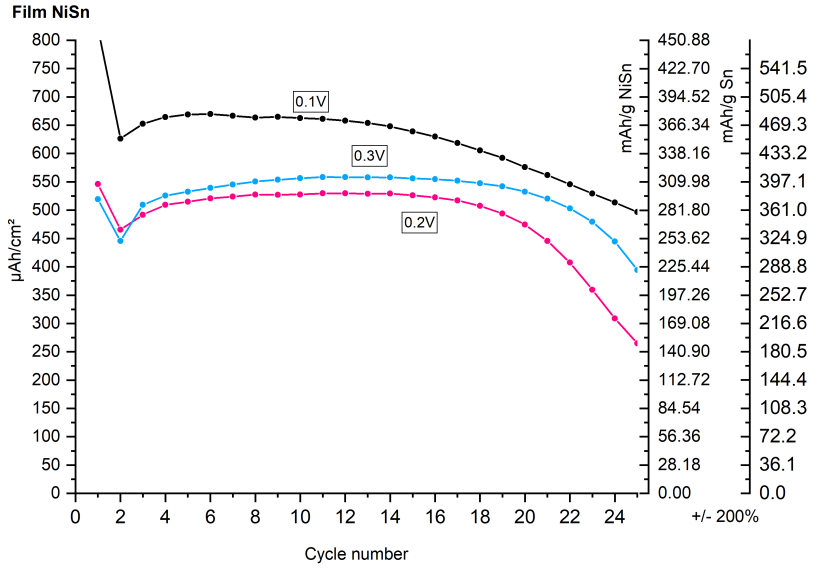

Figure 3.22: Specific capacity of NiSn film for different lower limits of potential up to 1V

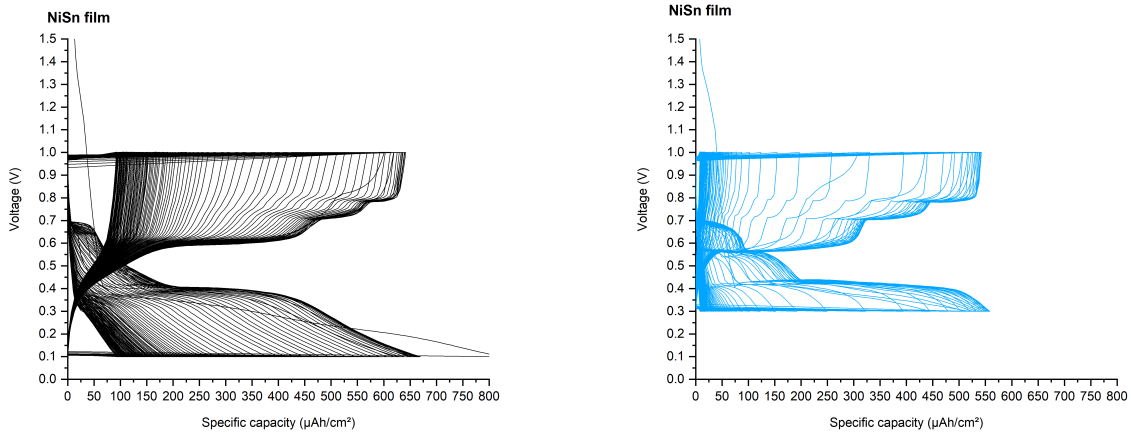

Figure 3.23: NiSn film: Ecell-Capacity curves at different lower limits of potential (black = 0.1V, blue= 0.3V)

The first batteries cycled were films to get a reference of achievable performances. Comparing films efficiency with nanowires structures may highlight the added value of a 3D structure.
Cycling tests were performed by discharging the battery to 0.1, 0.2 and 0.3V and recharging up to 1V (figure 3.22).
In all cases, the first cycle capacity is much higher than the following capacities values and is irreversible. The difference between the first cycle capacity and the following much more reversible capacities is mainly due to the formation of the SEI/electrolyte decomposition (see

Theoretical background section 1.3.2) and to the cycling of other compounds such as oxidised compounds present on the surface.[66]
As general observation, more is discharged the battery (up to lower potential), better are the performances in term of longevity (number of cycles) and maximum value of capacity but lower is the stability of the capacity.
Indeed, discharging up to lower potential allows to alloy more Li ions and to use more of the active matter inside the electrode. Therefore, the capacity value is higher.
The difference of life cycle could be explained by the formation of the SEI. Indeed, the SEI formation was studied at different potentials and it was shown that SEI formed at low potential are thicker.[20]
The SEI formed in samples cycled to lower potential could be more resistant and stable through cycling, allowing better performances while the SEI formed at higher potential is less stable and, if broken, could consume more of the battery material while increasing the internal resistance, decreasing therefore the performances.
The stability can also be explained by the quantity of SEI formed: at lower potential, more Li ions are alloyed in the material, causing a larger volume expansion which breaks the SEI already formed which will consume more of the electrolyte. The larger volume expansion weakens also the structure.

In this case, the results given by the samples discharged to 0.2 and 0.3 V are pretty close and are both lower than the one discharged to 0.1V.
In general, a specific capacity of 500-650 $\mu A/cm^2$ is obtained for film with a life cycle of 20-25 cycles. The capacity is consistent with values found in literature [34]. According to this article, the life cycle and the specific capacity could be improved by changing the electrodeposition parameters (time and current) as explained in the electrodeposition results (section 3.1). Indeed, the morphology and predominant phase of the sample are controlled by electrodeposition conditions and have a great influence on properties. A predominant metastable phase could improve the batteries behaviour.

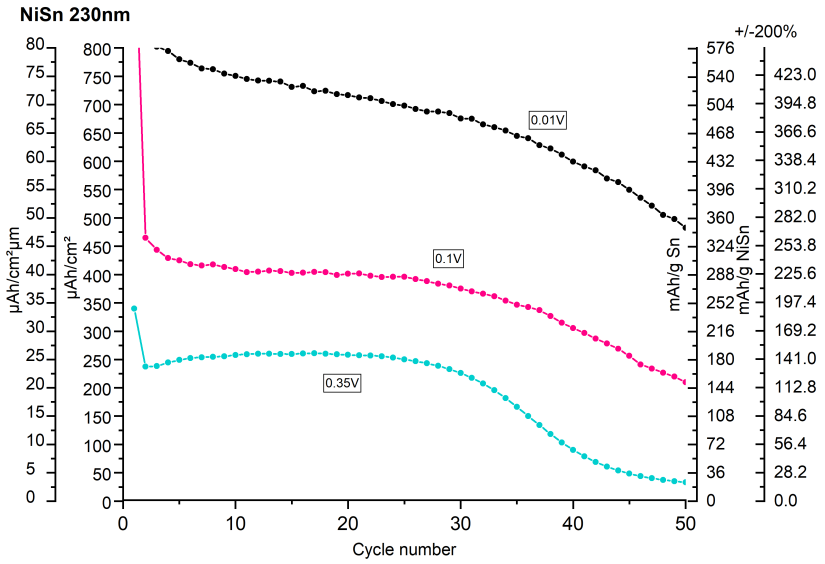

Figure 3.24: Specific capacity of NiSn 230nm-diameter nanowires for different potential lower limits up to 1V

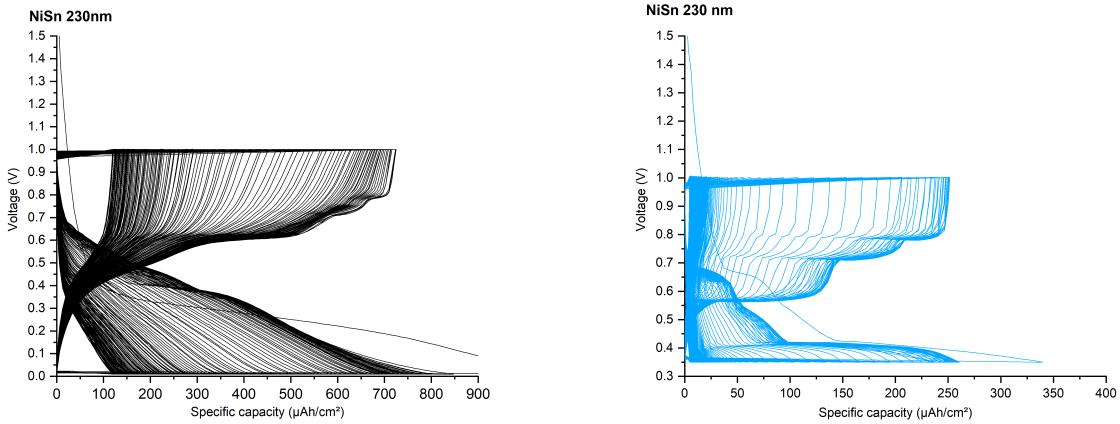

Figure 3.25: NiSn 230nm-diameter nanowires: Ecell-Capacity curves at different lower potential limits (black = 0.01V, blue= 0.35V)

For large nanowires of 230nm-diameter (figure 3.24) the difference between samples discharged to 0.01, 0.1 and 0.35V is more important.
The sample discharged to 0.35V has the lowest performances with a life cycle of 35 cycles and a specific capacity of 250 $\mu A/cm^2$ while the sample discharged to 0.01V can reach 750 $\mu A/cm^2$ and stays important during almost 50 cycles.
These results are smaller than what was obtained for other alloys with similar structure and same architecture (1400 $\mu A/cm^2$) [36] or than other nanowires structures as core-shell (800 mA/g) [67] but a large material loss is suspected explaining the difference in the comparison. An error of around 200% is expected for the mass of the sample. Indeed, the difference between measured and calculated values in addition to material loss during processing and cycling can increases significantly the error of the mass determination (see "methods" section 2).

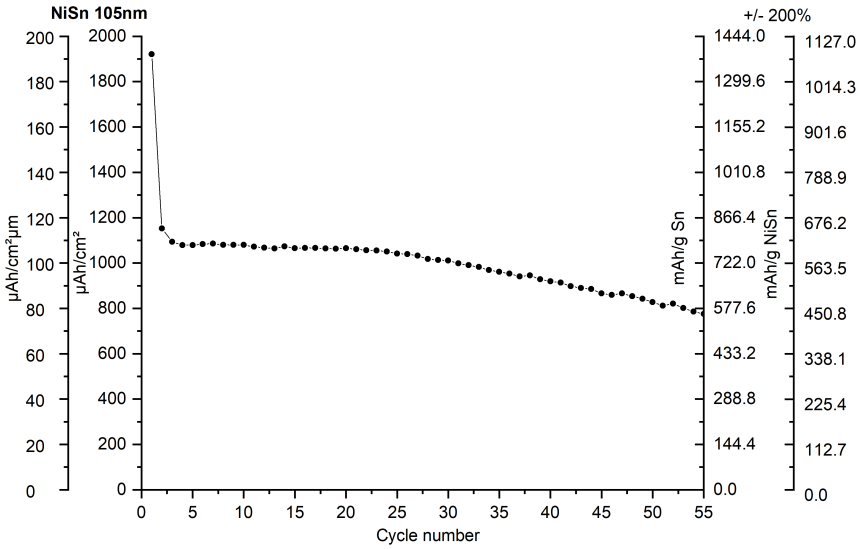

Figure 3.26: Specific capacity of NiSn 105nm-diameter nanowires

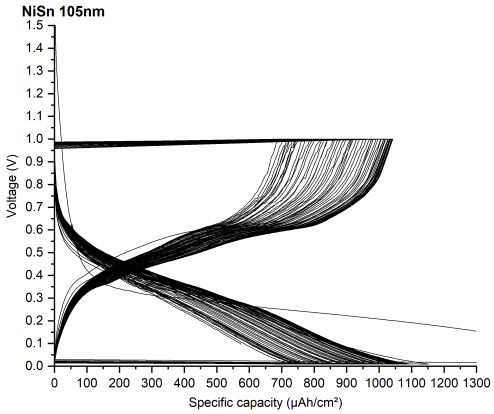

Figure 3.27: NiSn 105nm-diameter nanowires: Ecell-Capacity curves

For intermediate nanowires size of 105nm diameter (figure 3.26), the specific capacity is much higher and stable than for all other samples. It achieves a reversible specific capacity of $1100\mu A/cm^2$ and stays stable over 55 cycles. Furthermore, the potential-capacity curve of the sample has less significant steps. It could signify that the sample has less phase transformations during alloying with Li.

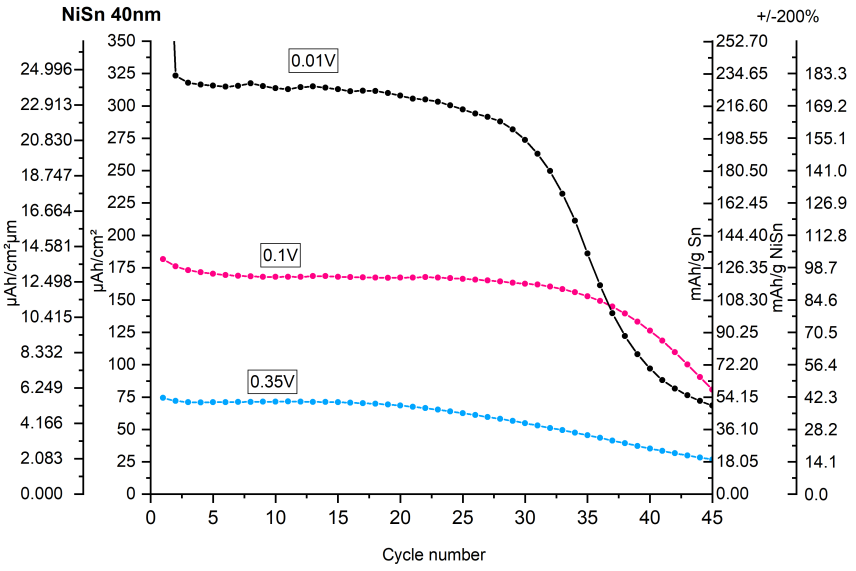

Figure 3.28: Specific capacity of NiSn 40 nm-diameter nanowires for different potential lower limits up to 1V

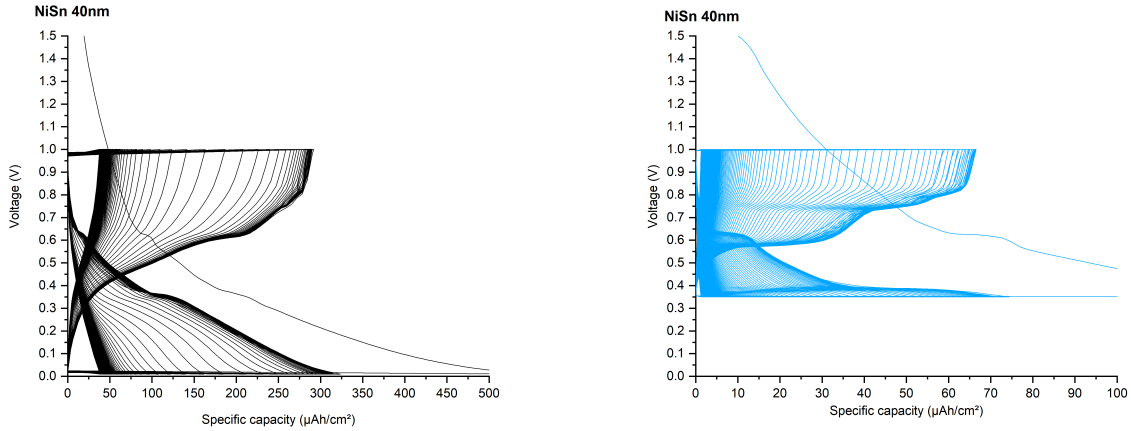

Figure 3.29: NiSn 40nm-diameter nanowires: Ecell-Capacity curves at different lower potential limits (black = 0.01V, blue= 0.35V)

For small nanowires of 40nm-diameter (figure 3.28) the difference between sample discharged to 0.01, 0.1 and 0.35V is more important.
The sample discharged to 0.35V has the lowest performances with a life cycle of 27 cycles and a specific capacity of $75\mu A/cm^2$ while the sample discharged to 0.01V can reach $325\mu A/cm^2$ and stays important during more than 35 cycles.

All these results are quite surprising because it highlights that the films have higher specific capacity than some 3D arrays structure.
Indeed, nanowires of 40nm-diameter and 230nm-diameter have lower capacity values than film for same potential limits while 105nm-diameter seems more promising. However, the nanowires structure seems to have a larger life cycle than films.

As already mentioned, the low values of specific capacity for nanowires could come from a not fully complete specimen. Indeed, during the additional process step that is performed on nanowires and not on film (polycarbonate template dissolution), some parts of the sample can detach and lose contact with the current collector. Moreover, the drying step, before the battery assembling, was noticed to cause more damages to nanowire morphology than films (due to a shrinking of the lattice). The complexity of a 3D array geometry makes it less stable under manipulation than a simple film configuration, moreover the adhesion between the sample and the substrate is suspected to be stronger for films than nanowires arrays.
This, with the huge mass approximation error (of +/- 200%), could explain the difference of specific capacity by loss of active materials. Other tests have to performed to verify this assumption or to confirm the higher capacity value of films.
The absence of core-shell structure could be one reason to the fragility of the samples which caused the hypothetical loss of active material during processing. Indeed, the presence of an inactive, stable core could improve the stability of the system under manipulation and cycling.

At the same time, performances of nanowires of different diameters are compared. The intermediate diameter (105nm) presents better performances in terms of longevity and specific capacity.
One possible explanation to this, is the better contact surface and adhesion between 105nm-diameter nanowires and substrate and a higher mechanical stability with no ends agglomeration of the nanowires compared to 40nm-diameter nanowires. Furthermore, the space volume between nanowires is larger for larger diameter nanowires, allowing a easier and faster access to electrolyte and ions.
In addition to that, the 105nm-diameter nanowires have a larger active surface area between the electrode and electrolyte than 230nm-diameter nanowires making the sample more efficient to make reactions between more active materials and the electrolyte.

Another possibility is simply the higher quality of the sample of NiSn 105nm-diameter nanowires compared to the others.

3.2.4 Specific results and comparison: Sn

It is complex to give a complete interpretation of Sn results (figure 3.30). Indeed, the samples tested have a particular geometry composed of very small nanowires (1-2μm high in average) and some large crystals on the top (see figure 3.15). The curves for lower potential cycling present a very limited life cycle of less than 5 cycles, which was expected of pure tin. Indeed, as discussed in the theory, lithiation of pure tin is accompanied by a huge volume variation, destroying quickly the sample by formation of large SEI and contact loss with active materials.
One could explain the larger life cycle (35 cycles) of the 0.35V cycled sample by a restrained lithiation process leading to a smaller volume expansion and therefore a better stability.
Finally, it can be seen that the maximum specific capacity by area attained by pure Sn (1100 $\mu Ah/cm^2$) is in general higher than NiSn. Result which is logical since pure Sn samples are composed of more active material compared to NiSn samples. This is confirmed by the specific capacity by active mass (Sn mass).

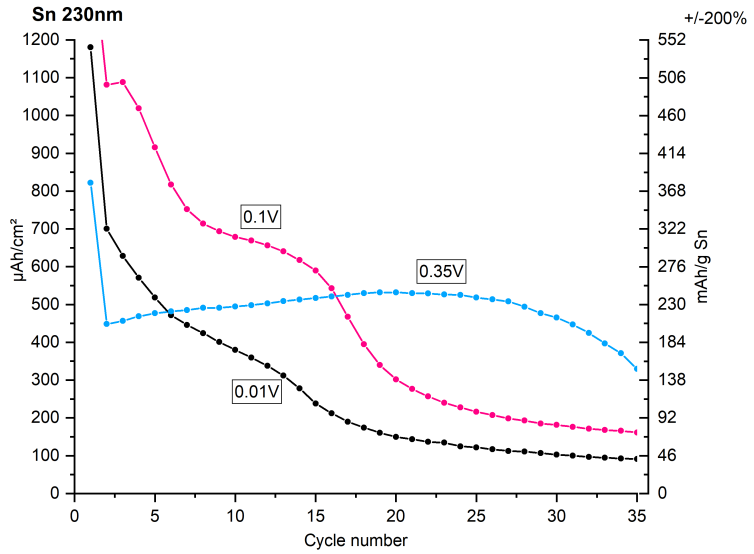

Figure 3.30: Specific capacity of Sn 230 nm diameter nanowires for different potential lower limits up to 1V

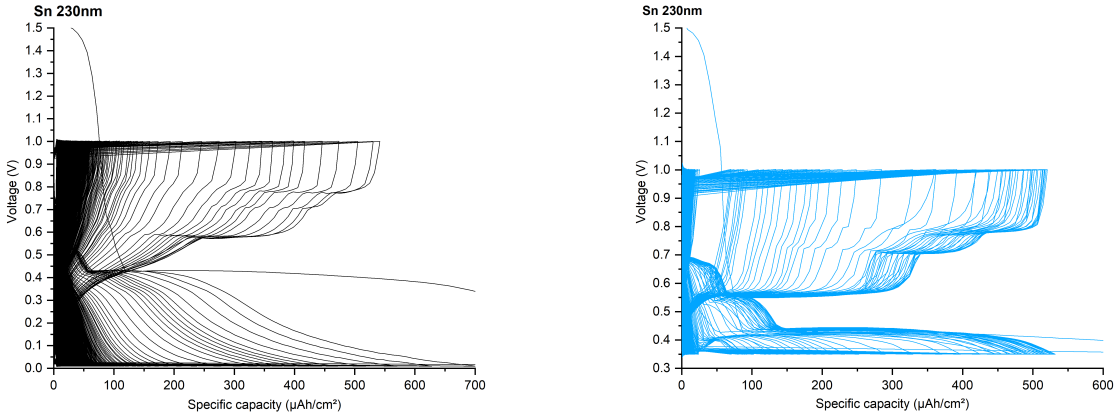

Figure 3.31: Sn 230nm-diameter nanowires: Ecell-Capacity curves at different lower potential limits (black = 0.01V, blue= 0.35V)

If we compare these results with tin oxide nanowires in literature, we can see that SnO_2 has a larger capacity of $\approx 1000\ mAh/g$. [68]
Whereas, the Sn system suffers from the same mass approximation error as NiSn samples.
It is therefore complicated to compare them with the gravimetric specific capacity.
Other interesting results were obtained with a core-shell nanorods systems (Sn coating on Ni nanorods structure), with a longer life cycle of more than 100 cycles and a specific capacity of 560 mAh/g.[29][41]

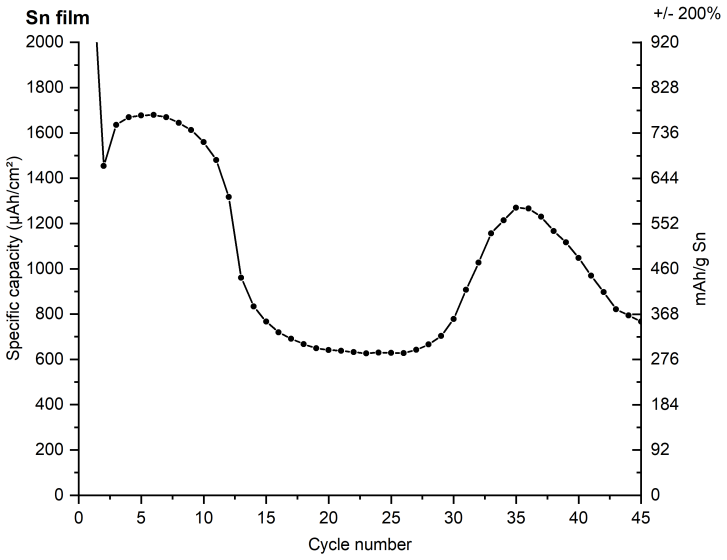

Figure 3.32: Specific capacity of Sn film

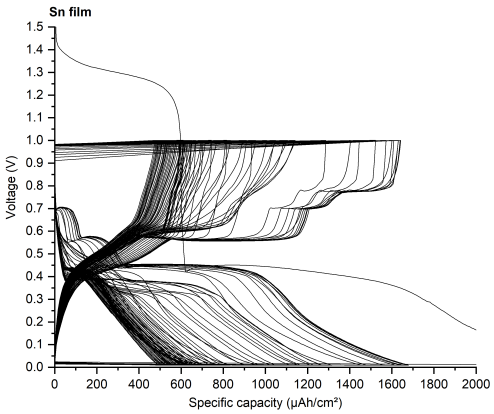

Figure 3.33: Sn film: Ecell-Capacity curve cycled from 0.01V to 1V

The film sample of pure Sn present results with a very unusual shape (figure 3.32).
This unusual double peak of pure tin can suggest a mechanical deformations/movements which have an influence on the proper functioning of the electrode inside the battery as a contact loss with the current collector.
Sn films present a very high specific capacity of $1600 \mu Ah/cm^2$ but only during few cycles as predicted by the theory. The values linked to the first peak are consistent with literature value (940 mAh/g at first cycle and 200 mAh/g after some cycles). [62] In this paper, a heat treatment was applied to alloy the tin with the substrate (Cu) to make a stronger interface leading to much better properties. Another article which shows the same value for specific capacity, was able to increase the electrodes performances by controlling the microstructure of the film by using pulsed electrodeposition in place of constant electrodeposition. Smaller crystal grains and stronger adhesion are possible thanks to pulsed electrodeposition. [61]

All these cases are still far from the desired sample with a specific capacity close to pure tin capacity (994 mAh/g Sn) along with a long life cycle needed for most applications even if the best configurations allow to achieve better results than graphene Li-ion batteries (372 mAh/g) in terms of capacity delivered.[66]

3.2.5 Coulombic efficiency curves

Another interesting test to perform is cycling batteries at different currents of discharge. Lower is the discharge current, better are the performances. Performing this test allows to highlight the difference of performances for different discharging rates.
The coulombic efficiency gives the ratio between charge and discharge capacity, informing about the reversibility of the reactions.[69] [70]

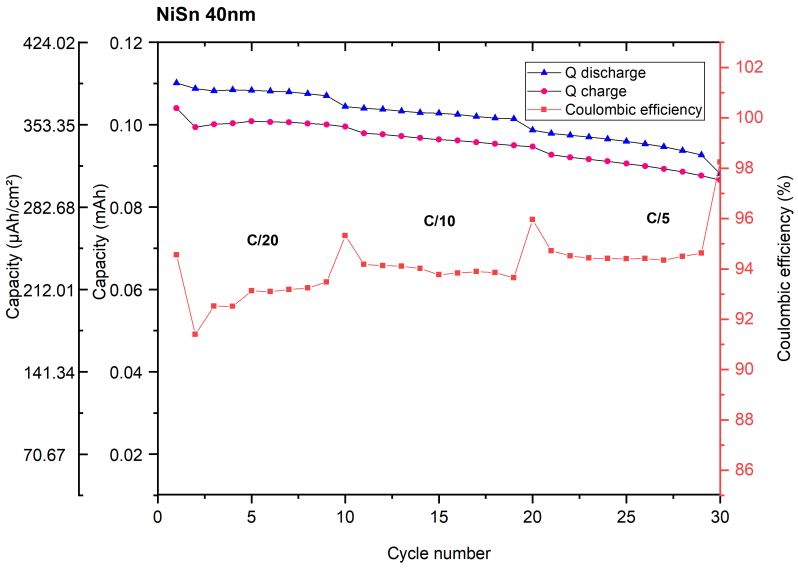

Figure 3.34: Coulombic efficiency, charge and discharge capacity of NiSn 40nm-diameter nanowires

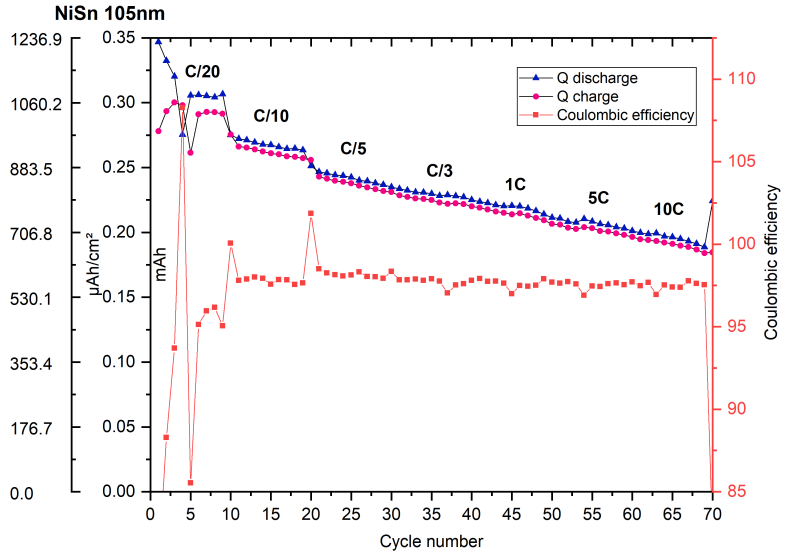

Figure 3.35: Coulombic efficiency, charge and discharge capacity of NiSn 105nm-diameter nanowires (Restart of the testing system after 10 cycles)

On figure 3.36, the gap between 10 and 20 cycles is not representative of intern mechanisms but is due to a restart of the testing device. The step at the 10^{th} cycle on figure 3.35 is probably due to resting time caused also by this restart.
The first value of coulombic efficiency is lower than the following ones due to the large irreversible part of the first cycle discharge capacity absorbed by the formation of SEI, electrolyte

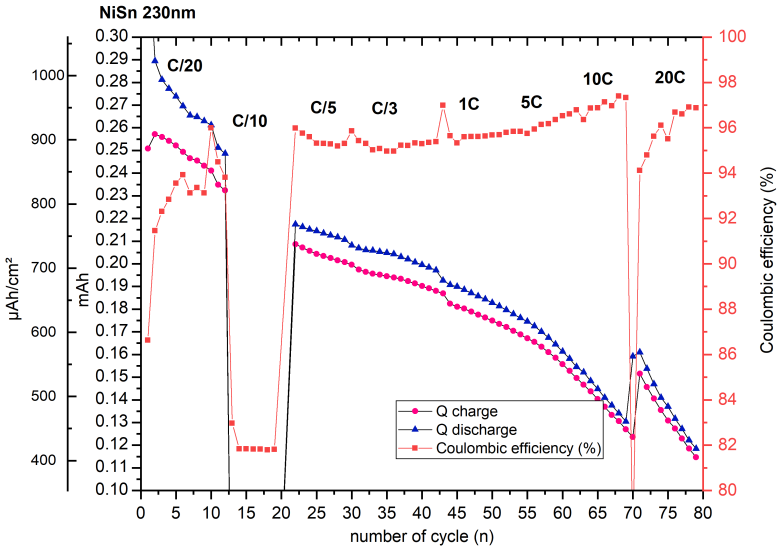

Figure 3.36: Coulombic efficiency, charge and discharge capacity of NiSn 230nm-diameter nanowires (Restart of the testing system after 10 cycles)

decomposition and cycling of surface's impurities (as oxides).[66]
The low difference of capacity in function of the discharge rate indicates that the cells performances are not greatly influenced by the discharge rate. This could be due to the large amount of accessible active compound. Indeed, the nanowire shape (with high surface area) allows an easy access for the ions from the electrolyte to the active material of the electrode.
However the fast fading of the cells capacities limited the test to low discharge rates (see Appendix 3.3.2). Indeed, after only few cycles, the capacity of the batteries decreases strongly and the results are not exact anymore since the discharge current is calculated in function of the initial capacity. A strong capacity loss leads to a much higher discharge current for the cycling cell.
The coulombic efficiency is high and stays between 90-97%.

3.2.6 Conclusion

Different samples of NiSn or pure Sn films and nanowires were cycled to identify their capacity, life cycle, potential and coulombic efficiency.
The NiSn 230nm and 40nm-diameters achieved lower capacities than films with a longer life cycle, while the 105nm-diameter nanowires achieved the best results with a high capacity of 1100 $\mu Ah/cm^2$ and a life cycle of 55 cycles. Some assumptions were made to explain this behaviour. Pure Sn was able to have larger capacities at the expense of its life cycle as predicted in the theory.

The comparison between the samples and with the literature has to be taken with some distance since the quality of the samples is susceptible to be low. Indeed, the nanowires samples are fragile and easily deformed or detached from the substrate during processing. Moreover the supposed error on the determination of the mass is huge. It is, therefore, complicated to draw any conclusion from those results which have to be confirmed by more tests.

3.3 Cycled samples

Some post-cycled samples were collected and analyzed with the SEM. The multiple residues of solvent, separator, SEI, ... make the observation of the samples very complicated and only observations at high scale were possible.
Moreover the samples were cycled until complete loss of capacity and stayed long time in the electrolyte before being disassembled and washed. Deterioration could have happened after capacity loss. It is therefore complicated to draw conclusions from these images.

3.3.1 Films

Sn film sample and NiSn film sample were observed.

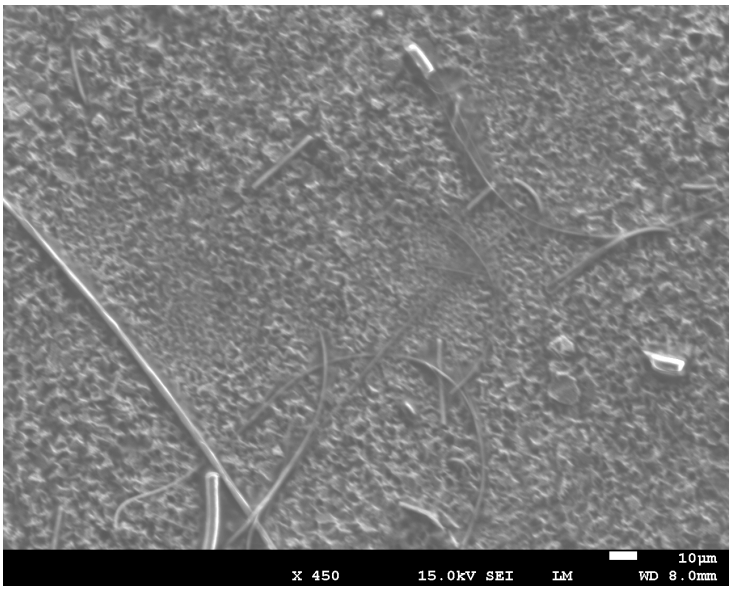

Figure 3.37: Sn film after cycling

On the Sn film, we can observe a rough surface (figure 3.37). By comparing it with the observations given in the study of Minoru Inaba [71], on figure 3.38, it appears that the surface of the film is deformed under cycling due to the volume change upon lithiation. This volume change breaks the SEI formed and an increase of surface area leads to a strong electrolyte decomposition and new SEI formation. These reactions affect strongly the irreversible part of the capacity during first cycles.
If Sn film is compared with NiSn film (figure 3.39) which seems to have a less rough surface, it seems to confirm that the volume change upon lithiation is lower and therefore lower is the deformation of the surface.

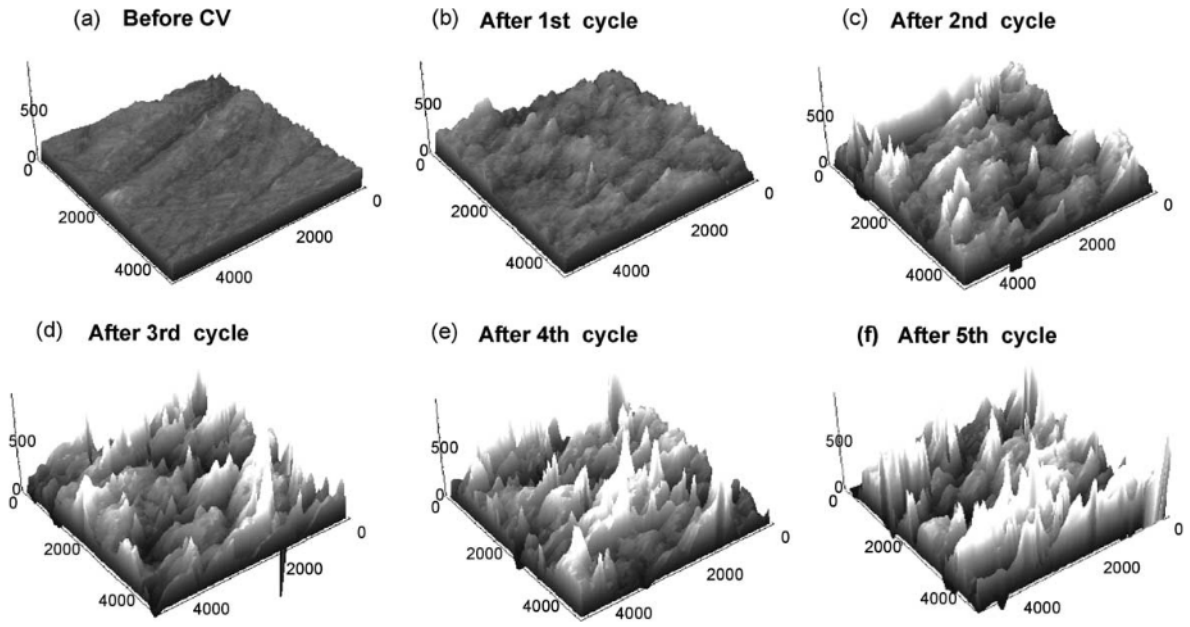

Figure 3.38: Three-dimensional AFM images of electrodeposited Sn thin film (a) before and (b–f) after cyclic voltammetry in 1 M LiClO4/PC (from [71])

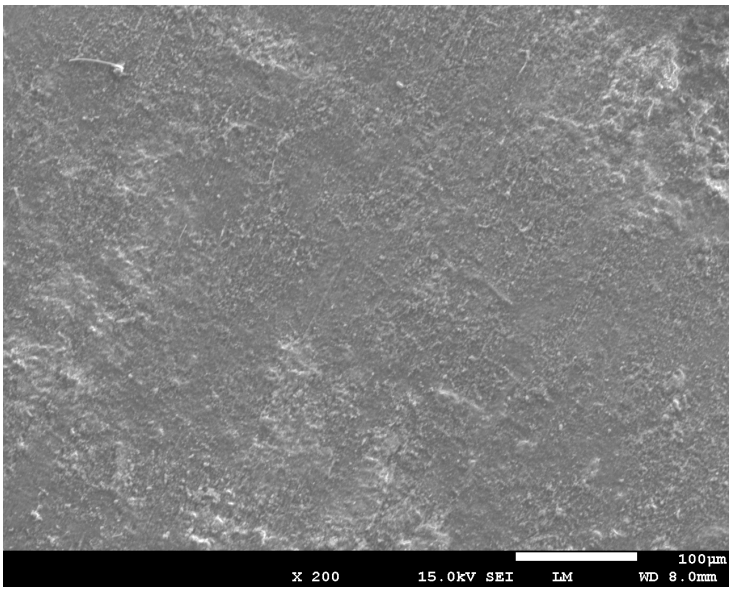

Figure 3.39: NiSn film after cycling

3.3.2 Nanowires

For nanowires, the morphology seems to also have suffered from cycling (figure 3.40). It is, however, difficult to draw any conclusions since the scale is too large to identify them and since the device remained during a long time in the electrolyte. The non-conductive porous shell which can be observed, created around the sample, is probably due to the SEI formation.

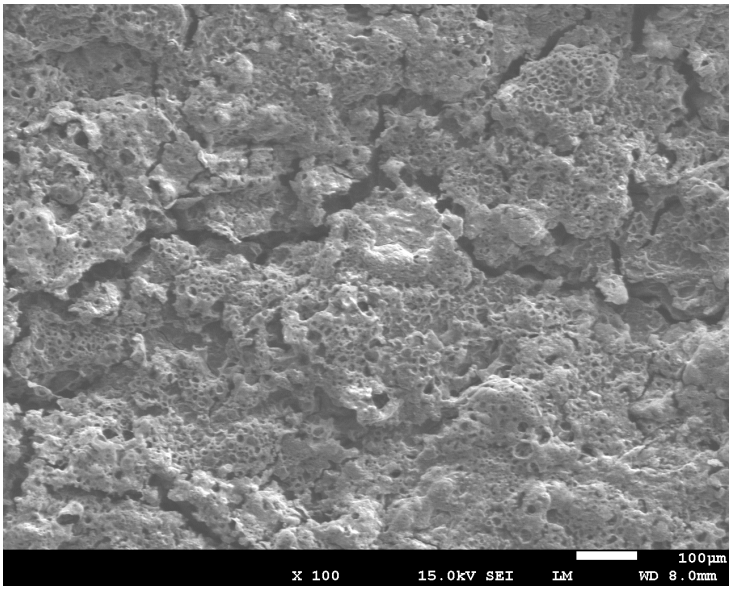

Figure 3.40: NiSn 230nm-diameter nanowires after cycling

Conclusions & Perspectives

This master thesis investigated a 3D interconnected nanowire network anode composed of NiSn alloy for Li-ion battery. The structure was compared with pure Sn samples (films and nanowires) and 2D NiSn anodes to emphasize the contribution of both 3D structures and Ni inactive matrix.

The first step was to grow the NiSn or Sn nanowires having different diameters (230nm, 105nm, 40nm) and the 2D films by cathodic electrodeposition from aqueous electrolytes.
The films were grown without facing any issue. The production of NiSn nanowires by cathodic electrodeposition, at the opposite of Sn nanowires, was successful. Well defined NiSn nanowires networks with homogeneous heights were observed by SEM. The networks seem structured for nanowires having 230nm and 105nm-diameter but some agglomerations were observed for 40nm-diameter nanowires, representative of a weaker structure. The deposition of Sn nanowires, however, produced non-homogeneous samples with some spots of preferential growth surrounded by a background of very small nanowires. The Sn electrolyte composition could be improved, indeed some indications about changing the pH of the solution were given in the Methods chapter thanks to an analysis of the Pourbaix diagram of $Sn - H_20$.

To improve the adhesion between the nanowires and the Cu substrate, alumina-coated silicon membranes were used as "pressing" membranes but metallic deposition occurred on the membrane preventing the formation of homogeneous deposited samples. Other strategies could be explored as thermal treatments, pulsed electrodeposition, "screw" nanowires or glued systems. The adhesion is suspected to be one of the main causes behind the poor battery performances obtained, due to a detachment of the sample from the current collector and a probable loss of mass during and after deposition.
It has also been shown that the surface morphology influences greatly the performances of the electrodes. Pulsed deposition and surface treatments could also be performed for this reason. Some studies about the exact predominant phase of the sample could be performed through XRD analysis.

The evolution of behaviour of different galvanostatically cycled samples suggests an amorphization of the samples through cycling and a high capacity loss (irreversible part) due to SEI formation or oxidation at the first cycles.

The intermediate-diameter size of nanowires (105nm) achieved the best results at low potential limitation (1V-0.01V) with a specific capacity of 1000 $\mu A/cm^2$ and a life cycle of 55 cycles compared to 325 $\mu A/cm^2$ and 35 cycles for 40nm-diameter nanowires, 750 $\mu A/cm^2$ during 45 cycles for 230nm-diameters nanowires and against 650 $\mu A/cm^2$ during 22 cycles for NiSn film. Pure Sn samples achieved higher values of specific capacity for films (1600 $\mu A/cm^2$) at the expense of the life cycle of 10 cycles. The deposition of Sn nanowires faced some issues and the resulting samples performances are very low and probably not representative of the real performances.

These results highlight both the interest of working with an inactive matrix material, Ni in this case, to achieve longer life time than for pure active material, Sn, and the higher specific capacity achieved by 3D structures compared to 2D structures, i.e. films.
The fact that the intermediate-size (105nm) nanowires achieved better performances could be explained by a compromise of larger interface area compared to 230nm-diameter nanowires and of a stronger structure with larger voids between nanowires compared the 40nm-diameter nanowires. But the quality of the samples and the adhesion between the anode and the current collector are suspected to be the main reason behind the poor battery performances achieved if the results are compared with what is done in literature.
More tests should be performed to verify the correctness and the reproducibility of the results. But more importantly, research on other adhesion techniques should be carried on in order to achieve better performances since adhesion and mass loss seem to jeopardize the samples quality.

Appendix

Template dissolution The dissolution of the polycarbonate template was not completely successful for some samples (figure 3.41).

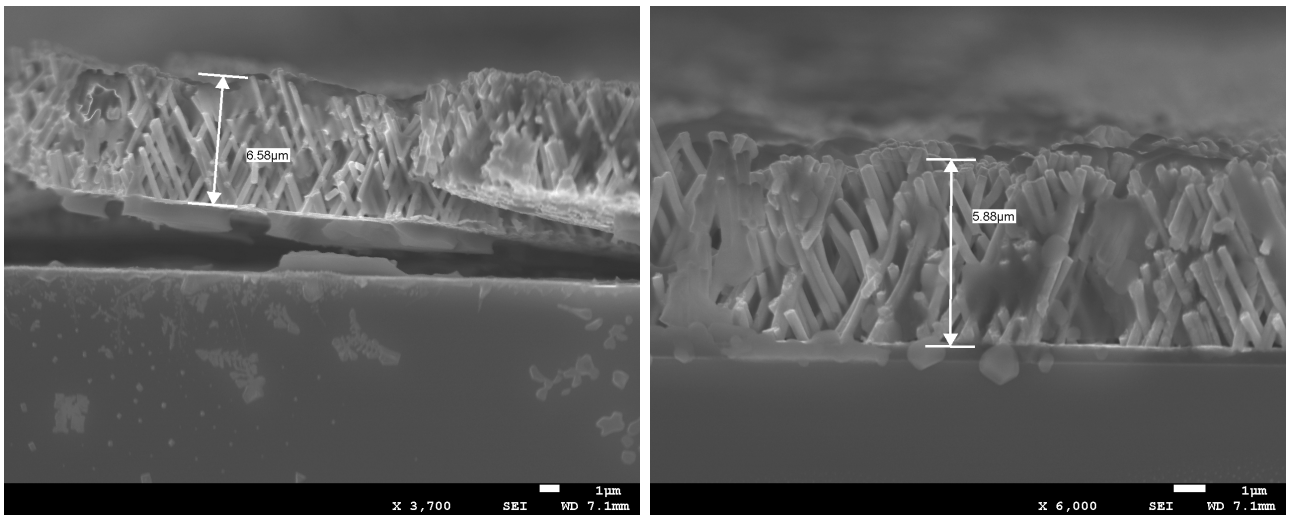

(a) Tilted view (x3700) (b) Side view (x6000)

Figure 3.41: NiSn 230nm-diameter nanowires with PC template residues

For small nanowires a long dissolution time (around 1h) with multiple baths of solvent is suggested to achieve better results.

Film support of nanowires A thin film is grown between the nanowires and the substrate during the electrodeposition of the nanowires. Here is a view of this film surface peeled of the substrate.

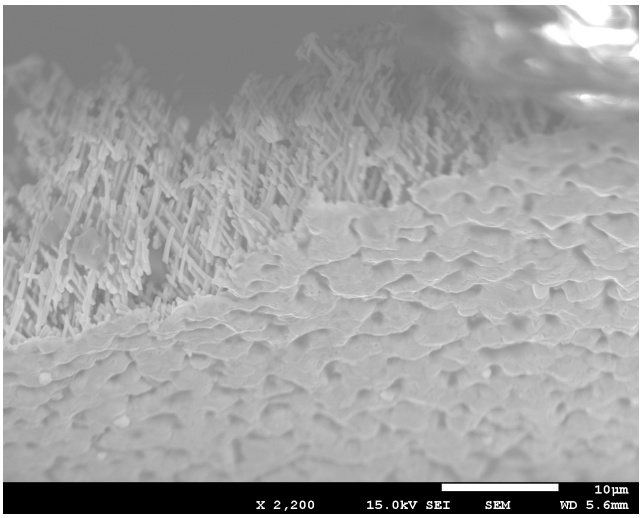

Figure 3.42: Sn 230nm-diameter nanowires detached from the substrate (ground angle view)

Fast fading of capacity The fast fading of capacity of the samples makes the test of different discharge rates meaningless (figure 3.43).

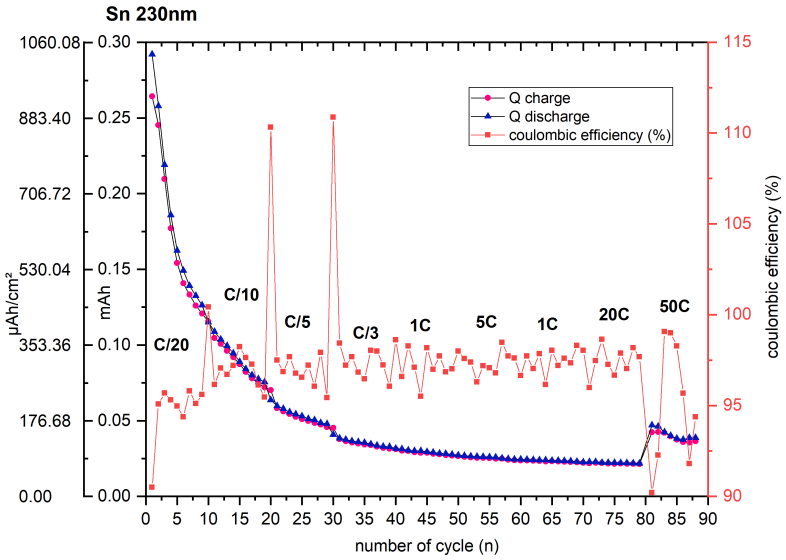

Figure 3.43: Coulombic efficiency, charge and discharge capacity of Sn 230nm-diameter nanowires

References

[1] Yang Xu, Min Zhou, and Yong Lei. "Nanoarchitectured Array Electrodes for Rechargeable Lithium-and Sodium-Ion Batteries". *Advanced Energy Materials* 6.10 (2016), p. 1502514.

[2] APERe. *Observatoire belge des énergies renouvelables*. https://www.apere.org/fr/observatoire-energies-renouvelables. 2019.

[3] LeParisien. *Transports : les chiffres alarmants de la pollution automobile*. http://www.leparisien.fr/environnement/ville-durable/transports-les-chiffres-alarmants-de-la-pollution-automobile-28-04-2015-4731551.php. 2015.

[4] C. Deluzarche. *Transport et CO2 : quelle part des émissions ?* https://www.futura-sciences.com/planete/questions-reponses/pollution-transport-co2-part-emissions-1017/. 2016.

[5] D. Linden. "Handbook of batteries". *Fuel and Energy Abstracts* 36.4 (1995), p. 265.

[6] N. Thomas. *China Is Building the Batteries of the Future*. https://foreignpolicy.com/2019/04/02/china-is-building-the-batteries-of-the-future-tesla-li-ion/. 2019.

[7] Jeffrey W Long et al. "Three-dimensional battery architectures". *Chemical Reviews* 104.10 (2004), pp. 4463–4492.

[8] Vladimir S Bagotsky, Alexander M Skundin, and Yurij M Volfkovich. *Electrochemical power sources: batteries, fuel cells, and supercapacitors*. John Wiley & Sons, 2015.

[9] Wikipédia. *Fuel Cell*. https://en.wikipedia.org/wiki/Fuel_cell. 2019.

[10] Wikipédia. *Supercapacitors*. https://en.wikipedia.org/wiki/Supercapacitor. 2019.

[11] Wikipédia. *Electric battery*. https://en.wikipedia.org/wiki/Electric_battery. 2019.

[12] Wikipédia. *Redox*. https://en.wikipedia.org/wiki/Redox. 2019.

[13] Darrel F. Untereker et al. "8 - Power Sources and Capacitors for Pacemakers and Implantable Cardioverter-Defibrillators". *Clinical Cardiac Pacing, Defibrillation and Resynchronization Therapy (Fifth Edition)*. Ed. by Kenneth A. Ellenbogen et al. Fifth Edition. Elsevier, 2017, pp. 251–269. ISBN: 978-0-323-37804-8.

[14] Jung-Ki Park. *Principles and applications of lithium secondary batteries*. John Wiley & Sons, 2012.

[15] Unknown. *Battery cell comparison*. https://www.epectec.com/batteries/cell-comparison.html. 2019.

[16] M Rosa Palacin. "Recent advances in rechargeable battery materials: a chemist's perspective". *Chemical Society Reviews* 38.9 (2009), pp. 2565–2575.

[17] Sung You Hong et al. "Charge carriers in rechargeable batteries: Na ions vs. Li ions". *Energy & Environmental Science* 6.7 (2013), pp. 2067–2081.

[18] C. Delenne. *La voiture électrique :Des avantages mais pas seulement*. http://voiture-electrique07.e-monsite.com/pages/batterie.html.

[19] John B Goodenough and Kyu-Sung Park. "The Li-ion rechargeable battery: a perspective". *Journal of the American Chemical Society* 135.4 (2013), pp. 1167–1176.

[20] Peng Lu et al. "Chemistry, impedance, and morphology evolution in solid electrolyte interphase films during formation in lithium ion batteries". *The Journal of Physical Chemistry C* 118.2 (2014), pp. 896–903.

[21] Jacques V. *Batteries Lithium-ion : Avantages et inconvénients*. http://energie-futur.com/batteries-lithium-ion-avantages-et-inconvenients/. 2015.

[22] Unknown. *La production mondiale de lithium*. https://www.planetoscope.com/matieres-premieres/671-production-mondiale-de-lithium.html. 2012.

[23] B. Gourcerol. *Quelle place pour l'Europe dans le marché du lithium ?* http://www.mineralinfo.fr/ecomine/quelle-place-leurope-marche-lithium. 2018.

[24] Simoen M. Hache E. Seck G-S. *Quelle criticité du lithium dans un contexte d'électrification du parc automobile mondial ?* http://www.panorama-ifpen.fr/criticite-du-lithium/. 2018.

[25] F. Marco. *Le lithium une ressource stratégique*. http://canabae.enseigne.ac-lyon.fr/spip/spip.php?article705. 2011.

[26] Manuel Salazar Salvo. *Chili. Le lithium dans les mains de la famille Pinochet*. https://www.courrierinternational.com/article/2009/10/08/le-lithium-dans-les-mains-de-la-famille-pinochet. 2009.

[27] A. Katwala. *The spiralling environmental cost of our lithium battery addiction*. https://www.wired.co.uk/article/lithium-batteries-environment-impact. 2018.

[28] Naoki Nitta et al. "Li-ion battery materials: present and future". *Materials today* 18.5 (2015), pp. 252–264.

[29] Xilin Chen et al. "3D tin anodes prepared by electrodeposition on a virus scaffold". *Journal of Power Sources* 211 (2012), pp. 129–132.

[30] Robert A Huggins. "Lithium alloy negative electrodes". *Journal of Power Sources* 81 (1999), pp. 13–19.

[31] Abhishek Lahiri and Frank Endres. "Electrodeposition of nanostructured materials from aqueous, organic and ionic liquid electrolytes for Li-ion and Na-ion batteries: a comparative review". *Journal of The Electrochemical Society* 164.9 (2017), pp. D597–D612.

[32] Hui Wu et al. "Stable cycling of double-walled silicon nanotube battery anodes through solid–electrolyte interphase control". *Nature nanotechnology* 7.5 (2012), p. 310.

[33] Candace K Chan et al. "High-performance lithium battery anodes using silicon nanowires". *Nature nanotechnology* 3.1 (2008), p. 31.

[34] Jusef Hassoun, S Panero, and B Scrosati. "Electrodeposited Ni–Sn intermetallic electrodes for advanced lithium ion batteries". *Journal of Power Sources* 160.2 (2006), pp. 1336–1341.

[35] Miao Tian et al. "Stable high areal capacity lithium-ion battery anodes based on three-dimensional Ni–Sn nanowire networks". *Journal of Power Sources* 211 (2012), pp. 46–51.

[36] Alexandru Vlad et al. "Three-dimensional interconnected Nicore–NiOshell nanowire networks for lithium microbattery architectures". *Journal of Materials Chemistry A* 4.5 (2016), pp. 1603–1607.

[37] Debra R Rolison et al. "Multifunctional 3D nanoarchitectures for energy storage and conversion". *Chemical Society Reviews* 38.1 (2009), pp. 226–252.

[38] Hitomi Mukaibo et al. "Electrodeposited Sn-Ni alloy film as a high capacity anode material for lithium-ion secondary batteries". *Electrochemical and Solid-State Letters* 6.10 (2003), A218–A220.

[39] Alexandru Vlad et al. "Three-dimensional interconnected Nicore–NiOshell nanowire networks for lithium microbattery architectures". *Journal of Materials Chemistry A* 4.5 (2016), pp. 1603–1607.

[40] it4ip. *Track-etching technology*. https://www.it4ip-iontracktechnology.com/innovation/track-etching-technology//.

[41] Jusef Hassoun et al. "High-rate, long-life Ni–Sn nanostructured electrodes for lithium-ion batteries". *Advanced Materials* 19.12 (2007), pp. 1632–1635.

[42] V.-A. Antohe and al. "pH sensitive capacitive detectors based on localized nanowire arraysnanotechnology & device integration routes." (2012).

[43] E. Roy. "Elaboration Electrochimique et Caractérisations de Nanofils d'Antimoine et d'Or". *Université de Marne la Vallée, 2* (2002).

[44] Lycée Galilée Franqueville-Saint-Pierre. "Ni-H2O Pourbaix diagramme" (consulted 2019). URL: http://lycees.ac-rouen.fr/galilee/nickelpotentielpH.html.

[45] Honorata Kazimierczak. "Electrochemical phase diagrams" (consulted 2019). URL: https://slideplayer.pl/slide/59860/.

[46] Ashraf T. Al-Hinai, Muna H. Al-Hinai, and Joydeep Dutta. "Application of Eh-pH diagram for room temperature precipitation of zinc stannate microcubes in an aqueous media". *Materials Research Bulletin* 49 (2014), pp. 645–650. ISSN: 0025-5408. DOI: https://doi.org/10.1016/j.materresbull.2013.10.011. URL: http://www.sciencedirect.com/science/article/pii/S0025540813008404.

[47] H. Mukaibo, T. Momma, and T. Osaka. "Changes of electro-deposited Sn–Ni alloy thin film for lithium ion battery anodes during charge discharge cycling". *Journal of Power Sources* 146.1 (2005). Selected papers pressented at the 12th International Meeting on Lithium Batteries, pp. 457–463. ISSN: 0378-7753. DOI: https://doi.org/10.1016/j.jpowsour.2005.03.043. URL: http://www.sciencedirect.com/science/article/pii/S0378775305004349.

[48] Joaquin de la Torre Medina et al. "Large-scale 3-D interconnected Ni nanotube networks with controlled structural and magnetic properties". *Scientific Reports* 8.1 (2018), p. 14555. ISSN: 2045-2322.

[49] Filinchuk F. et al. "Solid-State Micro-Batteries with nanowire Electrodes: from Materials to Integration". *action de recherche concertée* (consulted 2019).

[50] Matt Carter. *Guide to research techniques in neuroscience*. Academic Press, 2015.

[51] NanoScience Instruments. *Scanning Electron Microscopy*. https://www.nanoscience.com/techniques/scanning-electron-microscopy/. 2019.

[52] Jörgen Bergström. "2 - Experimental Characterization Techniques". *Mechanics of Solid Polymers*. Ed. by Jörgen Bergström. William Andrew Publishing, 2015, pp. 19–114. ISBN: 978-0-323-31150-2. DOI: https://doi.org/10.1016/B978-0-323-31150-2.00002-9. URL: http://www.sciencedirect.com/science/article/pii/B9780323311502000029.

[53] Unknown. *Electron Microscope Images Of Electrons*. http://www.bianoti.com/electron-microscope-images-of-electrons.html.

[54] Wikipédia. *Scanning electron microscope*. https://en.wikipedia.org/wiki/Scanning_electron_microscope. 2010.

[55] "How to Mix Backscattered and Secondary Electron Images". *Thermo Fisher Scientific Phenom-World BV* (2018). URL: https://www.azom.com/article.aspx?ArticleID=16390.

[56] A. Nanakoudis. *EDX analysis with a scanning electron microscope (SEM): how does it work?* https://blog.phenom-world.com/edx-analysis-scanning-electron-microscope-sem. 2018.

[57] L.Holtschi. "Synthesis and characterization of 3D nanowire networks for high-areal capacity Li-ion battery anodes" (2016).

[58] Da-wei Zhang et al. "Fabrication of Sn-Ni alloy film anode for Li-ion batteries by electrochemical deposition". *Transactions of Nonferrous Metals Society of China* 19.6 (2009), pp. 1489–1493.

[59] L. Piraux. "Transport phenomena in solids and nanostructures (MAPR 2471)" (2018).

[60] Miao Tian et al. "Enhancing Ni–Sn nanowire lithium-ion anode performance by tailoring active/inactive material interfaces". *Journal of Power Sources* 196.23 (2011), pp. 10207–10212. ISSN: 0378-7753. DOI: https://doi.org/10.1016/j.jpowsour.2011.08.062. URL: http://www.sciencedirect.com/science/article/pii/S0378775311016053.

[61] Koichi Ui et al. "Electrochemical characteristics of Sn film prepared by pulse electrodeposition method as negative electrode for lithium secondary batteries". *Journal of Power Sources* 189.1 (2009), pp. 224–229.

[62] Noriyuki Tamura et al. "Study on the anode behavior of Sn and Sn–Cu alloy thin-film electrodes". *Journal of Power Sources* 107.1 (2002), pp. 48–55.

[63] Pimpa Limthongkul et al. "Electrochemically-driven solid-state amorphization in lithium-silicon alloys and implications for lithium storage". *Acta Materialia* 51.4 (2003), pp. 1103–1113. ISSN: 1359-6454. DOI: https://doi.org/10.1016/S1359-6454(02)00514-1. URL: http://www.sciencedirect.com/science/article/pii/S1359645402005141.

[64] Dominique Larcher et al. "Recent findings and prospects in the field of pure metals as negative electrodes for Li-ion batteries". *Journal of Materials Chemistry* 17.36 (2007), pp. 3759–3772.

[65] Kejie Zhao et al. "Fracture and debonding in lithium-ion batteries with electrodes of hollow core–shell nanostructures". *Journal of Power Sources* 218 (2012), pp. 6–14. ISSN: 0378-7753. DOI: https://doi.org/10.1016/j.jpowsour.2012.06.074. URL: http://www.sciencedirect.com/science/article/pii/S0378775312010841.

[66] Guoxiu Wang et al. "Sn/graphene nanocomposite with 3D architecture for enhanced reversible lithium storage in lithium ion batteries". *Journal of Materials Chemistry* 19.44 (2009), pp. 8378–8384.

[67] Jin-Yun Liao and Arumugam Manthiram. "Mesoporous TiO2-Sn/C Core-Shell Nanowire Arrays as High-Performance 3D Anodes for Li-Ion Batteries". *Advanced Energy Materials* 4.14 (2014), p. 1400403.

[68] Z Ying et al. "Characterization of Sn O 2 nanowires as an anode material for Li-ion batteries". *applied Physics letters* 87.11 (2005), p. 113108.

[69] AJ Smith et al. "Precision measurements of the coulombic efficiency of lithium-ion batteries and of electrode materials for lithium-ion batteries". *Journal of The Electrochemical Society* 157.2 (2010), A196–A202.

[70] Tsutomu Ohzuku et al. "Factor affecting the capacity retention of lithium-ion cells". *Journal of power sources* 54.1 (1995), pp. 99–102.

[71] Minoru Inaba, Takeshi Uno, and Akimasa Tasaka. “Irreversible capacity of electrodeposited Sn thin film anode”. *Journal of power sources* 146.1-2 (2005), pp. 473–477.

UNIVERSITÉ CATHOLIQUE DE LOUVAIN
École polytechnique de Louvain
Rue Archimède, 1 bte L6.11.01, 1348 Louvain-la-Neuve, Belgique | **www.uclouvain.be/epl**